The Effects of Fuels on Engine Throttle Transients

by

Jean-Charles W. Bossert

Bachelor of Science in Mechanical Engineering
The University of Texas at Austin
(1992)

SUBMITTED TO THE DEPARTMENT OF
MECHANICAL ENGINEERING IN PARTIAL
FULFILLMENT OF THE REQUIREMENTS
FOR THE DEGREE OF

MASTER OF SCIENCE IN MECHANICAL ENGINEERING

at the

MASSACHUSETTS INSTITUTE OF TECHNOLOGY

February 1994

Signature of Author_____
Department of Mechanical Engineering
January 14, 1994

Certified by _____
Wai K. Cheng
Associate Professor, Department of Mechanical Engineering
Thesis Supervisor

Accepted by _____
Ain A. Sonin
Chairman, Department Graduate Committee

(This page has been intentionally left blank.)

The Effects of Fuels on Engine Throttle Transients

by Jean-Charles Bossert

Submitted to the Department of Mechanical Engineering on January 14, 1994
in partial fulfillment of the requirements for the degree of
Master of science in Mechanical Engineering

ABSTRACT

Experiments to evaluate the effects of fuel composition on engine throttle transients were performed. The goal of these experiments was to interpret and quantify the difference between the amount of fuel injected and the amount of fuel burned as a change in liquid fuel mass inside the intake port during accelerations. The fuels chosen for this experiment were methanol-indolene blends: M0, M10, M25, M40, M60, M85, and M100. The transient was simulated by simultaneously opening the throttle while changing the amount of fuel injected to the engine to a predetermined fixed flow rate. The engine speed was kept at a constant 1800 Rpm while the intake pressure increased from 0.7 bar (part throttle) to 1.0 bar (wide open throttle). Once the engine reached steady state at wide open throttle, the throttle was returned to its original position. During the experiment, the ignition timing was kept constant, halfway between the MBT points of the wide open throttle condition and the part throttle condition. The measurements included the in-cylinder pressure, the fuel flow rate, and the exhaust relative air-fuel ratio. Each fuel was tested under six conditions: three levels of enrichment at wide open throttle (λ=1.0, λ=0.9, λ=0.8), and two sets of engine coolant temperatures (T=40°C, and T=80°C).

Using a three dimensional engine map of the fuel conversion efficiency it was possible to relate the Gross Indicated Mean Effective Pressure to the amount of fuel burned during each cycle. The map included the effects of the relative air to fuel ratio, the Gimep, and the ignition timing.

The data showed a uniform increase in the change of fuel film mass from M0 to M100 for the warmed up engine condition. Under stoichiometric condition the liquid film mass increased from 0.10 to 0.22 gram. However, in the low engine coolant temperature condition, there was no measurable change in fuel film mass from M0 to M60. A transition occurred between M60 and M85, where the change in fuel film mass increased by 200% from 0.2 to 0.4 gram.

The data indicates that there is a good correlation between the mass of fuel injected at WOT and the change of liquid film mass during the transient. Although the correlation is not as good for low coolant temperatures, the low temperature trend can be explained with a one dimensional heat transfer model of the intake port. The model indicates that under low coolant temperature, the port wall remains close to the boiling point of methanol under low intake pressure (part throttle). However, under high intake pressure (wide open throttle) the average port wall temperature is below the boiling point of methanol, causing a significant increase of liquid film mass inside the intake port. The model also shows that the increase in volatility of methanol blends is offset by the stoichiometric requirement of the fuel.

ACKNOWLEDGMENTS

The three semesters I have spent at the Sloan Automotive Lab. kept me busy. This experience has been very rewarding and taught me a lot about research and graduate school. All this could not have been possible without the help and contribution from so many people. Where should I start?

The first person that I should thank is professor Wai Cheng. Without his guidance, and knowledge I would probably still be taking data right now..... I also want to thank Professor John Heywood and Simone Hochgreb who have also greatly contributed to this research with their ideas during the meetings. These meetings were insightful and kept my research aimed in the right direction. However, all of this could not have been possible without the funding provided by the Industrial Consortium on engine/fuel Interactions. The consortium includes Chevron Research corp., the Department of Energy, Exxon Research and Engineering Company, Nippon Oil Company Ltd., and Shell Oil Company.

I want to use this opportunity to thank everybody who works at the Sloan Lab. Brian Corkum has played an important role in helping me with the experimental set up. Brian knows now "Everything You Always Wanted to Know about Dynamometers but Were Afraid to Ask". I also want to thank Joan Kenney who kept my spirits up and made sure that all the red tape was done on time....something that is easier said than done....But wait I am not finished....

All my friends at the Sloan Lab need to be thanked, specially my office mates: Pete, Jon, Koji, and Tung-Ching. These are the people that had to put up with me for a year and a half...I think they also deserve a diploma. But most of all I want to thank ALL my friends here at the lab for their patience, help, and expertise: Pete for ALL the questions he had to put up with, Jon for his Computer-Analytical-Math skills, Olivier the only one who could really "understand" me, the California man-Ed for his expertise on everyMicrosoft-computer-program, Kuo-Chiang for his expertise on fuel volatility modeling, Mike his expertise in turbulent flow and diffusion, K.D.M's knowledge of everything, Christine's company during the night shift, and Gatis' help in the math course.

Finally I want to thank my parents without whom all of this would not have been possible...to whom I owe so much .....and Gail who made it all worthwhile.

Jean-Charles Bossert
January 1994

Table of contents

List of Figures

List of Tables

CHAPTER 1 -- INTRODUCTION

1.1 Motivation

Since the early 1970's, the Environmental Protection Agency has been forcing automobile manufacturers for engines with greater fuel efficiency and lower emissions. The clean Air Act of 1990 and the California Air Resource Board have set strict emissions guidelines for the up coming years.

In order to meet these stringent requirements, the automotive industry has developed complex engine control systems, sophisticated fuel metering strategies and the associated sensors to improve emissions. Along with the hardware development, there is substantial research using reformulated fuels to reduce emissions. For example, methanol/gasoline blends offer promises in lowering emissions while decreasing the United States' dependency on foreign oil imports.

Another important motivation for this research is the consumer's satisfaction. The oil industry tries to satisfy its customers by providing fuels which give good driveability while meeting the emission levels set by the EPA. Therefore it is important to understand the phenomena that causes hesitation (uneven acceleration), and stumble (stepping during acceleration). The above discussions motivates the theme for this thesis: to study the fuel effects on the transient behavior of spark ignition engines with a matrix of methanol/gasoline mixtures.

1.2 Background

1.2.1 Transient Testing

Since 1975 all EPA certified vehicles must pass the Federal Testing Program (FTP). The test consists of a driving cycle simulating a typical trip. The vehicle is installed on a chassis dynamometer while the speed and load are changed. Figure 1.2.1 shows the speed versus time for the FTP 75 test [1]. During the test, samples of the exhaust gases are taken and analyzed. Under 1993 standards, each vehicle must not generate more than an overall 0.25 gram per mile for Non-Methane Organic Gases, 3.4 gram per mile for Carbon Monoxide, and 0.4 gram per mile for NOx. Each vehicle must go through the same transient test starting under cold and warmed up conditions.

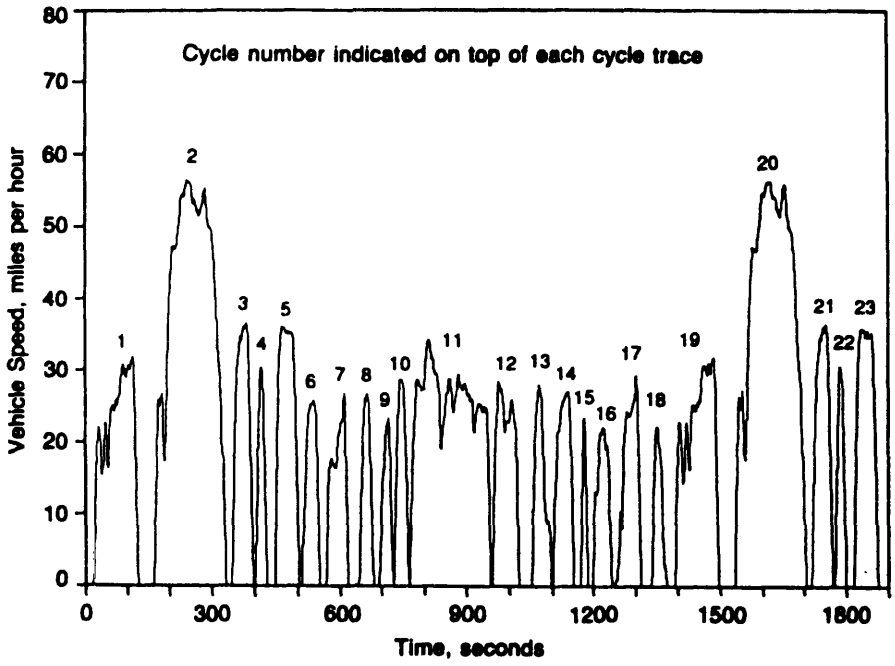

Figure 1.2.1 Speed versus time for the FTP 75 test[1].

Because of the various vehicle accelerations and decelerations in the FTP cycle, the test

procedure is transient in nature in the sense that there are rapid throttle and speed changes.

1.2.2 Emissions Control

Today's engines have a complex control system designed to optimize the engine's performance and emissions level. Emissions control hardware such as the catalytic converter set very strict guidelines over the air fuel ratio range. Figure 1.2.2 shows the window of operation of a three way catalytic converter[2]. Outside this window of operation, the catalytic converter's efficiency drops dramatically. For example, during a fuel rich situation, not enough oxygen is present in the exhaust gases, and the catalyst is unable to oxidize carbon monoxide and the unburned hydrocarbons. The reverse happens during lean conditions, too much oxygen is present, and the catalytic converter is unable to reduce NOx. Therefore, it is crucial to keep the engine operating inside the specified air/fuel control window to minimize the HC and NOx excursions.

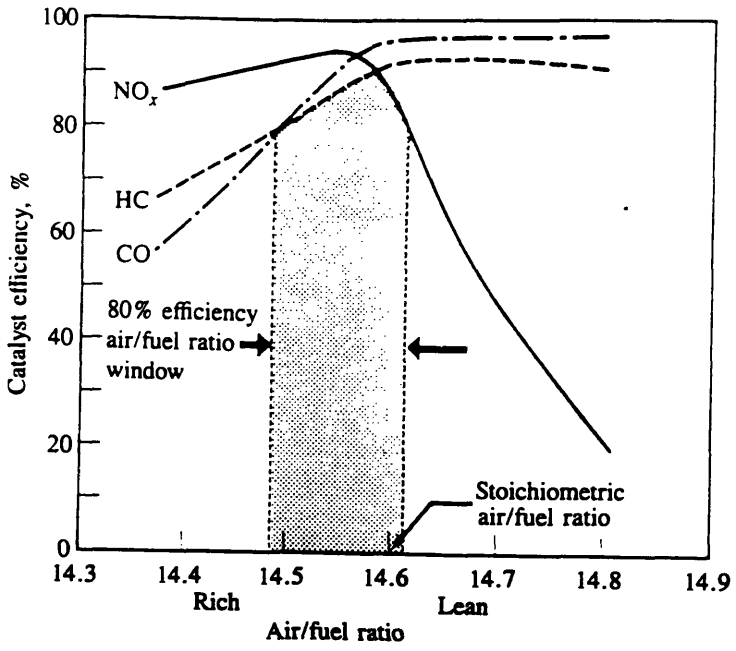

Figure 1.2.2 Efficiency of a three way catalytic Converter [2].

1.2.3 Air/fuel Control

The mixture preparation system of a modern engine provides a mixture of precise fuel air ratio delivered to the engine. Figure 1.2.3 shows a schematic of a typical control system. The air mass flow meter (usually a hot wire or film anemometer) sends a signal to the controller (the ECU). To keep the engine stable during rapid accelerations or decelerations, the throttle plate position sensor is used as a feed forward signal. Based on the air mass flowing to the engine, the controller determines the amount of fuel that needs to be injected in order to keep the mixture stoichiometric. Finally, the lambda sensor in the exhaust senses the relative air/fuel ratio burned. This signal is fed to the controller as an error signal. Therefore, the controller compensates partially when the exhaust gas air fuel ratio falls outside the specified range. Although lead/lag compensation schemes are used, the fuel metering system cannot always keep up with the air/fuel excursions during transients[3].

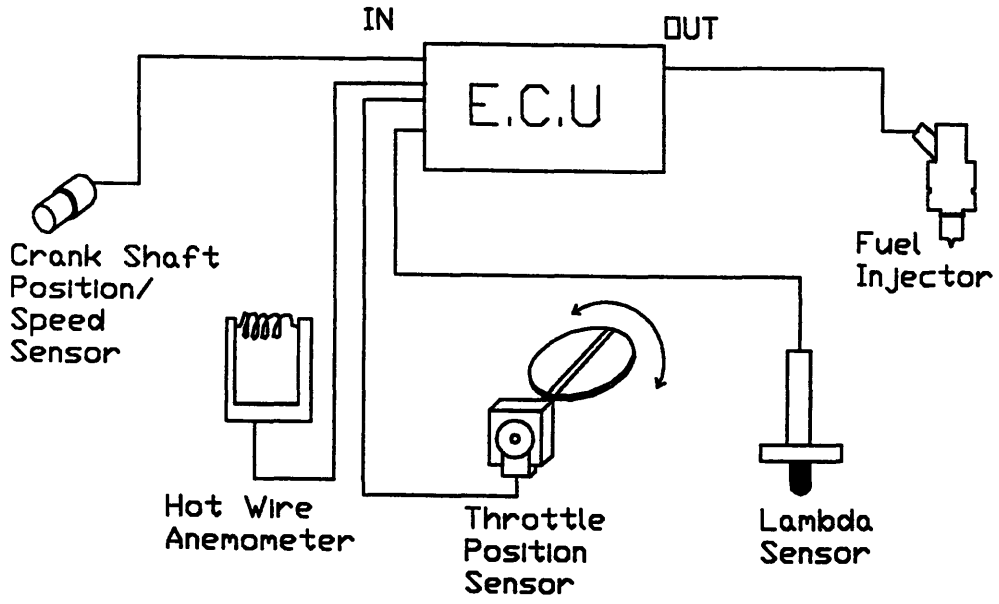

Figure 1.2.3 Diagram of a typical control system for a modern engine

Figure 1.2.4 shows typical air-fuel ratio excursions during the FTP cycle test[1]. There are three reasons for these fluctuations: the response time of the sensors, the controller's algorithm, but most important of all, the physical processes inside the intake port.

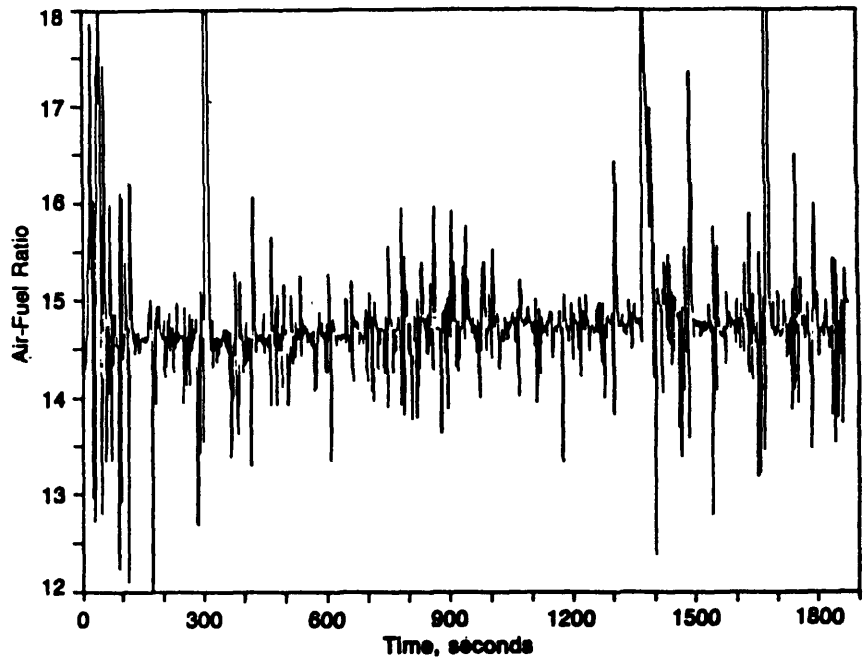

Figure 1.2.4 Typical air-fuel ratio excursions during the FTP cycle[1].

1.2.4 Air/fuel Transport

The most important factor affecting air-fuel ratio control during transients are the physical processes inside the intake port. Most engines today use a Multi-point fuel injection system, the system provides fuel to each cylinder by an individual injector. The injector is usually located approximately 10 cm up the intake port, aiming directly at the back of the intake valve. Figure 1.2.5 shows a schematic of a typical intake port in a modern engine.

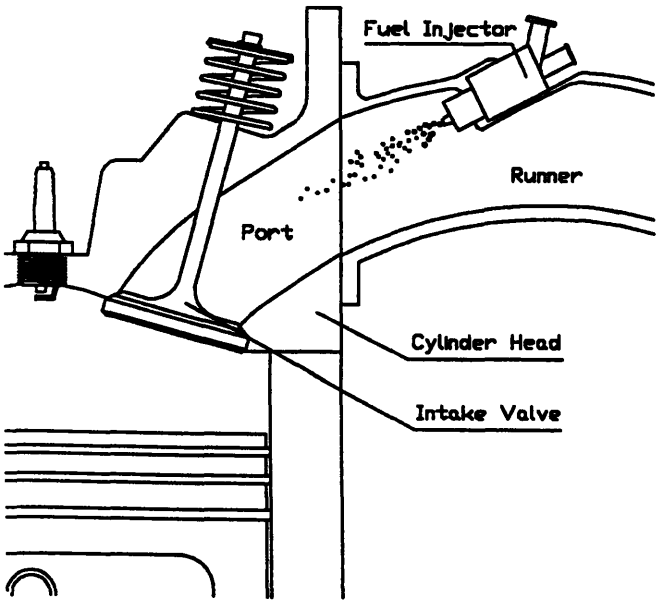

Figure 1.2.5 Schematic of a typical intake port in a modern engine.

The injector provides fuel metering and fuel atomization, which facilitates the evaporation of the fuel before entering the combustion chamber. After the fuel is injected, the liquid breaks up into fuel droplets. Some of the droplets evaporate in the air stream, others deposit on the port wall or the back of the intake valve. The droplets depositing on the port wall form a liquid film. This liquid film can evaporate or partially flow into the combustion chamber depending on operating conditions, such as speed, load and temperature. During transients, the manifold pressure and air flow rate change. These changes disrupt the dynamic equilibrium in the manifold. Mass transfer mechanisms such as diffusion and evaporation are altered, changing the size of the liquid film in the intake port. Although several computer models of the mass transfer processes inside the intake port have already presented[4,5,6,7], no model has yet been able to predict the effects of fuel composition on transient response. There are three major modes of fuel mass transfer into the cylinder:

1. Approximately adiabatic evaporation of fuel droplets in mid-air, and the subsequent

flow of fuel vapor into the cylinder during the intake flow.

2. Approximately isothermal evaporation from the liquid fuel film on the port wall and the subsequent flow of fuel vapor.
3. The liquid fuel film flow into the cylinder. The flow is driven by shear forces created by the air flow during the intake process.

1.3 Objective

The objective of this research is to relate the engine throttle transients behavior to fuel properties. A spark ignition engine has been tested with a set of 7 indolene/methanol blends. The experimental results will be interpreted via the fuel transport processes inside the intake manifold:

-The effects of fuel composition on the fuel film behavior.

-The effects of coolant temperature on the fuel film behavior.

-The physical processes governing fuel mass transfer through the intake port.

1.4 Methanol/Indolene Blends

Because methanol is an important choice as an alternative fuel, gasoline and methanol blends are used as the fuel for the experiments.

Methanol has advantages over gasoline in emissions characteristics. For example, methanol contains no sulfur, therefore does not create any sulfates during the combustion process. Other advantages include lower emissions of CO and Hydrocarbons. Methanol also has definite advantages from an engine designer's standpoint. For example, methanol has an antiknock index of 99, enabling the designers to increase the compression ratio, increasing the fuel conversion efficiency of the engine. These

advantages have boosted research in methanol, making it a feasible solution for meeting the up coming fuel economy and emission standards.

Table 1.1 Data on fuel Properties

Fuel	Methanol	Indolene
Chemical Formula	CH_3OH	$C_nH_{1.87n}$
Molecular Weight	32.04	≈110
Antiknock Index: (RON+MON)/2	99	87-84
Stoichiometric A/F Ratio	6.47	14.6
Q_{LHV} (MJ/kg)	20.0	44.0
Heat of Vaporization: kj/kg	1103	350

However, methanol has certain disadvantages that engineers still haven't been able to overcome. Methanol generates formaldehyde during combustion, a carcinogen and an ozone forming gas. Other disadvantages include a lower energy density and a lower stoichiometric air fuel ratio than gasoline. This means that an automobile would require twice as much methanol to travel the same distance compared to an automobile fueled with standard gasoline. Other problems arise due to methanol's corrosive properties. Fuel systems would need to be redesigned to be compatible with methanol. Another issue with methanol is safety. During combustion, methanol emits very little light. It would be a major safety hazard during accidents. Finally, due to its low stoichiometric air fuel ratio and its high heat of vaporization, methanol exhibits poor cold startability[8]. Table 1.1 compares the properties of methanol with the properties of indolene.

CHAPTER 2 -- EXPERIMENTAL APPARATUS

2.1 Engine and Dynamometer

The engine used in this research consists of a production spark ignition four stroke engine (Nissan SR20DE). The four cylinder engine has been modified to run on only one cylinder (cylinder #4). Figure 2.1 shows a schematic of the modifications done to the intake system. The intake runners to cylinder number 1, 2 , and 3 were blocked past the plenum chamber. Table 2.1 shows the engine specifications.

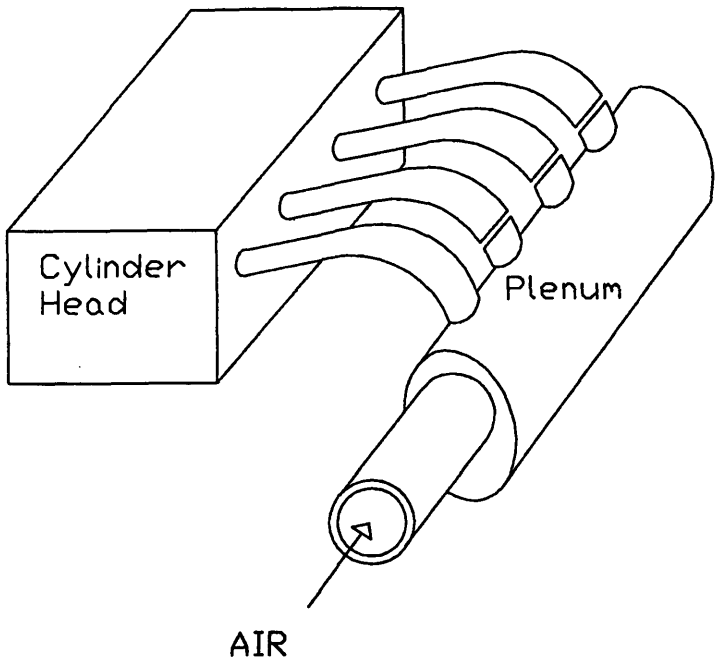

Figure 2.1 Schematic of the intake system

Table 2.1 Engine Specifications

Model	Nissan SR20DE
Type	4cylinders,4valves/ cylinder aluminum block and head.
Bore (mm)	86
Stroke (mm)	86
Clearance Volume (cm^3)	58.8
Displacement (cm^3)	1998
Compression Ratio	9.5:1
Valve Timing	IVO: 13 BTC IVC: 55 ABC EVO: 57 BBC EVC: 3 ATC

This engine has been in production since 1990 and is representative of today's state of the art engine design. The engine uses a port fuel injection system. Each injector forms 4 sprays, two sprays are aimed at the back of each intake valve, while the other two collide, enhancing mixing and evaporation. To isolate the effects of fuel composition on transients, the stock Electronic Control Unit has been replaced with a custom made open loop controller. The new controller gives us complete control over the injection pulse timing, injection duration, and the ignition timing. The engine coolant circuit has also been modified. The circuit is now connected to a heat exchanger running with city water. A gate valve provides the different levels of cooling necessary.

The engine is coupled to a dynamometer. The dynamometer has a three phase induction motor, a DC clutch and an eddy current brake. The motor is used to motor the engine during start up. The eddy current brake is used to control the engine speed during the experiment. The engine's crankshaft rotation is monitored via an inductive pick up. The sensor is hooked up to the dynamometer controller, whose main purpose is to keep the speed constant.

2.2 Sensors and Measurements

The air mass flow to the engine is monitored by a Kurz 505 laminar air flow element. The fuel flow to the engine is monitored by a digital oscilloscope, measuring the injection pulse duration (the injected volume per pulse as a function of pulse width has been calibrated separately by collecting the fuel injected in an ice-cooled cylinder). The exhaust gas equivalence ratio is measured with an Horiba lambda 110 controller and an oxygen sensor. The controller may be programmed to compensate for the fuel composition and the oxygen sensor sensitivity.

The cylinder pressure is measured with a Kistler 6051A piezoelectric pressure transducer. The output of the pressure transducer and the Horiba controller are converted to digital signals via a standard data acquisition card and stored on a hard disk. The clock of the acquisition card is triggered by the crank shaft encoder, giving one pulse every crank angle degrees (720 degrees per cycle). Therefore, one pressure point measurement is recorded every crank angle degree.

Thermocouples have been installed in the intake manifold, coolant system, oil pan, and exhaust pipe. These thermocouples assure us that the test conditions remain similar during each experiment.

2.3 Fuel and Air flow control

In order to simulate a throttle transient, both the air flow and the fuel flow to the engine must both be changed simultaneously. Figure 2.2 shows a schematic of the experimental set up. The throttle plate is connected to a pneumatic actuator, connected to a 40 psig air tank. The actuator is controlled by a 12 Volts DC three way valve. The system provides opening and closing of the throttle plate in the order of 30 to 40 msec.

The fuel injector is connected to a custom made injector driver. The injector driver amplifies TTL pulses to open and close the injector. The switch that controls the opening and closing of the throttle plate also controls which of the two pulse generators is used to control the injector driver. During accelerations the pneumatic actuator opens the throttle plate at the same time that the injection pulse is changed from T_1 to T_2. Each of the two pulse generators are triggered at 20 degrees before top dead center of the compression stroke (i.e. the injection is done once per cycle during closed valve).

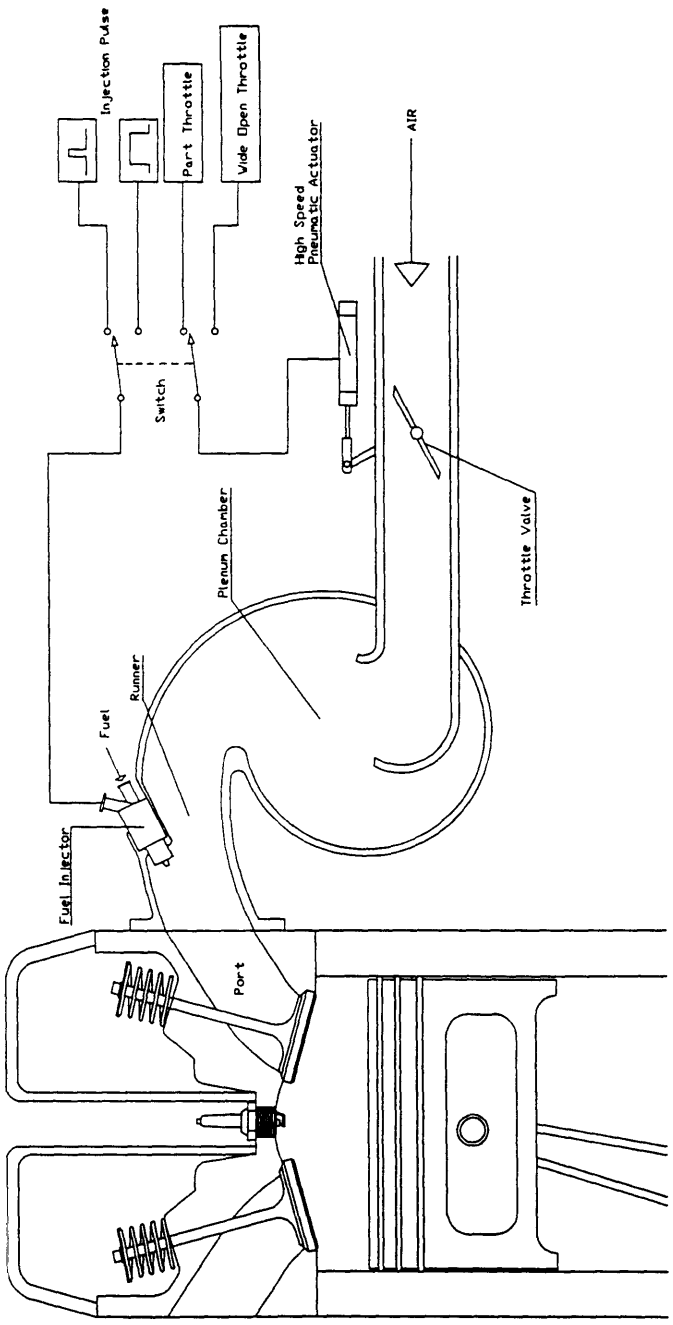

Figure 2.2 Experimental set up.

CHAPTER 3 -- EXPERIMENTAL PROCEDURE

3.1 Introduction

The following chapter presents the experimental test matrix as well as the complete data set recorded. The description will start with the fuel matrix chosen, followed by the test matrix, and finally by the testing procedure.

3.2 Fuel Matrix

The parameter that we control over each experiment is the fuel composition. We chose 7 fuel blends ranging from indolene to pure methanol: M0, M10, M25, M40, M60, M85, M100. The number following the M describes the volume percentage of methanol in an indolene fuel, i.e. M40 signifies 40% methanol, 60% indolene by volume. The blending of the fuels was done by refrigerating the fuels at 0°C first to minimize vapor losses.

3.3 Test Matrix

3.3.1 Operating Conditions

The experiments were designed to simulate a typical FTP driving cycle transient described in section 1.2.1. We chose to recreate a sudden throttle opening from a part throttle condition, followed by a sudden closing of the throttle back to the original position. Each experiment can be broken down into two sections: the up transient

(starting from part throttle at steady state finishing at steady state at Wide Open Throttle (WOT)), and the down transient (starting from steady state at WOT finishing at steady state at part throttle). All the experiments were performed at a constant speed: 1800 Rpm. The intake pressures were 0.7 bar for the part throttle case and 1.0 bar for the wide open throttle case. Other parameters that were kept constant throughout each experiment include the coolant temperature, the ignition timing, and the injector timing.

3.3.2 Control Parameters

Each fuel was tested under 6 conditions. To simulate the typical response of the engine's ECU three different levels of enrichment were used during wide open throttle: $\lambda_{t1}= 1.0$, $\lambda_{t2}=0.9$, $\lambda_{t3}=0.8$. These levels of enrichment are referred to as $\lambda_{target}(\lambda_t)$. The second parameter changed was the coolant temperature. All the experiments were performed under two coolant temperatures: $T_1=40^oC$, $T_2=80^oC$. The two temperatures chosen simulate a warming up condition and a fully warmed up condition. Table 3.1 shows the test matrix.

Table 3.1 Test Matrix

	T=40°C	T=40°C	T=40°C	T=80°C	T=80°C	T=80°C
M0-M100	$\lambda_{target}= 1.0$	$\lambda_{target}= 0.9$	$\lambda_{target}= 0.8$	$\lambda_{target}= 1.0$	$\lambda_{target}= 0.9$	$\lambda_{target}= 0.8$

The fuel flow to the engine at WOT was predetermined from the steady state fuel flow. For example, in the case where $\lambda_t=0.9$, the engine was ran at WOT with $\lambda=0.9$ and the fuel injection pulse was recorded. This injection pulse became T_2 in the experiment and remained fixed during the rest of the experiment. Figure 3.1 shows the air and fuel mass

flow to the engine during one of the experiments.

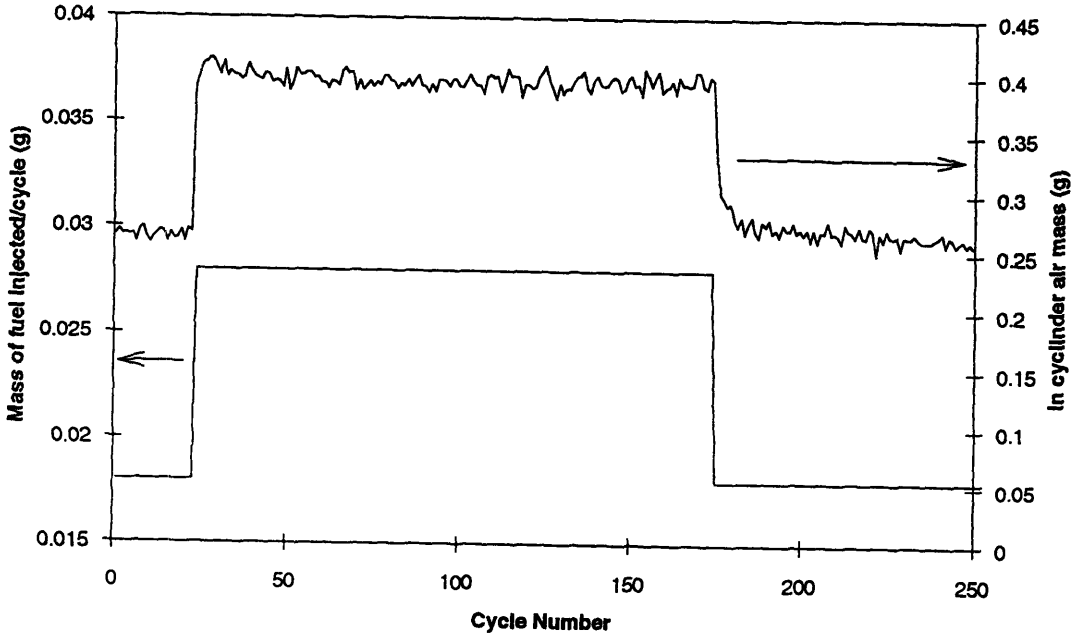

Figure 3.1 Air and fuel flow rate during the experiment

3.4 Test Procedure

All the experiments were performed at ambient temperature (about 22^{o} C). Prior to the start of the experiment, the engine was warmed up, and the MBT timing was recorded for the part throttle and WOT condition. The ignition timing was then set at the average of the two MBT points. In all the experiments the difference between the two MBT points was less than 4 degrees. The engine was run stoichiometric at 1800 Rpm at part throttle (intake pressure = 0.7 bar) for 15 minutes. The fuel injection pulse width was recorded and entered as T_1. The engine was then run 3 minutes at WOT (Pi = 1 bar) at the pre-selected enrichment level. The fuel injection pulse width was recorded and entered as T_2. The intake pressure was returned to 0.7 bar and the coolant system adjusted to maintain the selected temperature. Then the data acquisition system was started. Ten seconds later, the throttle control switch was turned on for 1 minute. The

switch was then returned to the part throttle position. The data acquisition system was turned off once the engine returned to steady state.

CHAPTER 4 -- DATA INTERPRETATION

4.1 Introduction

The main goal of the data analysis is to account for the air and fuel flow during each cycle. Using the data recorded, such as the lambda meter output, and the in-cylinder pressure measurement, expressions for the mass of fuel and air burned can be calculated.

4.2 Air and Fuel Flow

4.2.1 Air Flow

During transients, the air mass flow to the engine changes rapidly. Because the engine has been modified as a single cylinder engine, the pulsating air flow makes it difficult for conventional instruments to accurately measure the air flow on a cycle by cycle basis. To obtain an accurate measurement of the air flow, the air flow rate to the engine was mapped under steady state conditions as a function of compression pressure before spark (1 degree before ignition). Figure 4.1 shows the change of compression pressure for different air flow rates to the engine under several loads and equivalence ratios. Figure 4.1 indicates that the mapping is linear, and independent of the equivalence ratio. However, depending on engine temperature and ambient conditions, the slope of the line shown on figure 4.1 can change. Therefore, by using the steady state air flow measurements from the laminar air flow element at the steady-state part throttle and the wide open throttle conditions, we can find two points determining the equation of the line for each experiment. Once the equation for the line is known, the

compression pressure before spark is used to find the mass of air inside the cylinder during the transient.

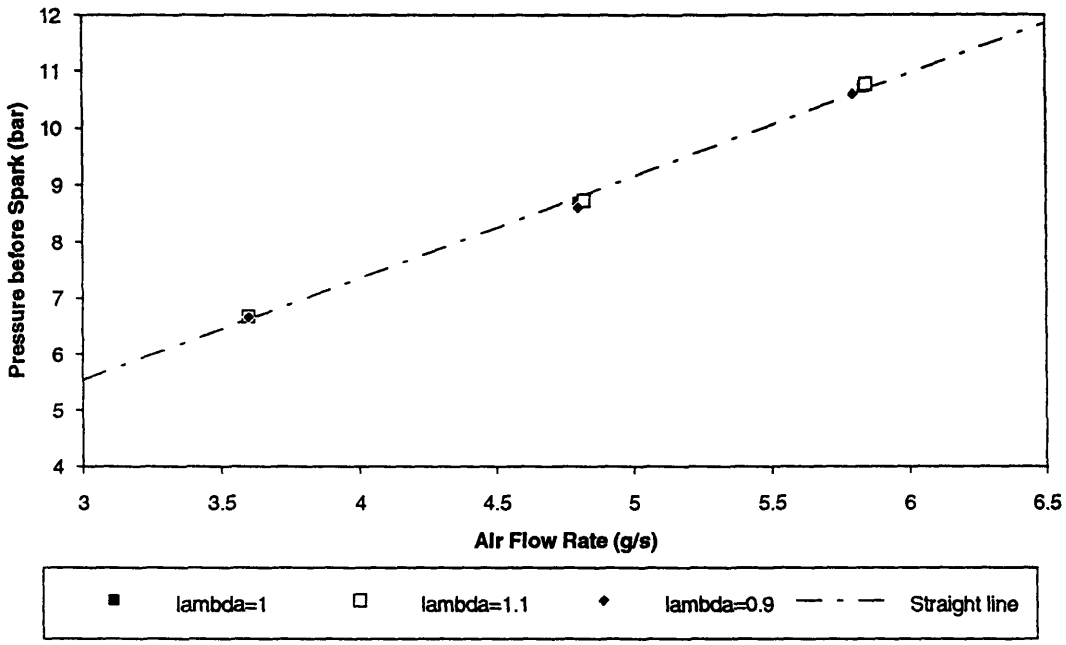

Figure 4.1 Mapping of the air flow as a function of compression pressure.

4.2.2 Fuel Flow

In order to obtain a mass balance of the fuel flow, two fuel flows are needed: the mass of fuel injected per cycle, and the mass of fuel burned during each cycle. The mass of fuel burned per cycle could be directly calculated from the lambda sensor output. However, it has been shown[9] that lambda sensors have response times on the order of 100 msec, which is inadequate for calculations on a cycle by cycle basis. Therefore a new method was developed, using the Gross Indicated Mean Effective Pressure (Gimep) and η_{ig} (the gross indicated fuel conversion efficiency). The Gimep is a measurement of the work done by the engine during the compression and the expansion stroke divided by

the cylinder volume. The Gimep can be calculated by integrating the cylinder pressure over the displacement volume.

$$Gimep = \frac{\int PdV}{V_d} \text{ (eq.1)}$$

The Gimep can also be related to the mass of fuel burned using η_{ig}.

$$Gimep = \frac{\eta_{fig} \times M_{burned}}{Q_{HV}} \text{ (eq.2)}$$

The engine was mapped under several operating condition to measure η_{ig}. Figure 4.2 shows η_{ig} as a function of λ and GIMEP.

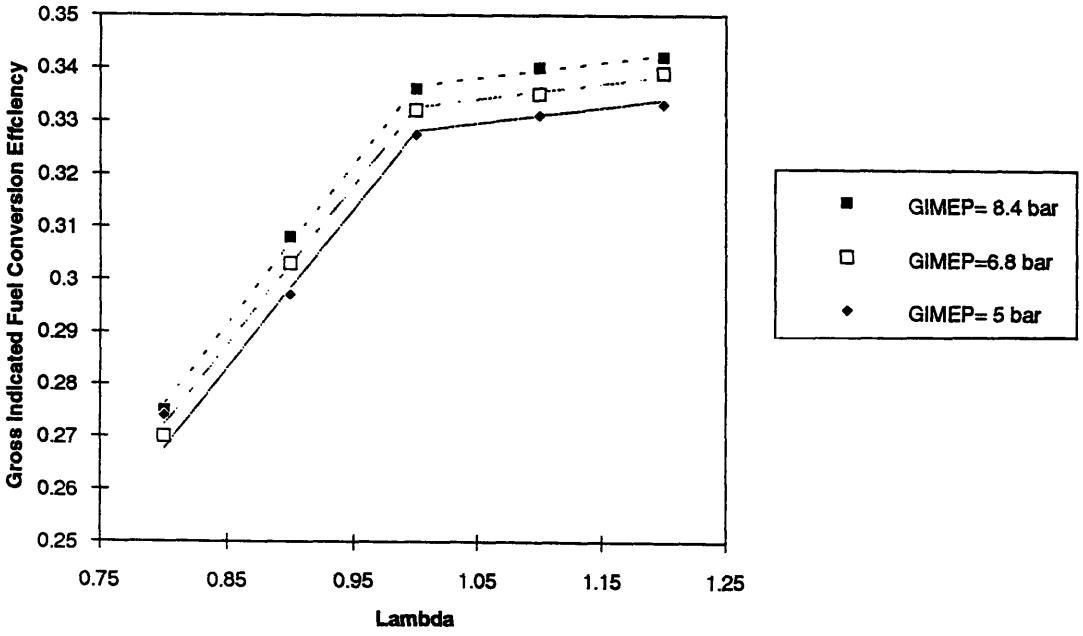

Figure 4.2 Mapping of the gross indicated fuel conversion efficiency.

The gross indicated fuel conversion efficiency is linear inside two distinct regions: the fuel rich region (λ<1.0), and the lean region (λ >1.0). Therefore the efficiency was mapped linearly as a function of λ for these two conditions. By using the lambda meter output and the Gimep measured, the fuel conversion efficiency can be calculated for each cycle.

Another important aspect of the fuel conversion efficiency is its dependence on the ignition timing. The timing must remain at MBT to maintain the fuel conversion efficiency optimum. Figure 4.3 shows varying fuel conversion efficiencies for different ignition timings. Although the MBT timing does not change by more than four degrees between the two steady state conditions (at Wide Open Throttle and at part throttle), lean and rich burning cycles during the transient significantly change the flame speed, changing the MBT timing, in turn changing the fuel conversion efficiency. However, it is possible to measure the amount of retard or advance based on the peak pressure angle. Therefore the peak pressure angle (θ_{pp}) was included to compensate for the change of MBT timing during the experiment.

$$\eta_{fig} = \frac{C_1 \times \lambda + C_2 \times Gimep + C_3}{(1 + (\theta_{pp} - \theta_{MBT})^2 \times C_4)} \text{(eq.3)}$$

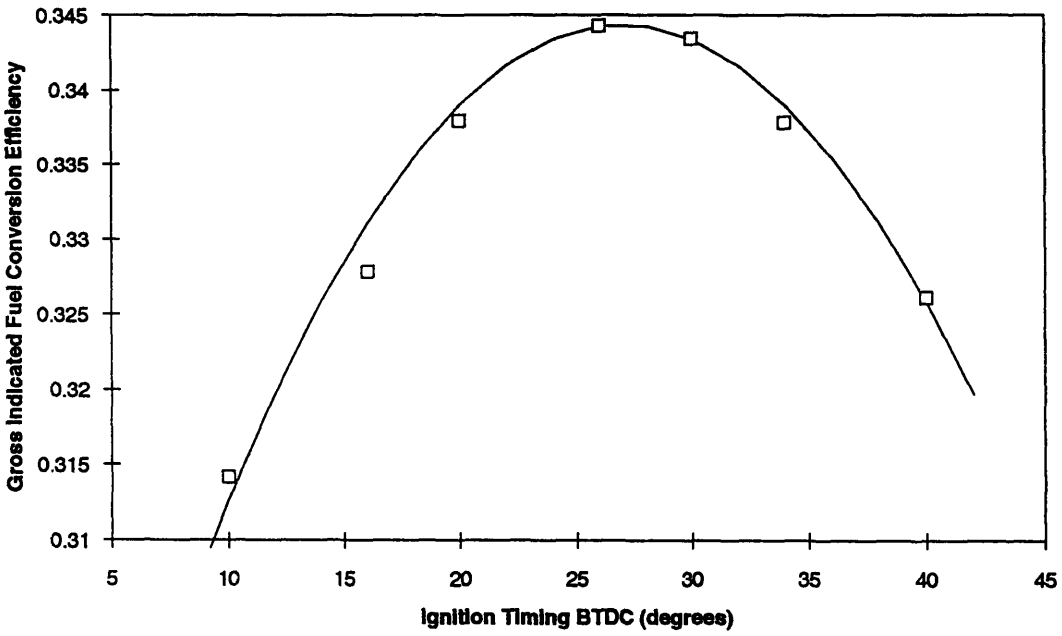

Figure 4.3 Gross indicated fuel conversion efficiency versus ignition timing.

Finally, by grouping these three engine maps together, the mass of fuel burned during each cycle can be calculated from the following measurements:

-Gross Indicated Mean Effective Pressure

-Relative air fuel ratio (λ)

-Peak Pressure Angle

The second fuel flow measurement necessary for the analysis is the amount of fuel injected. This volume can be directly measured from the pulse width (T1,T2) driving the injector. The pulse width was recorded with a digital oscilloscope during each experiment. Using the injector calibration curve the volume of fuel injected during each cycle can be calculated.

4.3 Data Analysis

4.3.1 Methodology

From the data recorded it is possible to calculate the mass of fuel burned and the mass of fuel injected during each cycle. With these measurements it is possible to calculate "the mass of fuel unaccounted for", the difference between the mass of fuel injected and the mass of fuel burned during each cycle. By summing up the mass of fuel unaccounted for over each cycle, we obtain the cumulative mass of fuel unaccounted for (C_{mf}). By assuming that all of the fuel injected is either burned inside the combustion chamber or stored inside the port in the form of a liquid film, we can interpret the cumulative mass of fuel unaccounted as a measure of the **change** in liquid film mass in the port.

$$Cmf = \sum_{i=1}^{i=n} \left[M_{inject_i} - M_{burned_i} \right] \quad \text{(eq.4)}$$

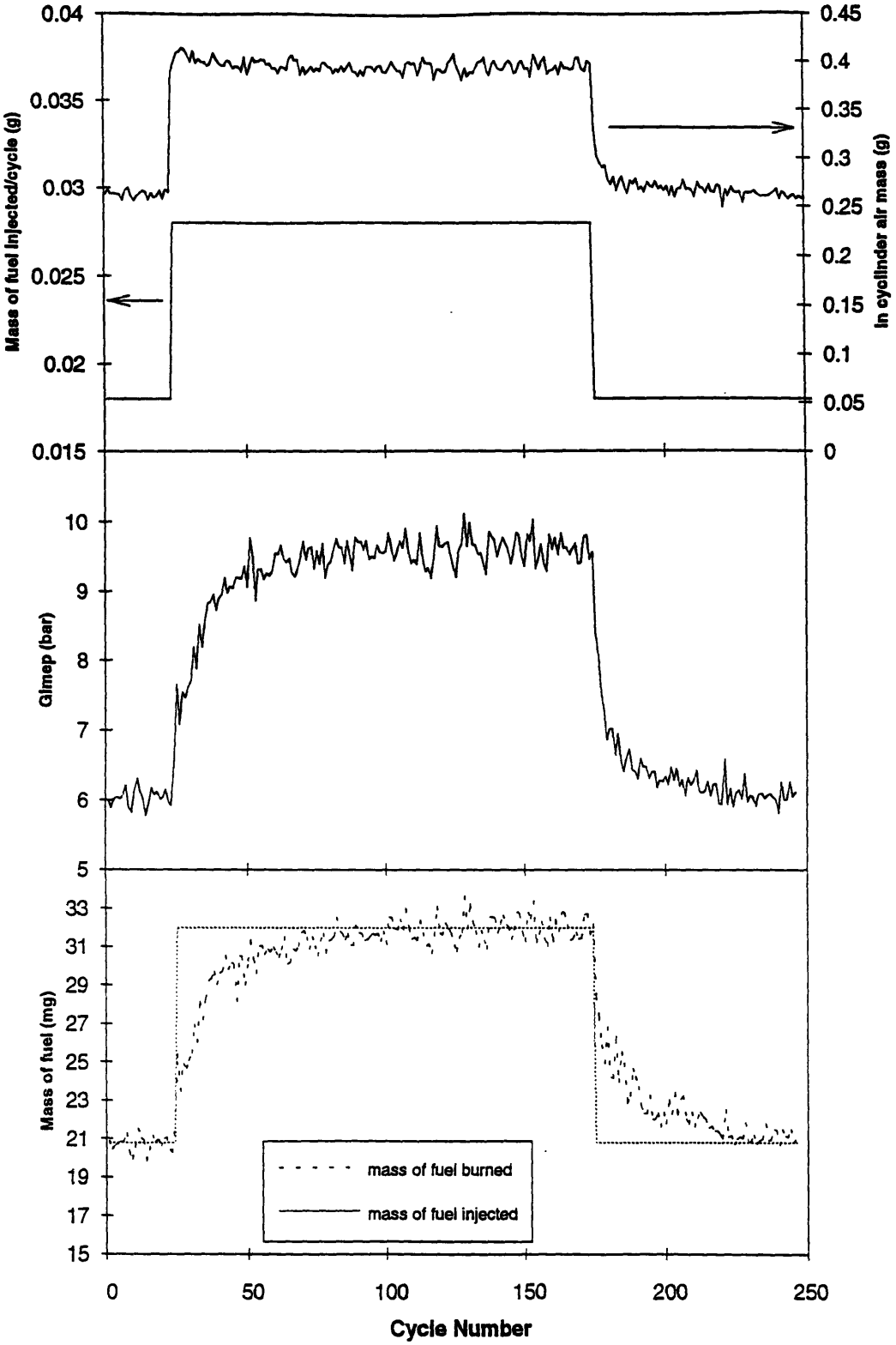

Figure 4.4 The first three steps in the Analysis for M0.

Figure 4.4 shows the different steps of the analysis for pure indolene. The first graph shows the fuel flow and the air flow to the engine obtained from the calibration showed on figure 4.1. The second graph shows the gross indicated mean effective pressure for each cycle, obtained from equation 1. The third graph compares the fuel mass burned and the fuel mass injected during each cycle, obtained from equation 2. Finally using equation 3 the "cumulative mass of fuel unaccounted for" is obtained, shown in figure 4.5.

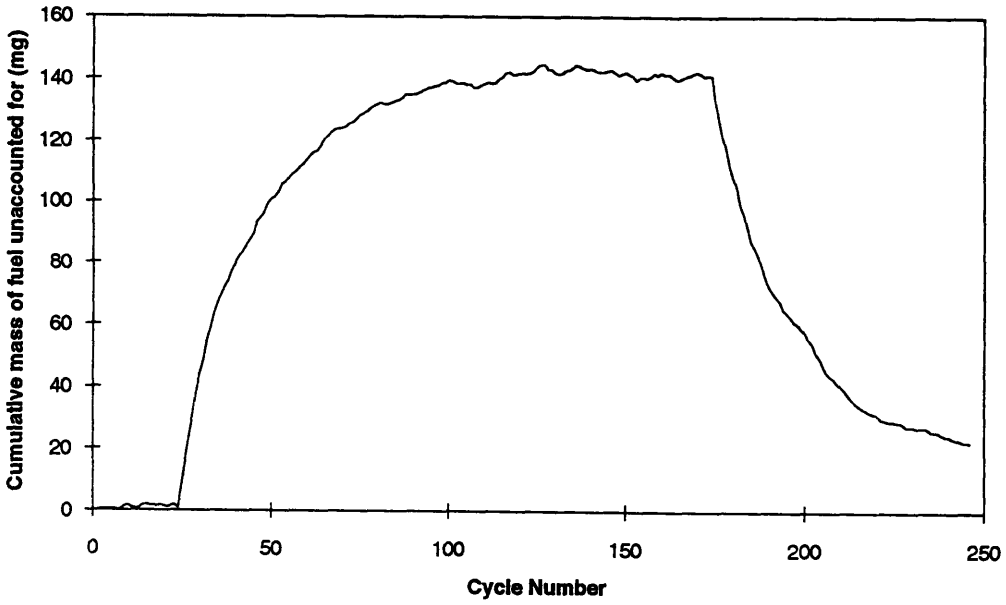

Figure 4.5 The cumulative mass of fuel unaccounted for for M0.

4.3.2 Accuracy of the mass of fuel unaccounted for

Section 4.3 described the procedure used in the analysis of the data . It is important to explain some of the difficulties encountered during the processing of the data.

Using the engine map described in section 4.2, the analysis calculated the fuel mass and the air mass inside the cylinder during each cycle. Problems arose when

redundant parameters were calculated and measured. For example, at the end of the up transient (just before closing the throttle), the engine is assumed to be at steady state since the lambda meter reading was stable. Therefore, by applying a conservation of mass inside the port, the mass of fuel burned per cycle should be equal to the mass of fuel injected per cycle. However, due to errors generated by the inaccuracy of the instruments, as well as errors in the engine map, the mass of fuel burned per cycle was within ±1% of the measured mass of fuel injected per cycle. When calculating the cumulative mass of fuel unaccounted for, the error was cumulated over about 150 cycles, amplifying the error. Figure 4.6 and 4.7 illustrate this example. Sample 3 plotted on figure 4.7 corresponds to a negative one percent error, whereas sample 2 corresponds to a positive one percent error. In order to avoid such an error, an algorithm was developed.

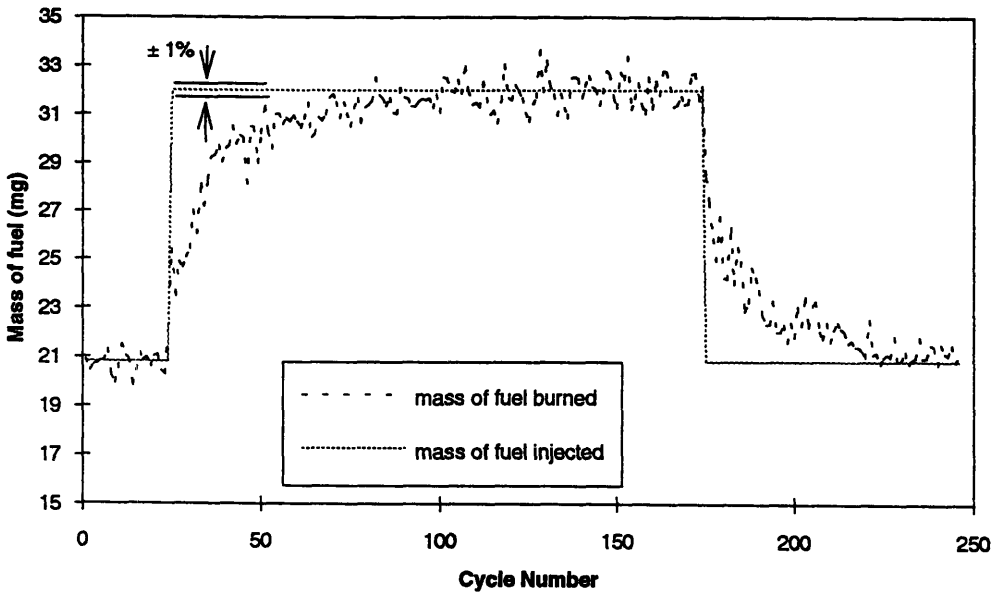

Figure 4.6 Adjustment of the mass of fuel injected at wide open throttle.

By assuming that the engine is at steady state before closing the throttle, the mass of fuel burned must be constant over the last few cycles at wide open throttle. Therefore, the slope of the cumulative mass of **fuel burned** must be equal to the mass of fuel injected at wide open throttle.

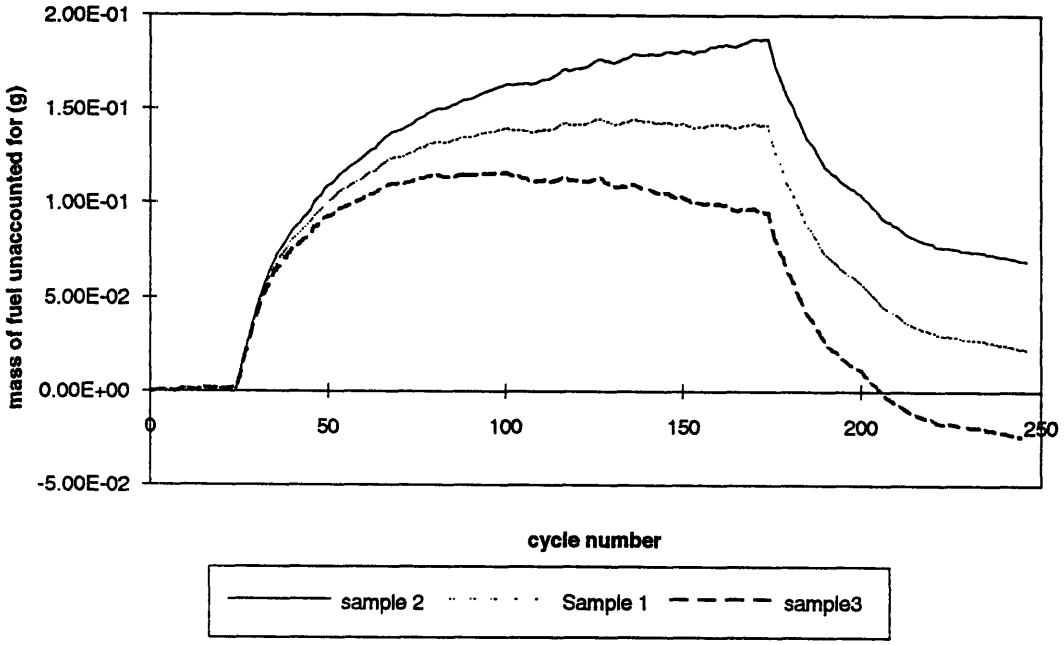

Figure 4.7 Effect of measurement error on the cumulative mass of fuel unaccounted for.

Figure 4.8 shows the straight line and the slope of the line before closing the throttle. Since the calculated mass of fuel burned was within ±1% of the measured fuel mass injected, the fuel mass injected at wide open throttle was calculated from the slope of the line for each experiment.

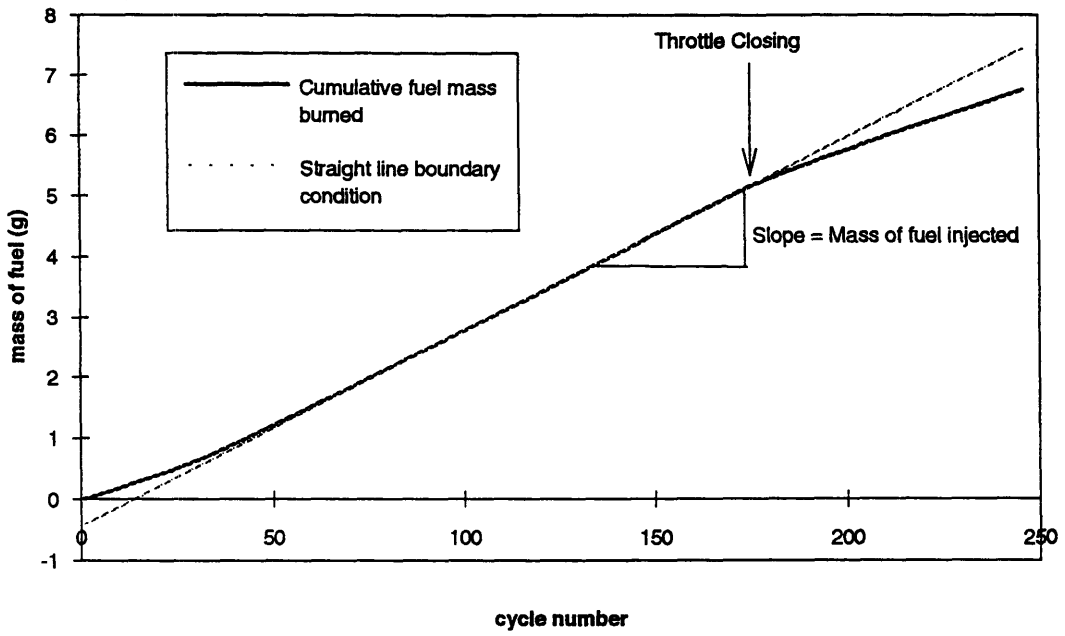

Figure 4.8 Obtaining the mass of fuel injected at wide open throttle from the cumulative mass of fuel burned.

4.4 Results

From the data it is possible to calculate the cumulative mass of fuel unaccounted for during each cycle. Although it is not precisely known as to where does this fuel goes (e.g. via the cylinder wall to the oil sump), a substantial amount of this fuel represents the change in mass of the liquid film stored inside the intake port. Appendix A contains the detailed data for each experiment (the air flow rate, fuel flow rate, Gimep, and exhaust relative air-fuel ratio). Appendix B contains the graphs of the cumulative fuel mass unaccounted for. The cumulative mass of fuel unaccounted for is plotted with a best fit curve using two time constants, one for the up transient and another for the down transient.

For the up transient: $C_{mf} = a \times \left(1 - e^{\frac{t}{\tau_1}}\right)$

For the down transient: $C_{mf} = a \times e^{\frac{t}{\tau 2}}$

Constant a is a measure of the change in fuel film mass between the wide open throttle condition and the part throttle condition. This constant was calculated for every experiment.

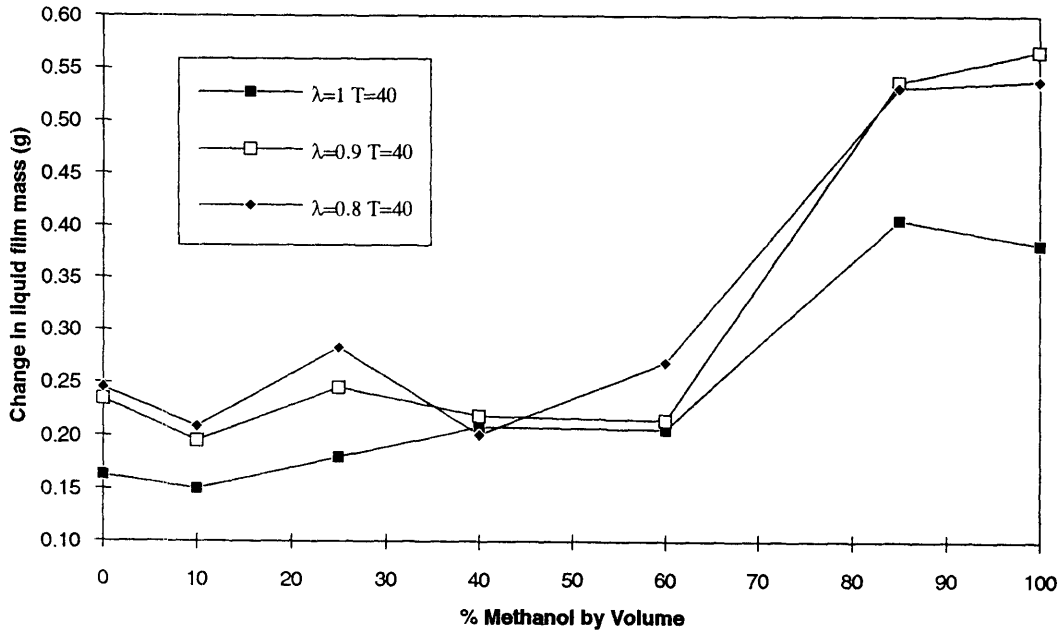

Figure 4.9 Change in fuel film mass for the low temperature experiment.

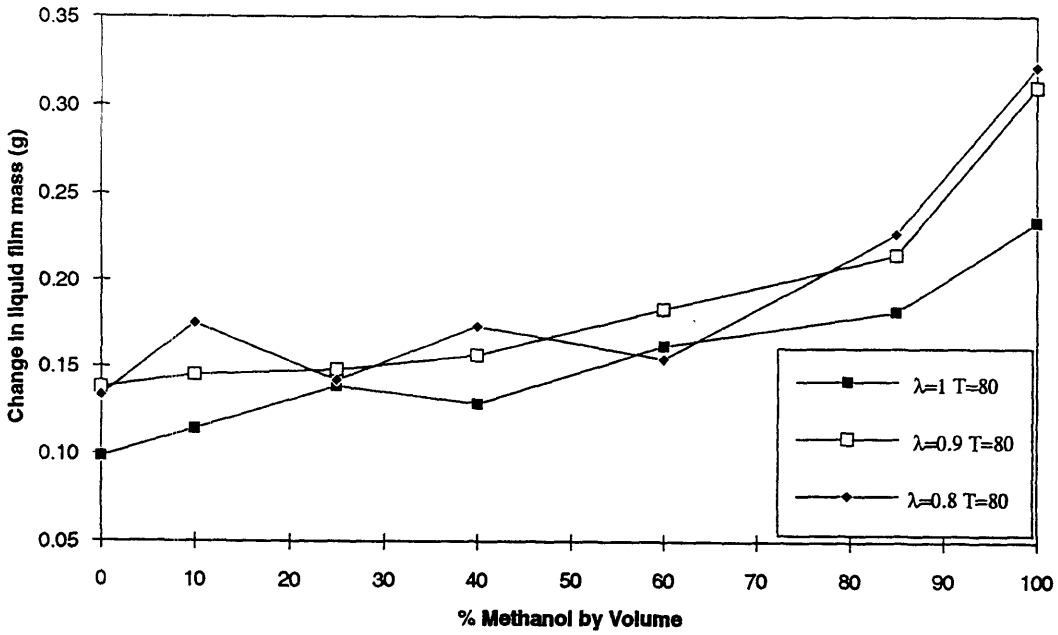

Figure 4.10 Change in fuel film mass for the high temperature experiment.

Figure 4.9, and figure 4.10 show the value of constant a for the cold and the hot coolant temperature experiments. For reference, the fuel mass injected per cycle at WOT at λ =1.0 for M0 is 0.031 gram. Figure 4.11, 4.12, 4.13 and 4.14 show the value of time constants τ_1 and τ_2 for the cold and the hot coolant temperature experiments.

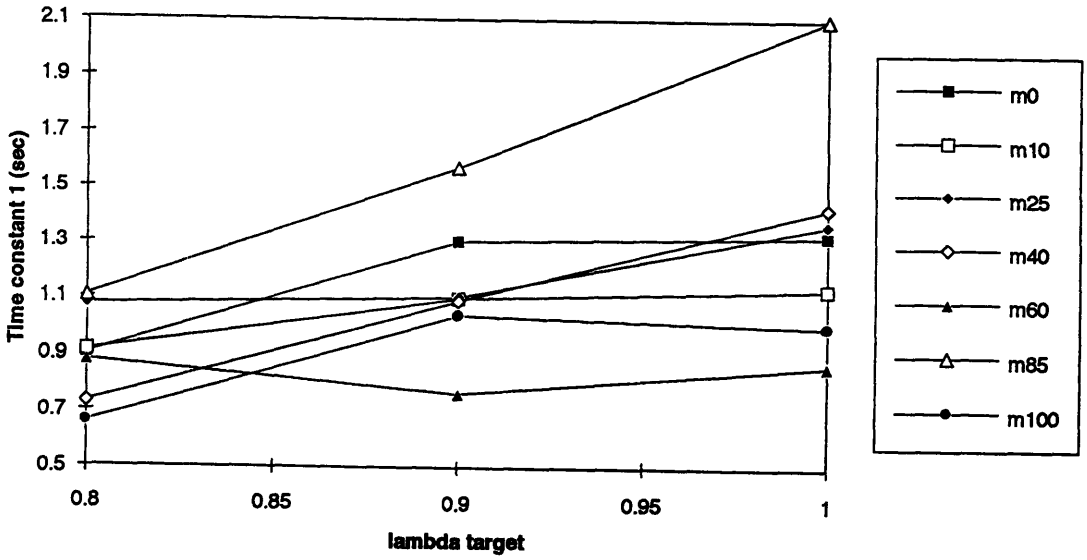

Figure 4.11 Time constant τ_1 for the cold coolant temperature experiment.

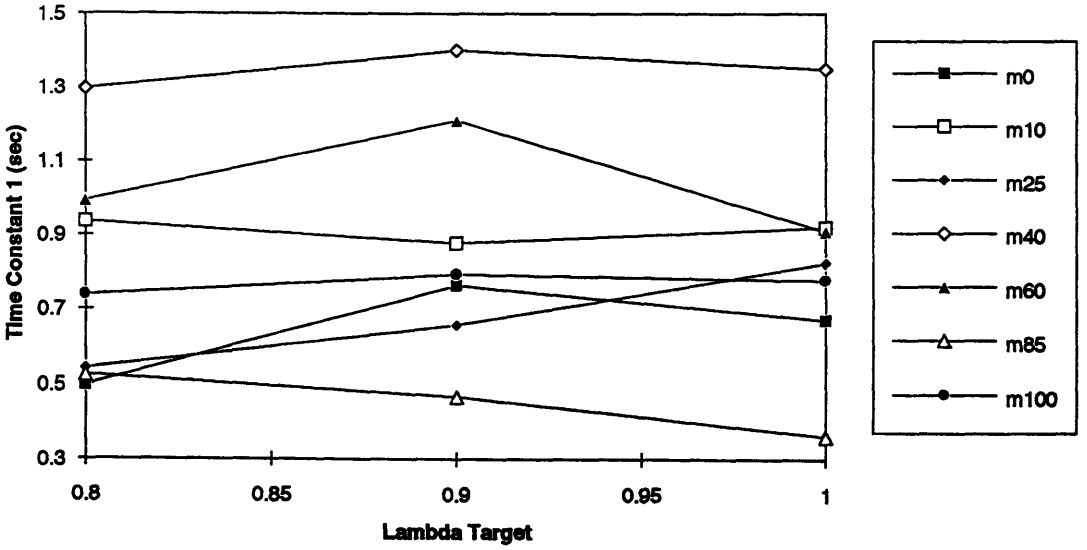

Figure 4.12 Time Constant τ_1 for the hot coolant temperature experiment.

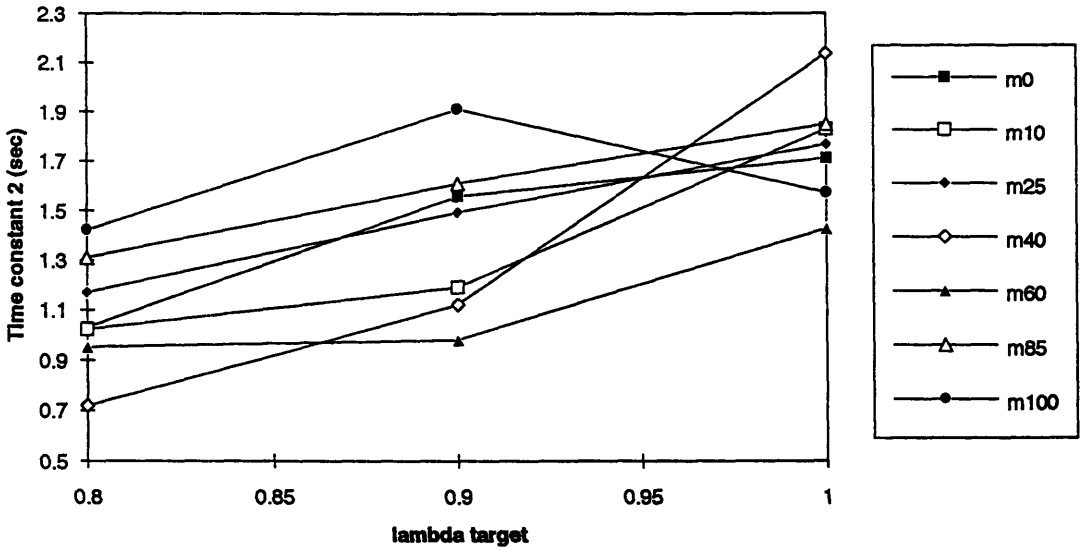

Figure 4.13 Time Constant τ_2 for the cold coolant temperature experiment.

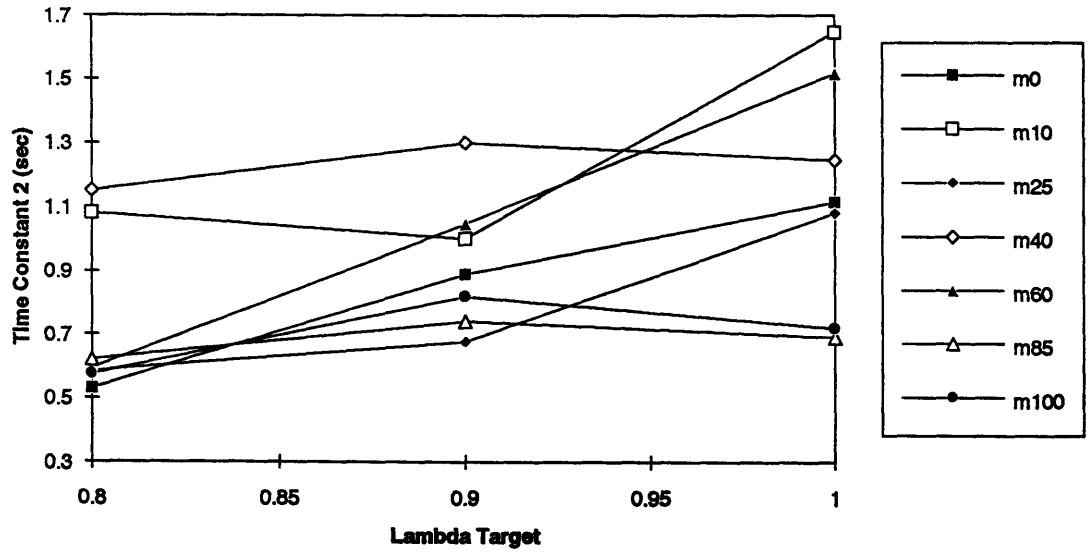

Figure 4.14 Time constant τ_2 for the hot coolant temperature experiment.

4.5 Fuel effects on driveability

In section 1.1, we mentioned that one of the major motivations for starting this research was to understand the effects of fuel composition on driveability ratings such as hesitation and stumble. Using the data from the throttle transient experiment, it is possible to quantify the transient response time of each fuel under the different test conditions. These response times may be interpreted as a measure of stumble and hesitation.

A standard method already used in the testing of fuels is the measurement of the response time of the torque curve of the engine (in our case the Gimep curve)[10]. Figure 4.15 shows a sample Gimep curve to illustrate the calculation. The response time is defined here as the rise time between 0% and 90% of the final Gimep value at wide open throttle.

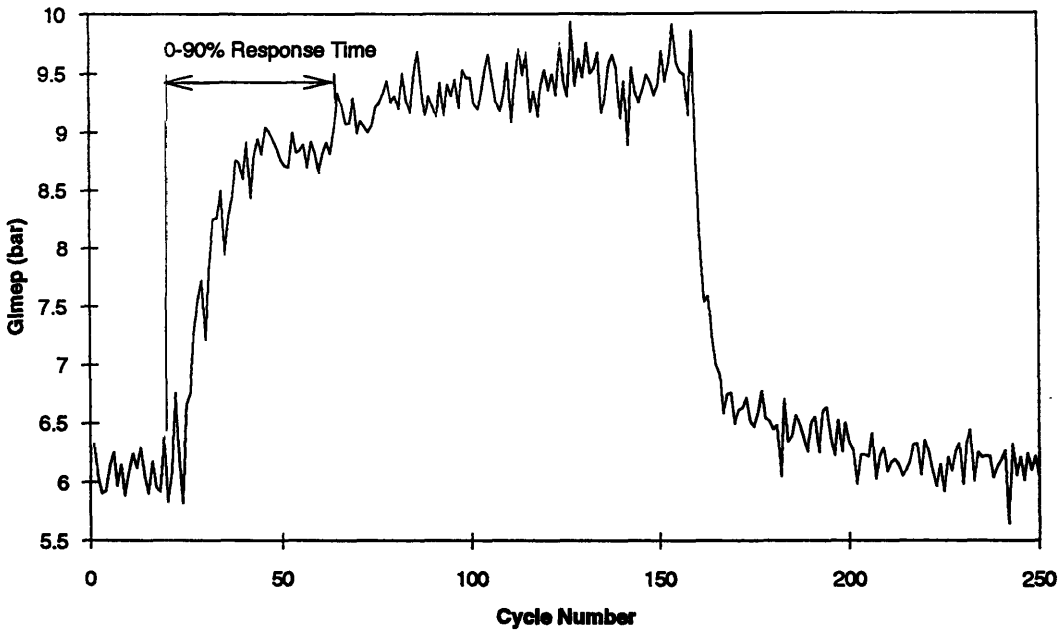

Figure 4.15 Sample Gimep curve with the 0-90% response time.

The response time was calculated for each fuel under the two coolant temperatures. The response times are showed in figures 4.16 and 4.17 as a function of methanol content. Figures 4.18 and 4.19 show the effect of lambda target on the response time.

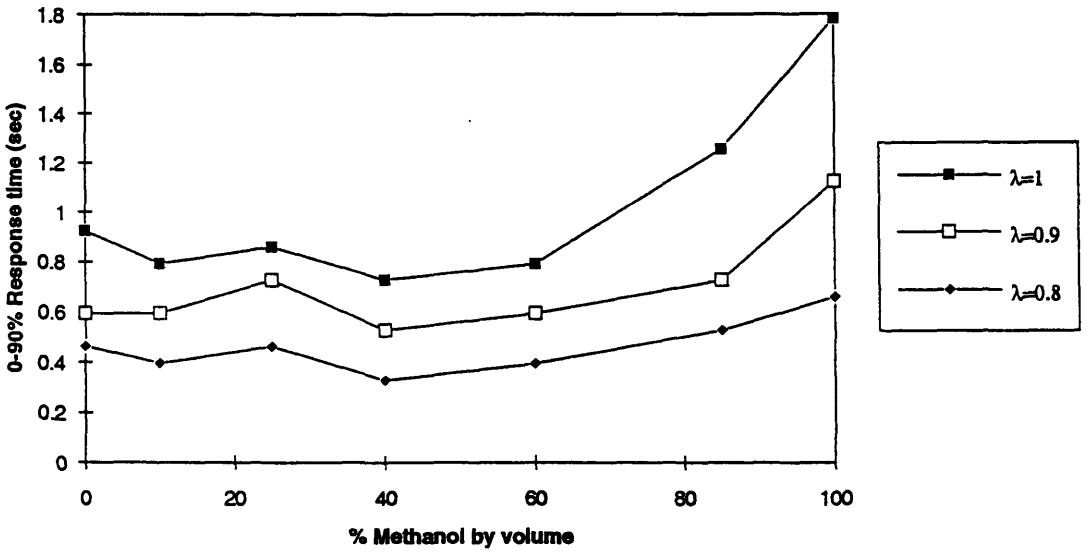

Figure 4.16 Effect of methanol content on the response time under cold coolant condition (T=40° C).

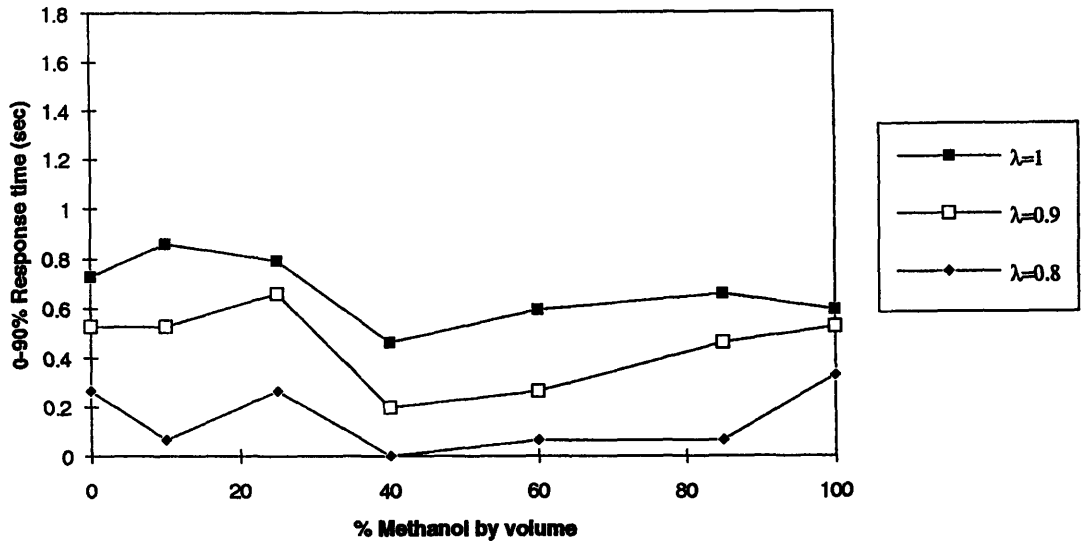

Figure 4.17 Effect of methanol content on the response time under hot coolant condition (T=80°C).

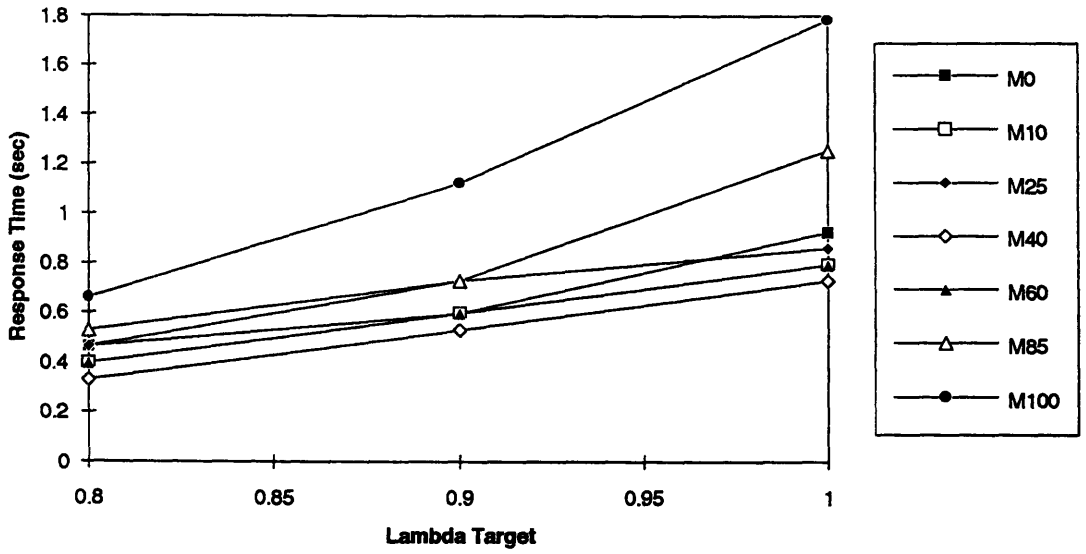

Figure 4.18 Effect of lambda target on the response time under cold coolant condition (T=40°C).

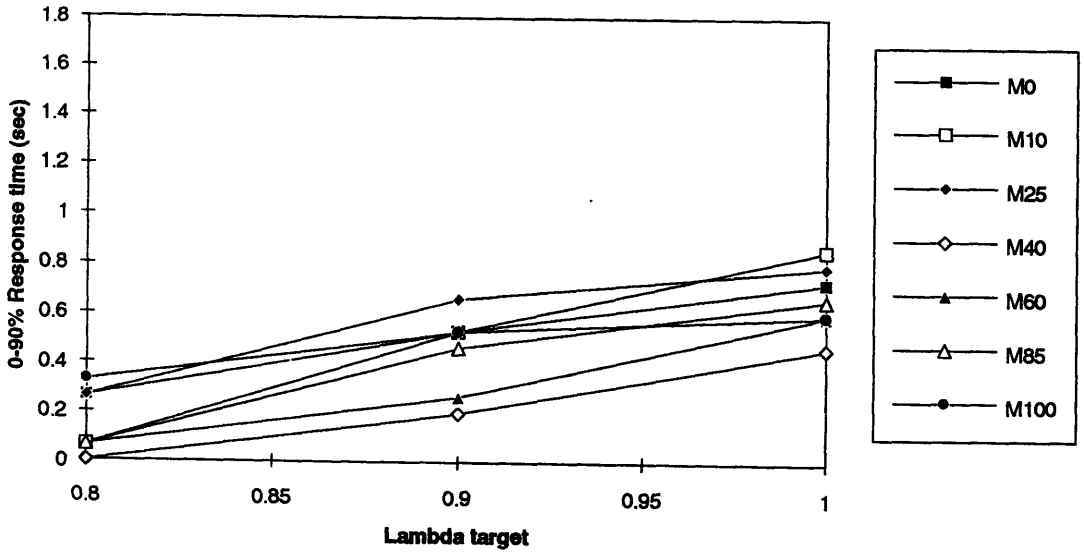

Figure 4.19 Effect of lambda target on the response time under hot coolant condition (T=80°C).

Figure 4.16 shows that under a coolant temperature of 40°C, the response time increases sharply between M60 and M100. This sharp increase of about 225% is not as sharp for the richer case. For λ_{target}=0.9, the increase is about 190% ,and for λ_{target}=0.8, the

increase is down to 170%. Figure 4.18 shows that although the enrichment decreases the response time by about 50% for M0 through M60, it is more noticeable for M85 and M100 where the response time decreases by 58% and 63%.

Under a coolant temperature of 80°C , the response time decreases between M25 and M40 by about 40%. The response time remains constant for the other fuels from M40 through M100.

CHAPTER 5 -- MODEL AND DISCUSSION

5.1 Discussion

Results in section 4.3 showed the absolute effect of methanol content on the change in liquid film mass during the transient. The relative effect of the methanol content on the change of film mass is illustrated in figure 5.1 and 5.2 In these two figures, the change in film mass for each fuel was normalized with the change in film mass for indolene under the same test conditions. These two graphs show that the enrichment used for λ_{target}=0.9, and λ_{target}=0.8 did not change the relative increase of liquid film mass between the methanol blends and the indolene fuel. It is also important to note that in the cold and the hot coolant conditions, the relative change in liquid film mass between methanol (M100) and indolene (M0) was about the same, in the order of 220 %.

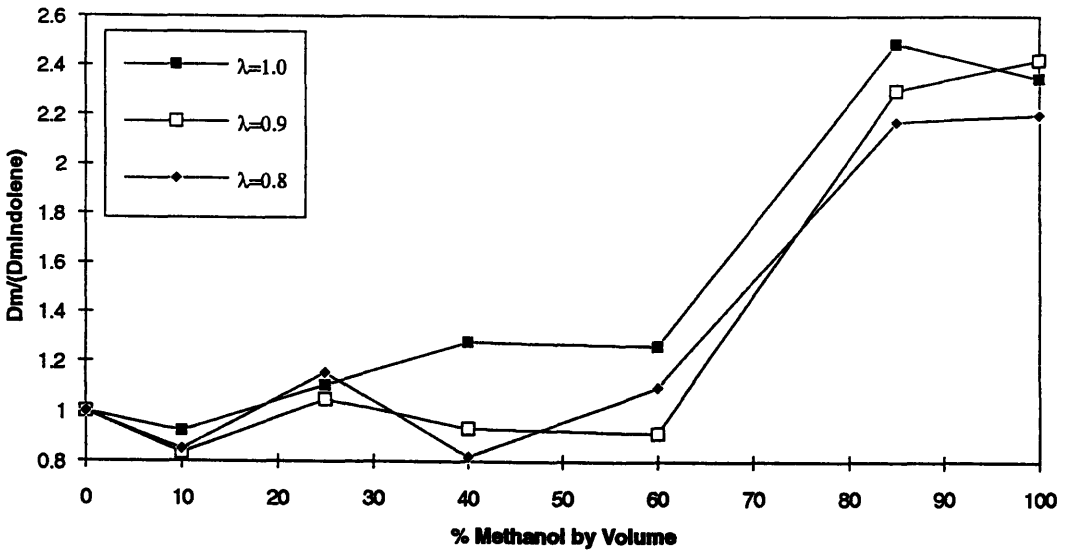

Figure 5.1 The relative effect of methanol content on the change in liquid film mass under cold coolant conditions.

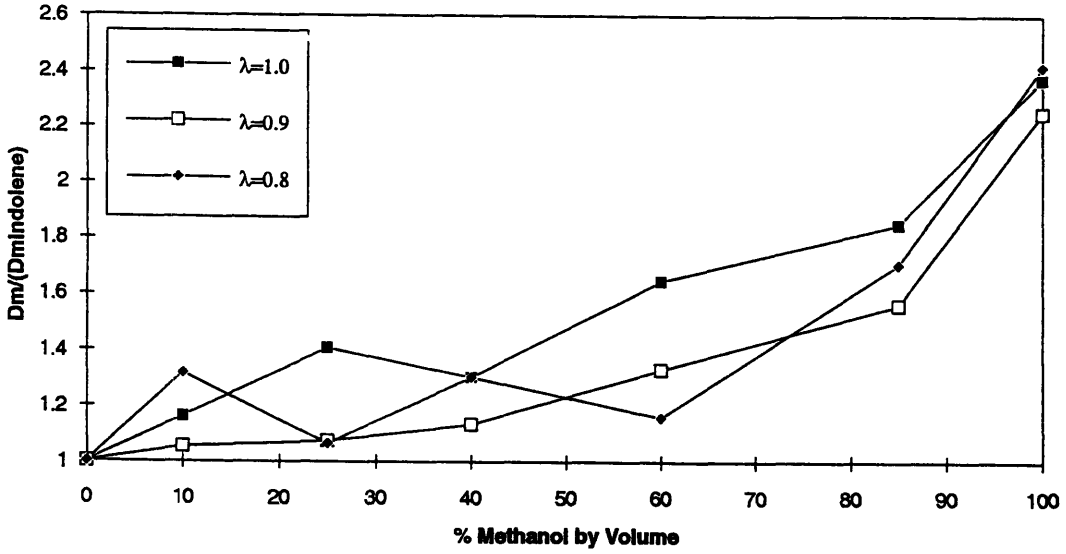

Figure 5.2 The relative effect of methanol content on the change in liquid film mass under hot coolant conditions.

There are many physical parameters that affect the transient response of a spark ignition engine. The mixture preparation process of the liquid film is dependent on the latent heat of vaporization, the fuel's distillation curve, the temperature of the intake manifold, the intake pressure, and the fuel's stoichiometric fuel-air ratio requirement. This last parameter has two effects on the mixture preparation process. As the stoichiometric requirement increases, the total energy required to vaporize the fuel increases accordingly [11]. The second effect is the possible change of the liquid film pattern inside the port. Since the injector is aimed directly at the back of the intake valves, the wetted surface area remains the same from cycle to cycle. Under steady state conditions, as the fuel evaporates, the film's surface area decreases, and then increases back to its original size at the time of the next injection. If the fuel used has a high stoichiometric requirement, then there will be twice as much fuel over the same surface area right after the injection process. Therefore, the liquid film thickness is likely to

scale with the stoichiometric requirement of the fuel used. As the film thickness increases, the mass transfer processes inside the manifold are changed. Because the liquid film flow to the combustion chamber is driven by surface shear forces of the intake charge, the film flow to the combustion chamber scales with the fuel film thickness :th. Equations 5 and 6 relate the shear stress to the film flow rate (assuming that the liquid film covers half of the port diameter) :

$$\left[\frac{dM}{dt}\right] = \frac{\pi \times dia \times th \times \rho_f \times V_f}{2} \quad \text{(eq.5)}$$

$$\tau_f = \frac{\mu_f \times V_f}{th} = f(\rho_m, \nu_m, U_m, R_m) \quad \text{(eq.6)}$$

Notation:

dia: manifold diameter

th: Fuel film thickness

ρ: density

V: Surface velocity of the film

μ: Dynamic Viscosity

ν: Kinematic viscosity

U: mean velocity

R: Specific gas constant

Subscripts:

f: fuel film

m: air-fuel mixture

By grouping equation 5 and 6 we can see that the fuel film flow rate to the combustion chamber scales with the square of the fuel film thickness: $\frac{dM}{dt} \propto (th)^2$

In a first attempt to explain the change of liquid film mass inside the intake port, we looked at the correlation between the change of liquid film mass and the mass of fuel injected per cycle.

Assuming that the absolute liquid film mass inside the intake port scaled with the mass of fuel injected during each cycle: $M_{film} \propto C \times M_{inj}$, the change in liquid film to the change in mass of fuel injected: $C_{mf} \propto C_1 \times [Minj]_{1.0bar} - C_2 \times [Minj]_{0.7barr}$.

For these transient experiments the correlation coefficient was poor when the coefficients C_1 and C_2 were both set equal to one. Figure 5.3 and 5.4 show the correlation under hot and cold coolant conditions. However, much better correlation was found when C_2 was neglected (C_2=0). Figure 5.5 show the correlation between the change of liquid film mass and the mass of fuel injected at wide open throttle. In this case correlation coefficients: r=0.94 (@ T=80°C), and r=0.91 (@ T=40°C) were found.

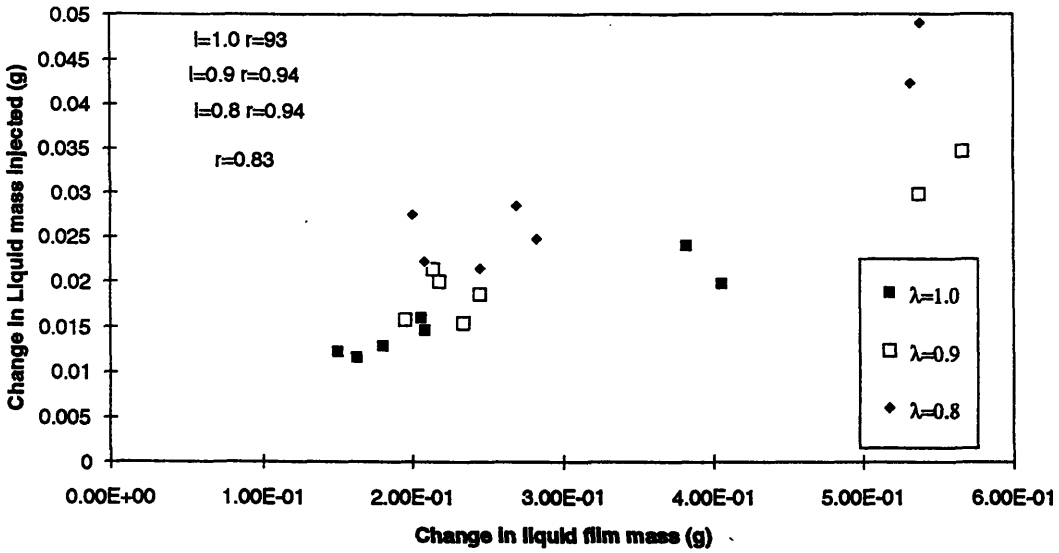

Figure 5.3 Correlation between the change of liquid film mass and the change of fuel mass injected (T=40°C).

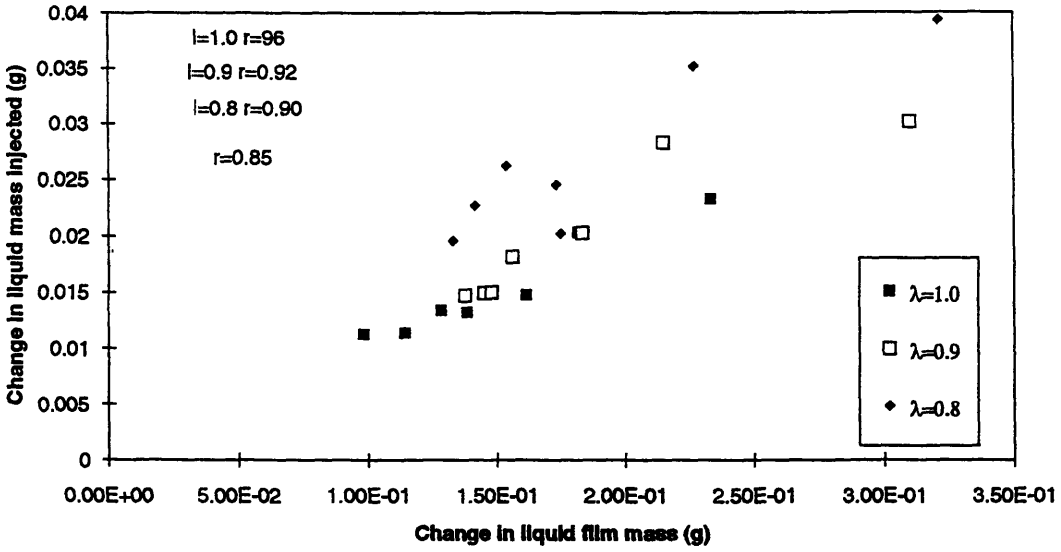

Figure 5.4 Correlation between the change of liquid film mass and the change of fuel mass injected (T=80°C).

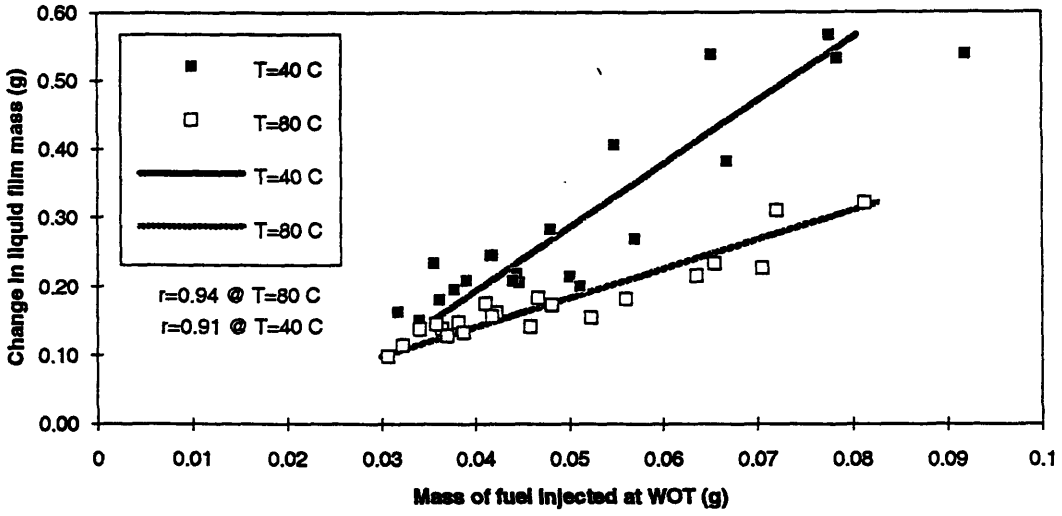

Figure 5.5 Correlation between the change of liquid film mass and the mass of fuel injected at wide open throttle.

There are several important preliminary results from the experiments. First, the data indicate a sharp increase in the change of film mass between M60 and M85 for the cold condition. The second important result is the relatively high change of film mass for pure methanol in the hot coolant condition. Although the coolant temperature (T=80°C) is above the boiling point of methanol (T=64.7 °C @ 1 ATM), the data indicates that there is a liquid film build up. There is good correlation between the mass of fuel injected at wide open throttle and the change of liquid film mass during the transient.

From these preliminary results we can conclude that the latent heat of vaporization of methanol plays an important role in the evaporation process. In order to obtain a better understanding of the physical processes inside the intake port we attempted to develop a simple model which would work with Multi-component fuels.

5.2 Indolene Model

Because indolene contains more than twenty components, a model was devised to simplify the analysis. This model was developed by Kuo-Chiang Chen at MIT[12]using SUPERTRAPP, a program written by the National Institute of Standards and Technology (NIST)[13] containing a library of thermophysical properties of hydrocarbon mixtures. The NIST program uses the Peng-Robinson equations of state to calculate the vapor-liquid equilibrium compositions. Although the program takes into account the non-ideal interactions between the components, it does not take into account the effects of the polar structure of methanol.

The goal of this model was to simplify the composition while keeping the same distillation parameters as the standard indolene: T10, T50, T90 and the Reid Vapor Pressure . T10, T50, and T90 refer to the temperature at which 10%, 50%, and 90% of the liquid evaporates under atmospheric pressure. The values obtained are shown in

table 5.1. Table 5.2 shows the content of the indolene model used.

Table 5.1 Distillation Parameters for Indolene and the Indolene Model.

	Indolene	Indolene Model
T10 (°C)	53.3	53.5
T50 (°C)	105	104.1
T90 (°C)	151.6	152.1
Reid Vapor Pressure (Psi)	8.74	8.5

Table 5.2 Content of the Indolene Model

Component Name	Volume %
N-Butane	6.1
Isopentane	18.6
2-Methylpentane	8.17
2-Methylhexane	9.3
Toluene	14.5
2,2,4-Trimethylpentane	24.76
Meta-Xylene	6
N-Nonane	2.6
Cumene	7
Decane	2.9

Using the indolene model, it was then possible to perform adiabatic and isothermal flash

calculations using SUPERTRAPP. However, it is important to point out that the NIST program performs steady state calculations, which might not always apply due to the dynamic processes inside the intake port. However, the steady state value will give an indication of the trend that the dynamic process will follow.

5.3 Modeling the Intake Port

The most crucial parameter for mixture preparation inside the intake port is the port wall temperature. Several papers have been published emphasizing the effects of cold manifold walls and cold valves on start-up and transient behavior [14,15,16,17]. Therefore, it is important to model the heat transfer between the combustion chamber/cooling jacket and the port wall/intake valves accurately. With an instrumented and heated intake valve, Martins J.J.G. et al. have obtained important differences in valve temperatures between gasoline and methanol under the same heating power[18]. For example, under the constant heating power (Q=100W), the methanol fuel lowered the valve temperature from 180°C to 65°C, compared to the gasoline case. In these experiments, the fuel injector was aimed directly at the back of the intake valve, preventing fuel interaction with the port wall. The heat transfer model presented in this section calculates the temperature and the fractional mass of fuel evaporated along the port wall, between the injector and the intake valve. To simplify the analysis several assumptions were made:

-The fuel injector creates a uniform fuel film over the intake port and the valve.

-The port wall temperature close to the combustion chamber is constant .

-The heat is conducted along the length of the port wall.

-All of the injected fuel is deposited on the port wall.

-The fuel film temperature is uniform across its thickness.

-The fuel film has uniform thickness along the port wall.

-There is no film flow.

Although the last assumption does not apply to an actual engine, the purpose here is to correlate the change in liquid film mass with the evaporation model of the fuels. Figure 5.6 shows a schematic of the intake port to illustrate the heat transfer analysis on the port wall.

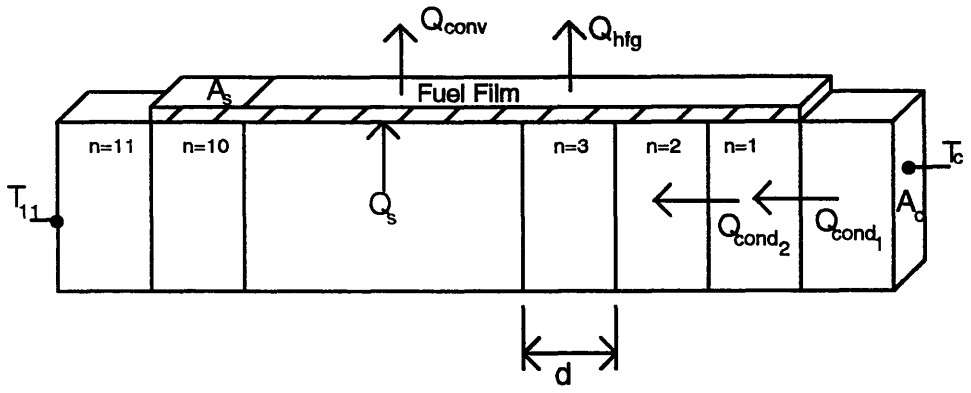

Figure 5.6 Schematic of the Intake Port wall.

The port wall was divided into 10 elements of equal surface area. Referring to figure 5.6, the first element represents the valve and the immediate region around the valve seat. This first element receives heat from the combustion chamber wall (Tc) by conduction. The wall temperature of each element is obtained by the energy balance between the heat flow into the element by conduction (Q_{cond_n}), and the energy leaving the element. The energy leaving the element is defined as the energy required to heat up the fuel from the injection temperature Tinj to the wall temperature T_n (Q_S) and vaporize it at the wall temperature (Q_{hfg}), the energy leaving the element by conduction to the next element ($Q_{cond_{n+1}}$), and the energy transferred at the surface due to forced convection. In the time τ for one engine cycle, the energy balance for each wall element becomes:

$$\left[\frac{[T_{n-1}-T_n]}{d}-\frac{[T_n-T_{n+1}]}{d}\right]\times K\times Ac\times\tau=\frac{Minj}{N}\times Cp\times[Tn-Tinj]+Mev_n\times hfg+h\times As\times[Tn-Tair]\times\tau$$

Notation:

Ac: heat conduction cross sectional area along the port

As: surface area of each element exposed to the intake air flow

C_p: specific heat of liquid fuel

d: Length of one segment

h: heat transfer coefficient (set equal to Watt/m^2.K) between the intake air and the fuel film

h_{fg}: latent heat of vaporization of the fuel

K: thermal conductivity of the port material (aluminum)

M_{inj}: mass of fuel injected per cycle

Mev_n: mass of fuel evaporated per cycle at element n

T_n: wall temperature at element n

T_c: combustion chamber wall temperature

τ: time for one cycle

There are two boundary conditions for the model. First, the combustion chamber temperature is constant (T_c=constant). Second, the end of the port wall is also held constant (T_{11}=constant). For practical purposes, T_{11} was held constant at 300°K. Assuming that the evaporation of the film reaches equilibrium before the end of the cycle, the NIST program can be used to relate the wall temperature (T_n) and the fractional mass of fuel evaporated per cycle for each element.

$[Mev]_n = X_n \times [M_{film}]$ eq.(5)

X_n: mass fraction of fuel evaporated at element n.

$[M_{film}]$: liquid fuel film mass at any element n. Since the surface area of each element is the same, and the film thickness is uniform.

X is a function of the temperature and pressure at the wall: $X=F(T_n,P_n)$

Although the total fuel film mass is unknown, it is reasonable to assume that the sum of the fuel mass evaporated over all the elements is equal to the mass of fuel injected

(assuming that there is no film flow present). Since the pressure inside the manifold is known, the model simplifies to two equations (eq.(4) and eq.(5)) and two unknowns (T_c and m_{film}). The solution to the model is obtained by iterating the fuel film mass until the fuel mass evaporated from the film equals to the fuel mass injected. The solution provides us with three sets of information: the fuel film mass necessary to generate the required mass of fuel vapor, the temperature profile along the port, and the fractional mass of fuel evaporated along the port wall.

5.4 Modeling Results

The port wall temperature model presented in section 5.3 solved for the **absolute** liquid film mass inside the port for a constant pressure and a constant combustion chamber wall temperature. The relative **change** of liquid fuel film mass between the part throttle and the wide open throttle case is calculated from the model by subtracting the liquid fuel film mass at part throttle from the liquid fuel film mass at wide open throttle. Figure 5.7 shows the effects of methanol content on the change of liquid fuel film mass for different boundary conditions. Represented here are three combustion chamber wall temperatures. For T_c=470^{o}K, the correlation coefficient between the model and the experimental results under high coolant temperature (T=80^{o}C) is r=0.97. Under low coolant temperature, (T=40^{o}C), the correlation works best for a combustion chamber wall temperature equal to 390^{o}K, r=0.95.

Figure 5.7 indicates that several transitions take place when the temperature of the combustion chamber wall increases.

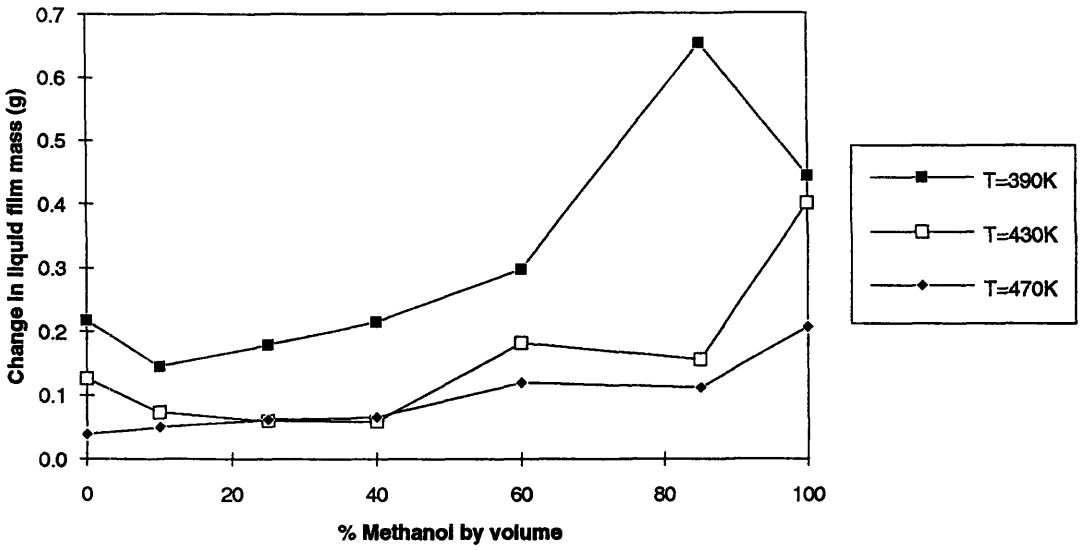

Figure 5.7 Effects of Methanol Content on the change of liquid fuel film mass for the model.

1. The first transition occurs between M0 and M60. The change in fuel film mass uniformly increases as the temperature decreases.

2. The second transition occurs between M60 and M100. As the combustion chamber wall decreases, there is a rapid increase in fuel film mass. The transition first occurs between M85 and M100 (between T=430^{o}K and 470^{o}K), then the transition mostly affects M85 between T=430^{o}K and T=390^{o}K).

The details of the analysis are shown in figures 5.8, 5.9, 5.10, and 5.11. Figures 5.8, and 5.9 show two samples of the temperature profile along the port under different combustion chamber wall temperatures (T=390^{o}K, and T=430^{o}K).

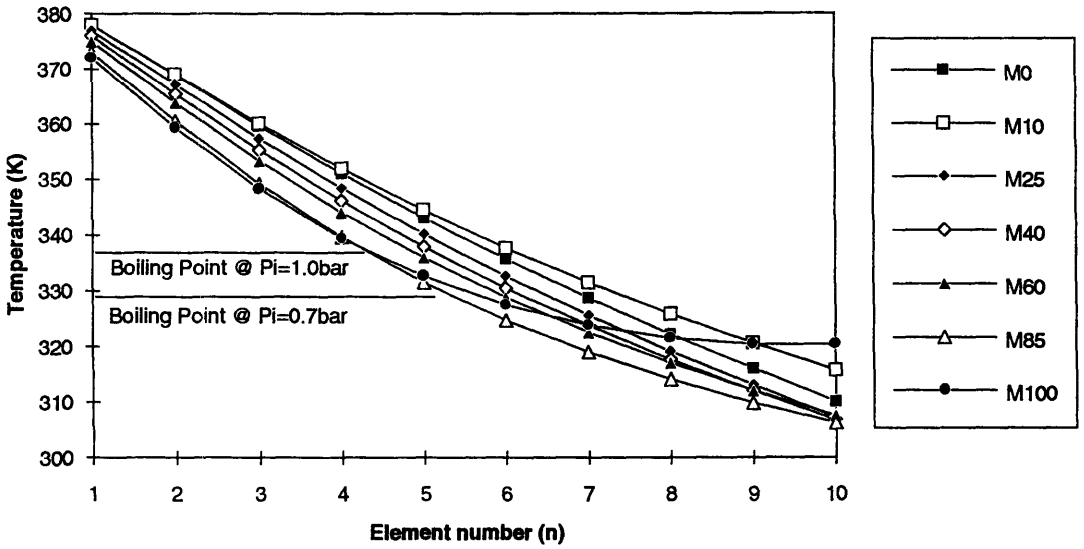

Figure 5.8 Temperature profile along the port wall (Tc=390^{o}K)

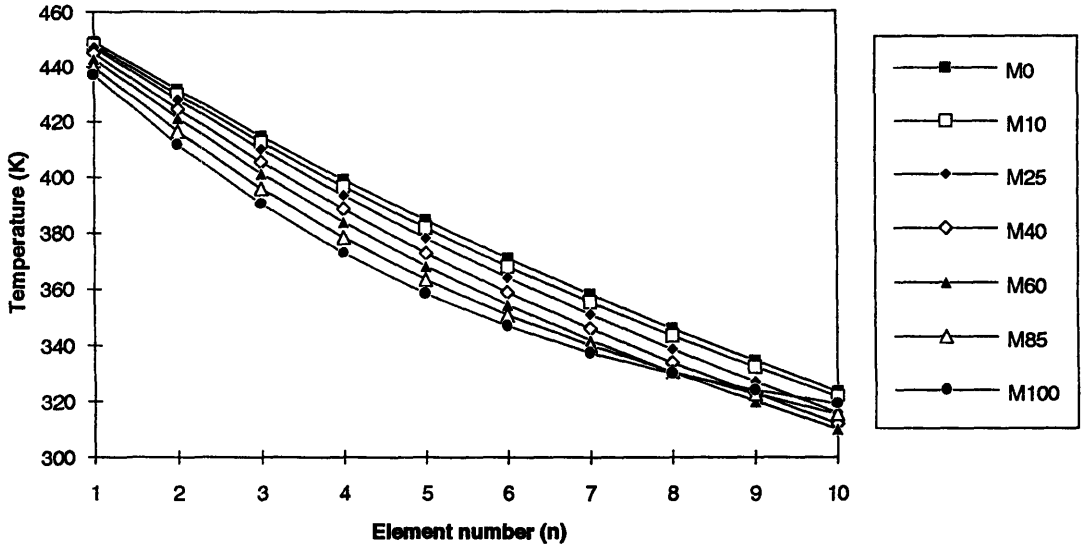

Figure 5.9 Temperature profile along the port wall (Tc=470^{o}K)

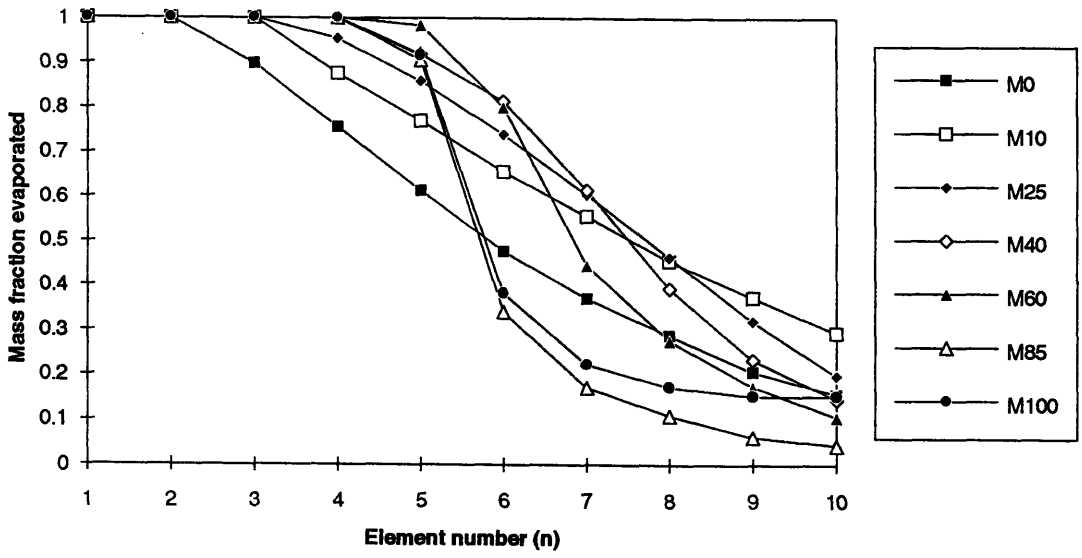

Figure 5.10 Mass fraction of fuel evaporated along the port wall (Tc=390^{o}K)

Figures 5.10 and 5.11 show the mass fraction of fuel evaporated along the port wall for each element under the different temperature profiles.

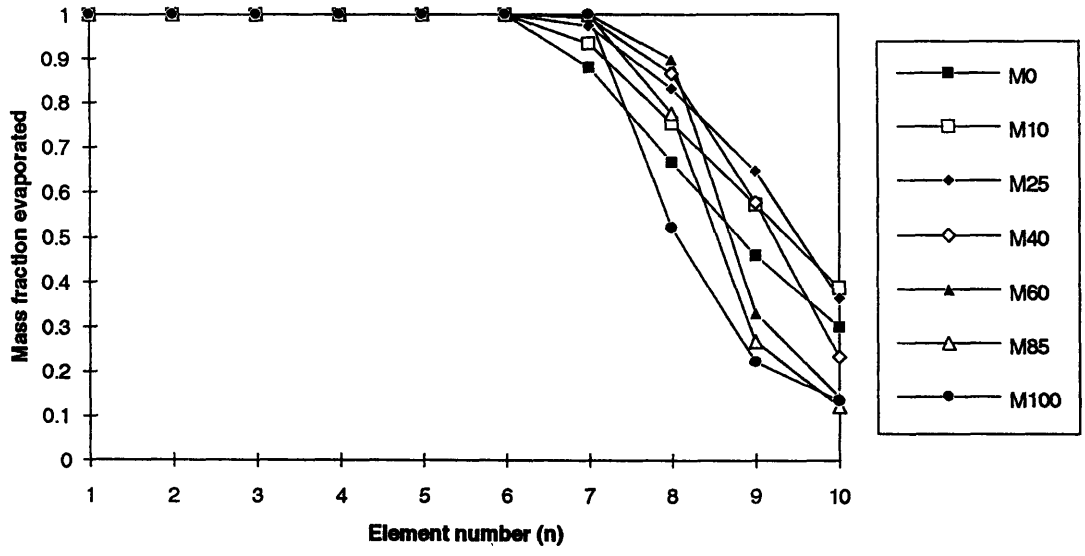

Figure 5.11 Mass fraction of fuel evaporated along the port wall (Tc=470^{o}K)

For methanol (M100), figures 5.8 and 5.10 show that for low temperatures, 6 out of the 10 elements are below the boiling point of methanol at wide open throttle. However, only 4 out of the 10 elements are below the boiling point of methanol at part throttle (Pi=0.7 bar). The model indicates that this is the major reason for the sudden change in liquid fuel film mass observed in the data under low coolant temperature. Because a significant portion of the liquid film area is below the boiling point of methanol at wide open throttle, a much larger fuel film mass is necessary to generate the necessary fuel vapor.

Figure 5.11 shows that M10, M25, and M40 have a better volatility along the port wall than indolene under the high combustion chamber wall temperature ($T=470^{o}K$). However, the increase in volatility is offset by the increase in the stoichiometric air-fuel ratio requirements of the methanol blends over indolene.

CHAPTER 6 -- CONCLUSION

6.1 Review of the Methodology

A method was developed to measure the effects of fuel composition on engine throttle transients. A parameter used to measure the effect of fuel composition was the change of the cumulative difference between the amount of fuel injected and the mass of fuel burned in the cylinder (obtained from the Gimep) This difference is interpreted as the change in liquid fuel mass inside the intake port (fuel film) between the initial (at P_i=0.7 bar) and final state of the transient (at P_i=1.0 bar). The method uses a detailed engine map of the gross indicated fuel conversion efficiency to calculate the mass of fuel burned on a cycle by cycle basis. The engine map includes parameters such as the Gross Indicated Mean Effective Pressure (Gimep), the Peak cylinder pressure angle, and the exhaust relative air to fuel ratio. The mass of fuel injected was calculated from the injector pulse width and the mass of fuel burned under steady state conditions. The change of liquid film mass over one cycle was calculated by subtracting the mass of fuel burned from the mass of fuel injected during the cycle. By summing the change of liquid film mass over the duration of the transient, we obtained the "cumulative mass of fuel unaccounted for" or, the change of liquid film mass between the two steady state conditions.

The second parameter used to evaluate the effects of fuel composition on engine throttle transients was the Gimep response time. The response time was defined as the 0 to 90% rise time of the Gimep curve.

6.2 Model and Discussion

The data indicates that there is good correlation between the mass of fuel injected at wide open throttle and the change of liquid film mass during the transient. This correlation holds true under hot and cold coolant temperatures. However, the correlation coefficient is not as good for the cold case. The higher scattering obtained under cold coolant conditions can be explained with the one dimensional model developed.

The model included a 10 component fuel model of indolene to simplify the calculations. The model explained the trends showed on figure 4.9 and 4.10.

The following main conclusions can be drawn from the data and the model presented here:

1. Under warmed up engine conditions (T=80°C) the correlations indicate that the change of liquid film mass scales directly with the fuel mass injected at wide open throttle. Although we anticipated the liquid film mass to scale with the change of fuel mass injected per cycle, it is not yet clear as to why the fuel mass injected at part throttle does not enter the equation.
2. Under warmed up and cold engine conditions there is no correlation between the change in fuel film mass inside the intake port and the 0-90% Gimep response time.
3. Under warmed up engine condition, the 0-90% Gimep response times were fastest and showed no change between M40 and M100.
4. Under low engine coolant temperature, the change of liquid film mass exhibits a rapid transition between M60-M85 and M100. This transition is in the order of 220%.
5. Using the one dimensional model, it appears that the transition under low coolant temperature is due to the intake port wall cooling below the boiling point of methanol at wide open throttle. Under low intake pressure, the liquid film is above its boiling

point, when the intake manifold pressure increases (at WOT), the liquid film is below its boiling point, causing a large increase of the response time, and a large increase in the change of liquid film mass.

REFERENCES

1. Gallopoulos N.E., "Bridging the Present to the Future in Personal Transportation - The Role of Internal Combustion Engines", SAE paper 920721, 1992.
2. Heywood, J.B., Internal Combustion Engine Fundamentals, McGraw-Hill Book Company, New York, 1988.
3. Benninger N.F., Plapp G., "Requirements and Performance of Engine Management Systems under Transient Conditions", SAE paper 910083, 1991.
4. Brown, C.N. and Ladommatros,N., "A Numerical Study of Fuel Evaporation and Transportation in the Intake Manifold of a Port-Injected Spark-Ignition Engine", Journal of Automobile Engineering, vol 205, 1991.
5. Yoshikawa Y.,Nakada T., Itoh T., Takagi Y., Kawasaki T., and Kawabe R., "Numerical Simulation System for Analyzing Fuel Film Flow in Gasoline Engine", SAE paper 930326, 1993.
6. Nagaishi H., Miwa H., Kawamura Y., Saitoh M., "An Analysis of Wall Flow and Behavior of Fuel in Induction Systems of Gasoline Engines", SAE paper 890837, 1989.
7. Benyettou F.M., Thelliez M., "Modeling of Unsteady Multiphase Flow in the Intake Manifold of Spark Ignition Engines", SAE paper 910392, 1991.
8. DeWitte, K., "Fuel Effects on the Starting Behavior of Engines", M.S. Thesis, Department of Mechanical Engineering, Massachusetts Institute of Technology, 1993.
9. Almkvist G., and Eriksson S., "An Analysis of Air to Fuel Response in a Multi Point Fuel Injected Engine under Transient Conditions", SAE paper 932753, 1993
10. Ogawa T., Araga T.,Okada M., Kato M., and Nakada M., "Analysis of Poor

Engine Response Caused by MTBE-Blended Gasoline from the Standpoint of Fuel Evaporation", SAE paper 920800, 1992.

11. Harrison A.J., "Enthalpy Requirement -- A New Fundamentally-Based Gasoline Volatility Parameter for Predicting Cold-Weather Driveability", SAE paper 881670, 1989.

12 Kuo-Chiang Chen, "Fuel Volatility Modeling", M.Sc. Thesis, Department of Mechanical Engineering, Massachusetts Institute of Technology, 1994.

13 Fly J.J., and Huber M.L., "NIST Thermophysical Properties of Hydrocarbon Mixtures Database (Supertrapp)", National Institute of Standards and Technology Standard Reference Database 4 -- Version 1.0, Gaithersburg, MD 20899, (July 1992).

14 Servati, B.H. and Herman, E.H., "Spray/Wall Interactions Simulations", SAE paper 890566, 1989.

15 Iwano H., Jaitoh M., Sawamoto K., and Nagaishi H., "An Analysis of Induction Port Fuel Behavior", SAE paper 912348, 1991.

16 Aquino C., and Plensdorf W.D., "An Evaluation of Local Heating as a Means of Fuel Evaporation for Gasoline Engines", SAE paper 860246, 1986.

17 Aquino C., "The Effects of Local Heating on A/F Ratio Control", SAE paper 820411, 1982.

18 Martins, J.J.G. and Finlay I.C., "Fuel Preparation in Port-Injected Engines", SAE paper 920518, 1992.

APPENDIX A

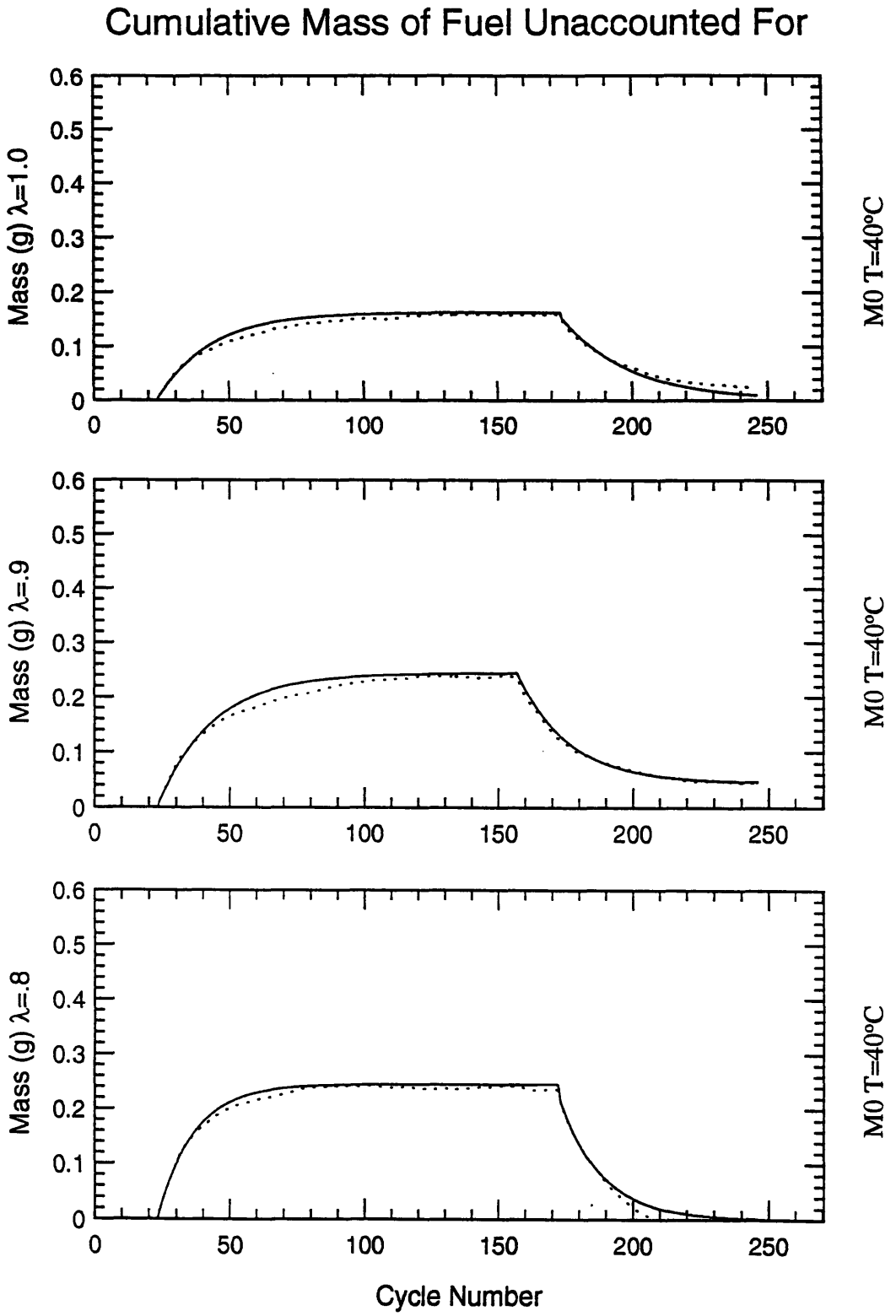
Cumulative Mass of Fuel Unaccounted For
Mass (g) λ=1.0
Mass (g) λ=.9
Mass (g) λ=.8
0.6
0.5
0.4
0.3
0.2
0.1
0
0
50
100
150
200
250
Cycle Number
M0 T=40°C
M0 T=40°C
M0 T=40°C

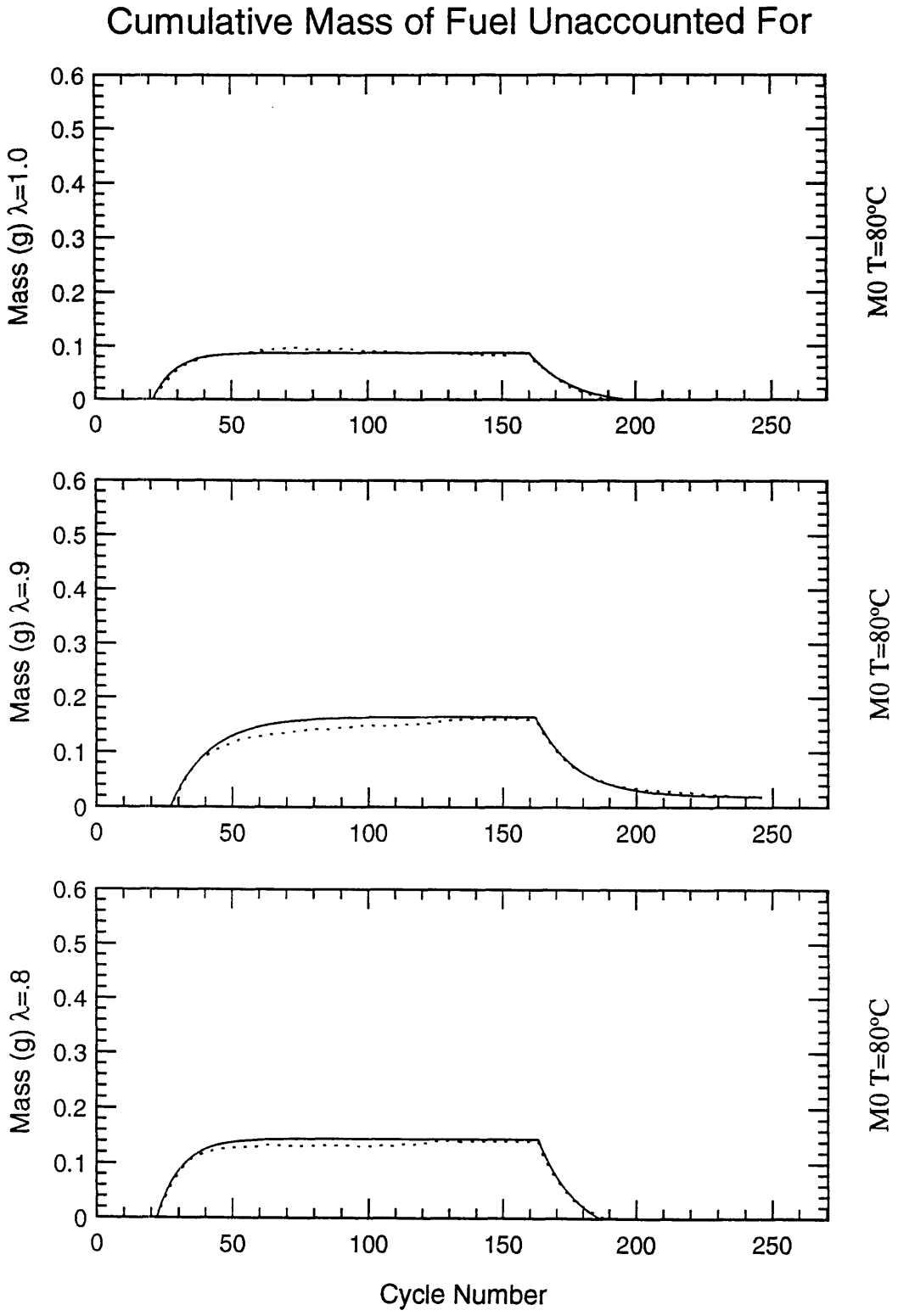
Cumulative Mass of Fuel Unaccounted For
Mass (g) λ=1.0
Mass (g) λ=.9
Mass (g) λ=.8
0.6
0.5
0.4
0.3
0.2
0.1
0
0
50
100
150
200
250
Cycle Number
M0 T=80°C
M0 T=80°C
M0 T=80°C

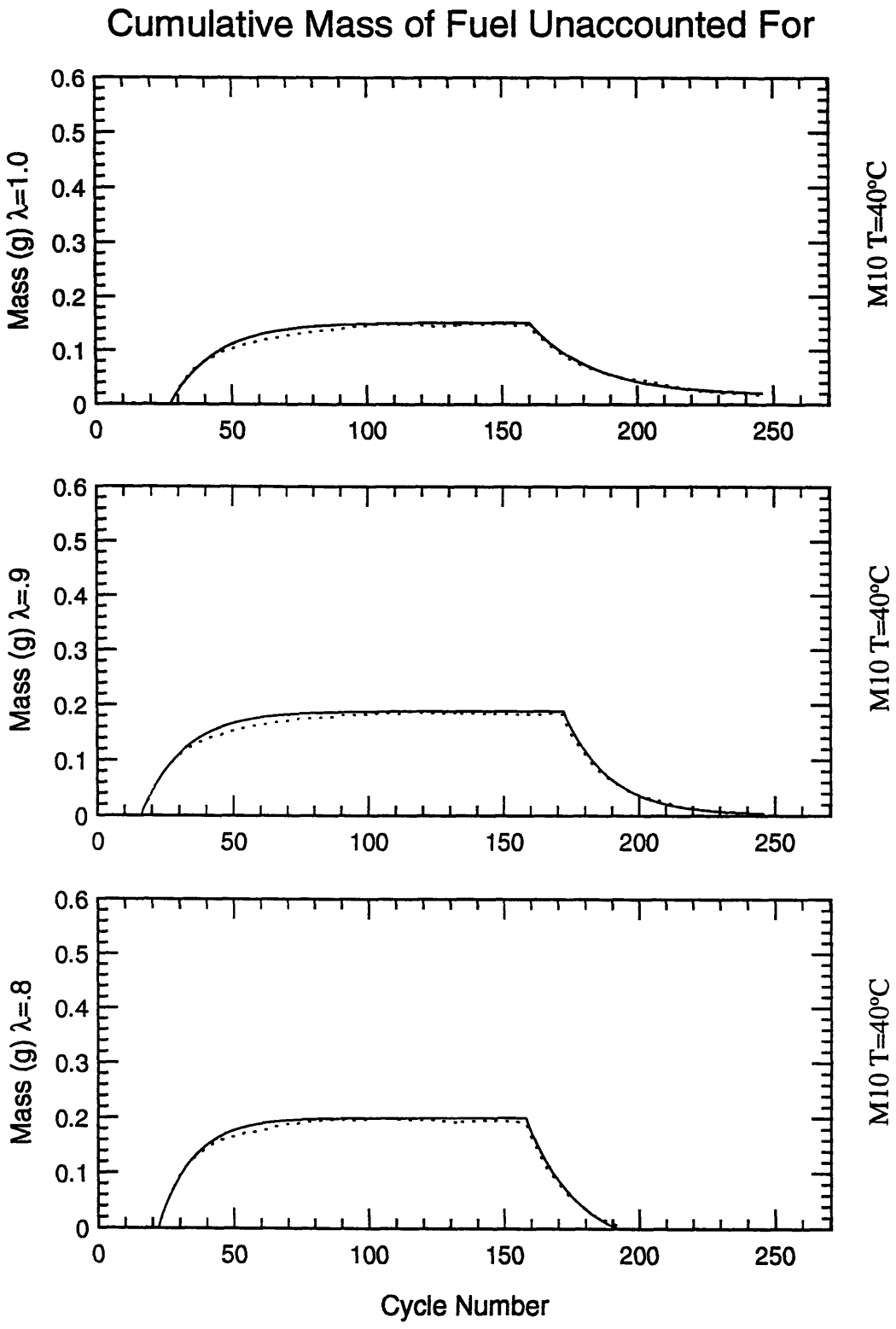
Cumulative Mass of Fuel Unaccounted For
Mass (g) λ=1.0
Mass (g) λ=.9
Mass (g) λ=.8
0.6
0.5
0.4
0.3
0.2
0.1
0
0
50
100
150
200
250
Cycle Number
M10 T=40°C
M10 T=40°C
M10 T=40°C

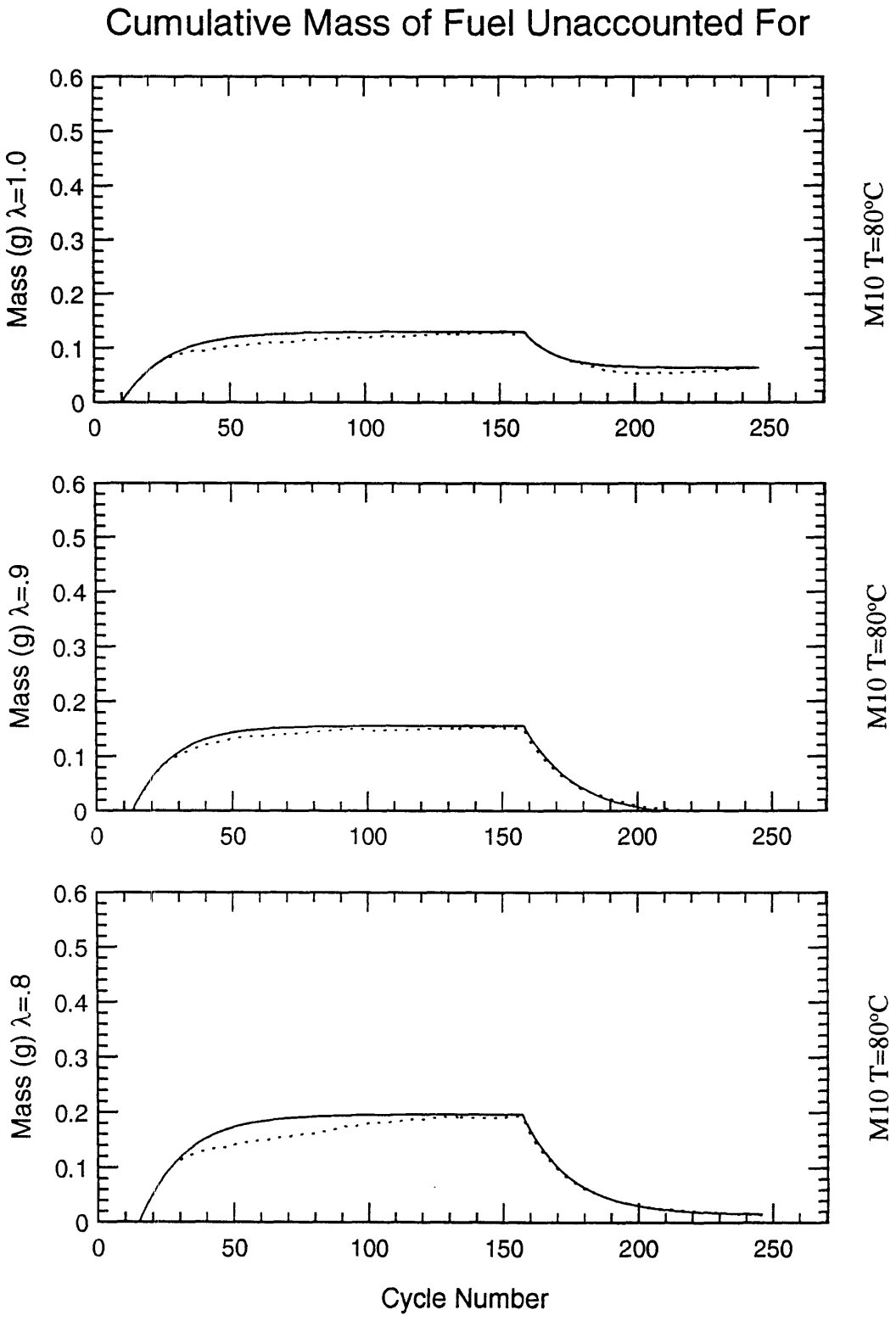
Cumulative Mass of Fuel Unaccounted For
Mass (g) λ=1.0
Mass (g) λ=.9
Mass (g) λ=.8
0.6
0.5
0.4
0.3
0.2
0.1
0
0
50
100
150
200
250
Cycle Number
M10 T=80°C
M10 T=80°C
M10 T=80°C

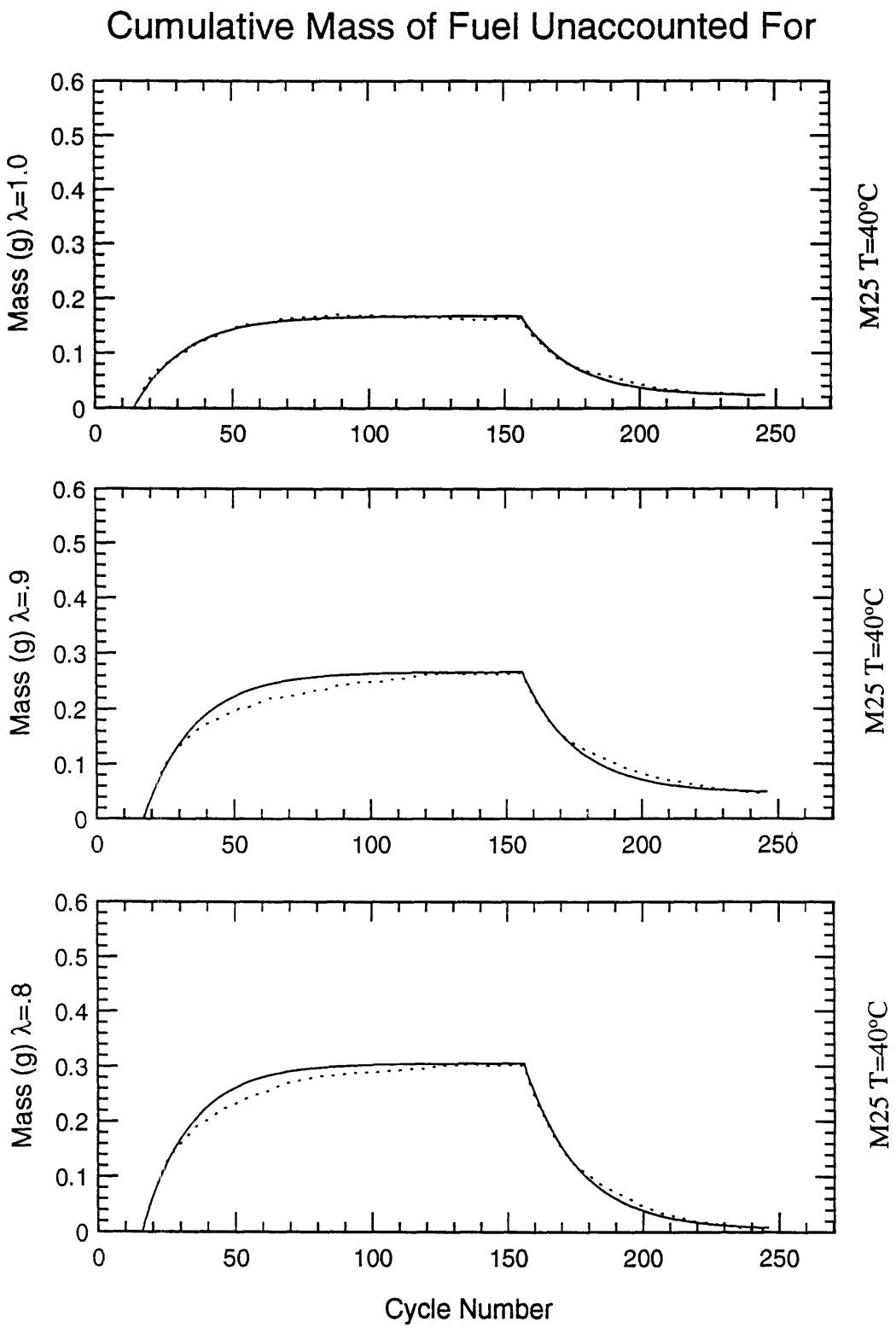
Cumulative Mass of Fuel Unaccounted For
Mass (g) λ=1.0
Mass (g) λ=.9
Mass (g) λ=.8
0.6
0.5
0.4
0.3
0.2
0.1
0
0
50
100
150
200
250
Cycle Number
M25 T=40°C
M25 T=40°C
M25 T=40°C

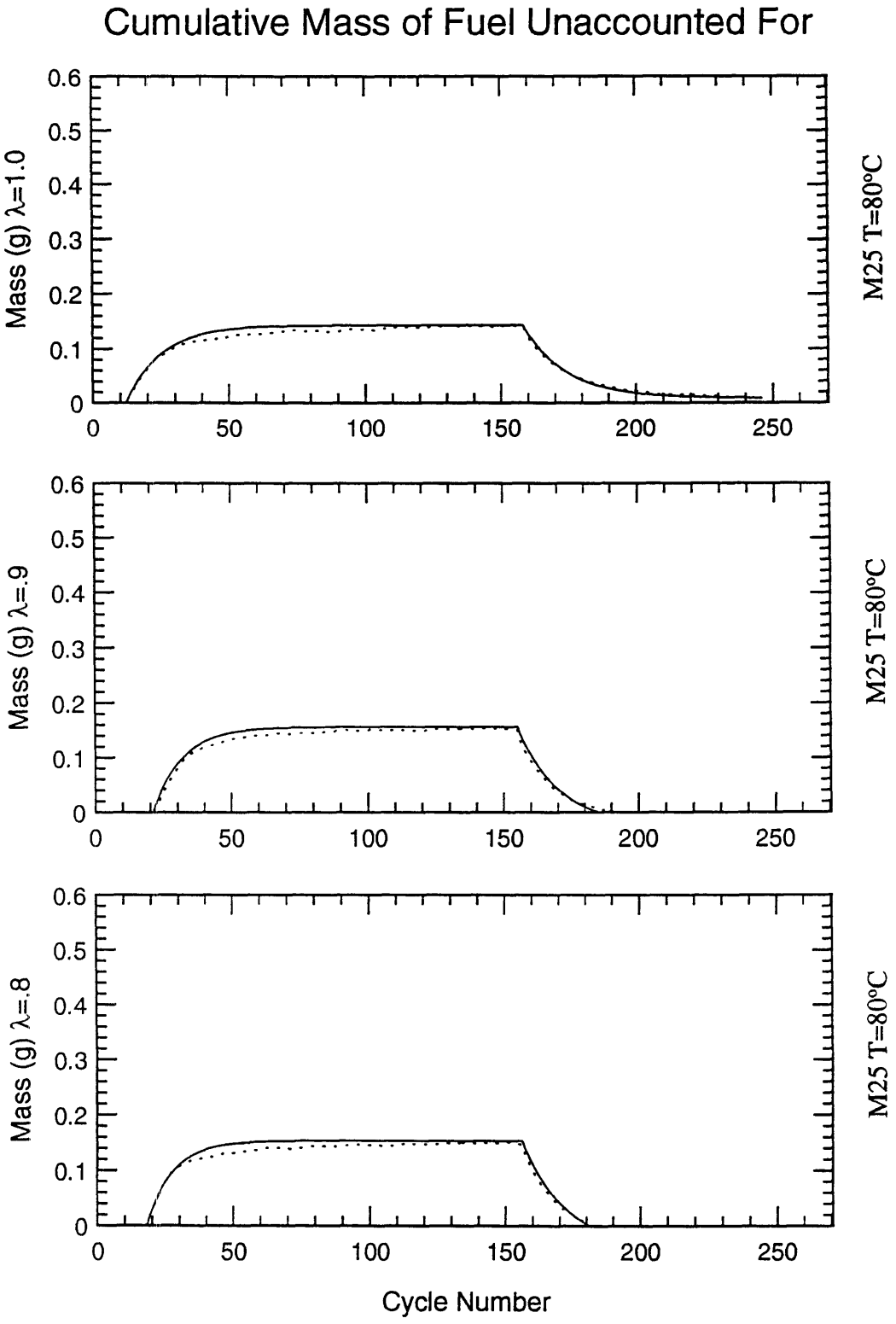
Cumulative Mass of Fuel Unaccounted For
Mass (g) λ=1.0
Mass (g) λ=.9
Mass (g) λ=.8
M25 T=80°C
M25 T=80°C
M25 T=80°C
0.6
0.5
0.4
0.3
0.2
0.1
0
0
50
100
150
200
250
Cycle Number

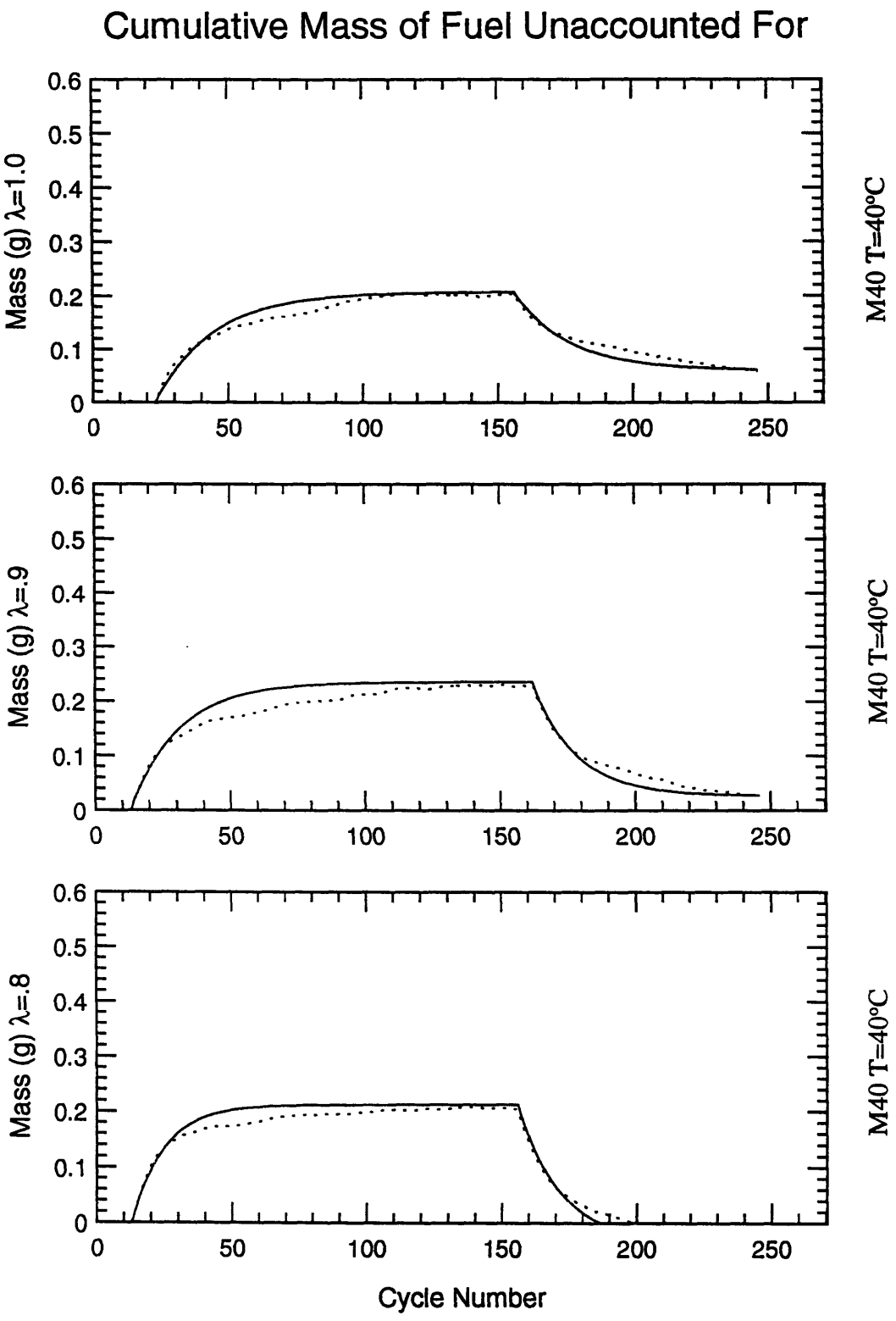
Cumulative Mass of Fuel Unaccounted For
Mass (g) λ=1.0
Mass (g) λ=.9
Mass (g) λ=.8
0.6
0.5
0.4
0.3
0.2
0.1
0
0
50
100
150
200
250
Cycle Number
M40 T=40°C
M40 T=40°C
M40 T=40°C

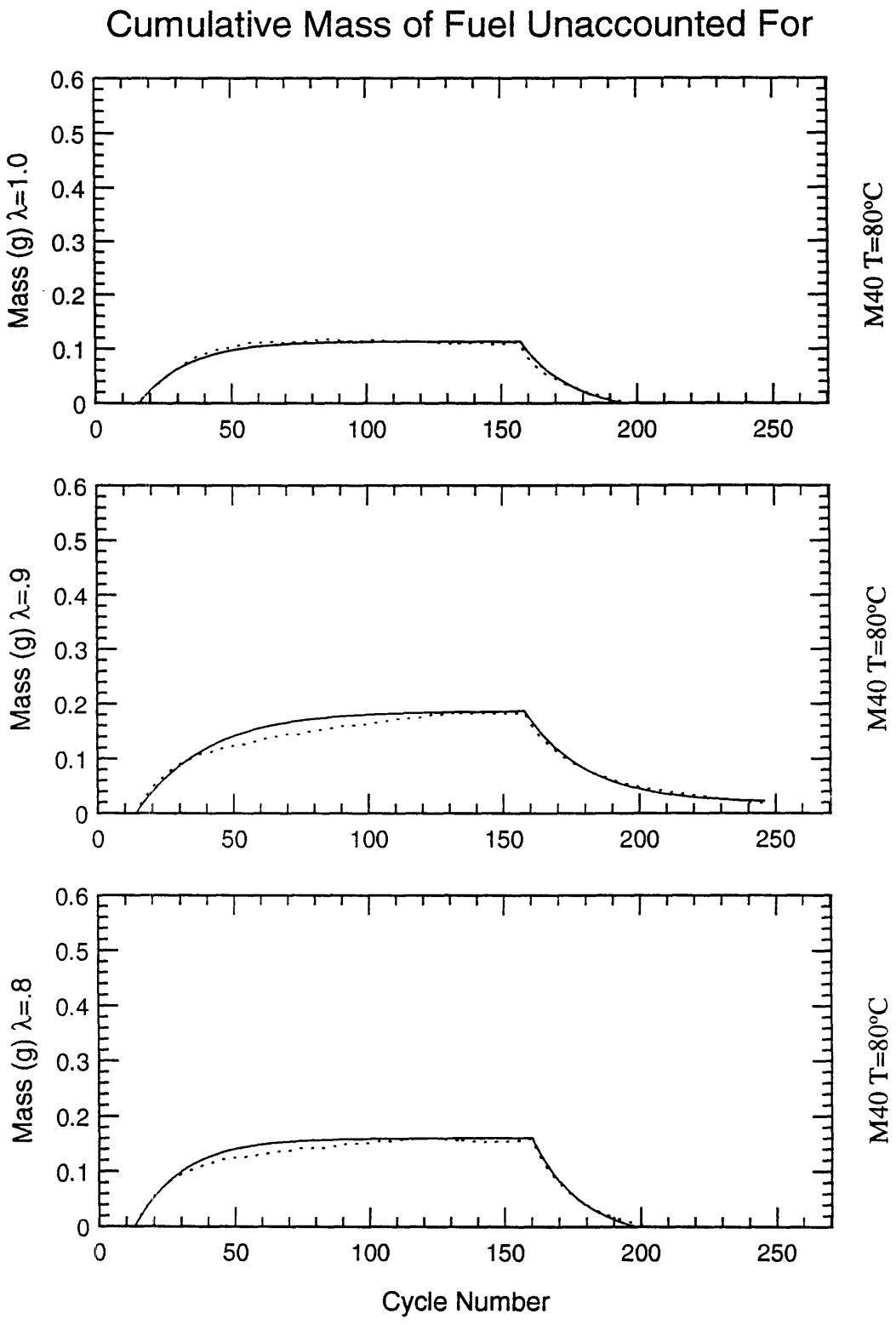
Cumulative Mass of Fuel Unaccounted For
Mass (g) λ=1.0
Mass (g) λ=.9
Mass (g) λ=.8
M40 T=80°C
M40 T=80°C
M40 T=80°C
0.6
0.5
0.4
0.3
0.2
0.1
0
0
50
100
150
200
250
Cycle Number

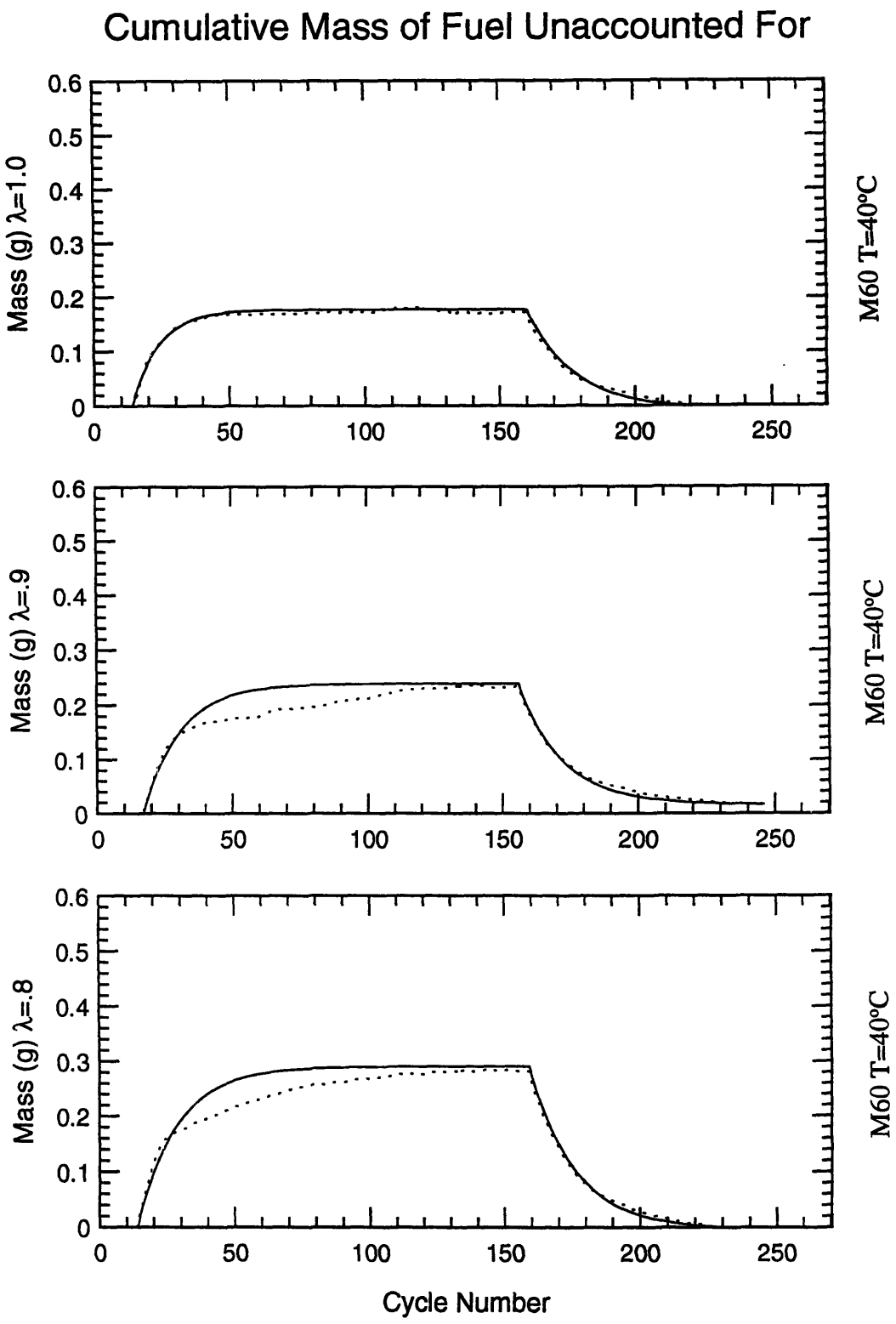
Cumulative Mass of Fuel Unaccounted For
Mass (g) λ=1.0
Mass (g) λ=.9
Mass (g) λ=.8
M60 T=40°C
M60 T=40°C
M60 T=40°C
0.6
0.5
0.4
0.3
0.2
0.1
0
0
50
100
150
200
250
Cycle Number

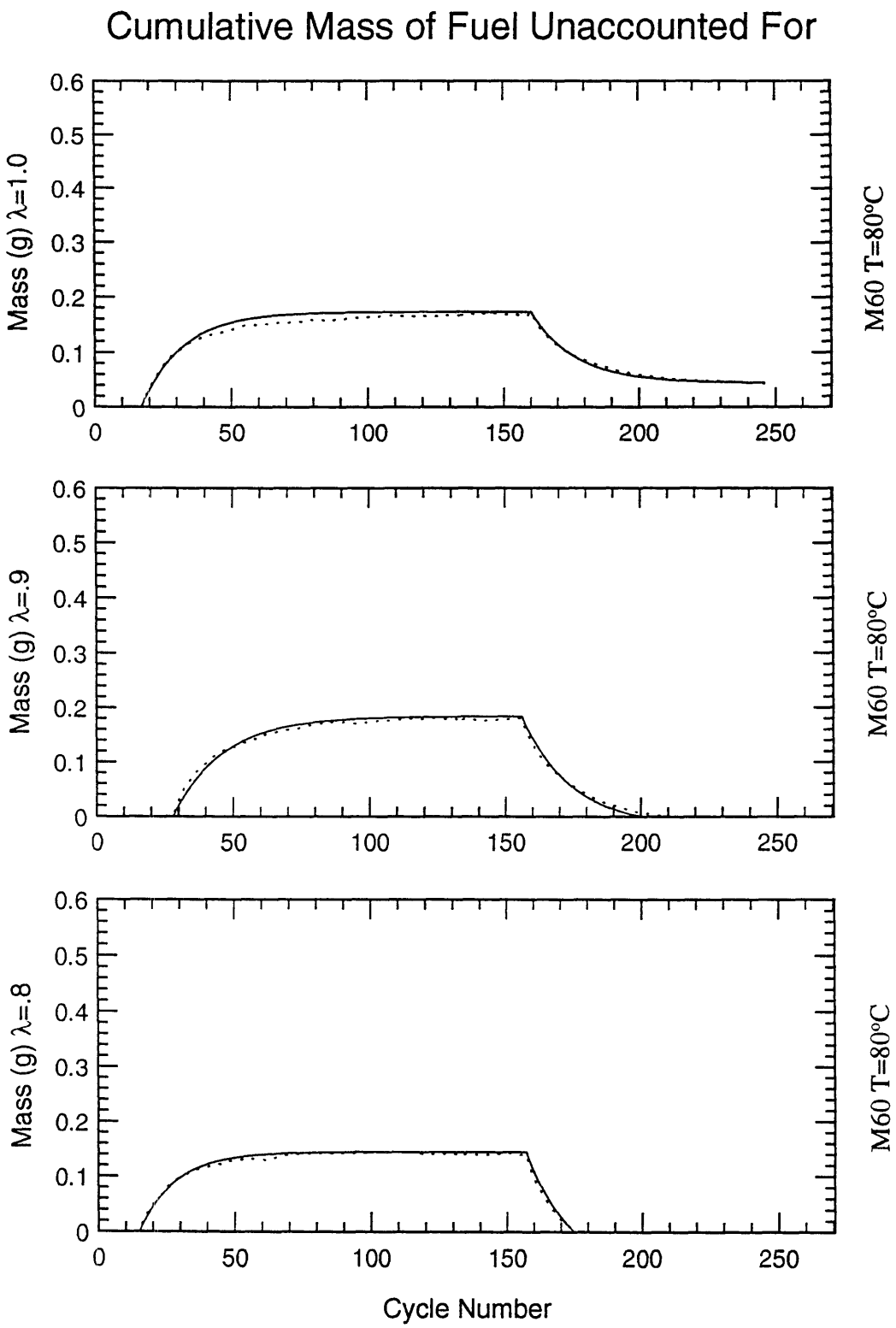
Cumulative Mass of Fuel Unaccounted For
Mass (g) λ=1.0
Mass (g) λ=.9
Mass (g) λ=.8
0.6
0.5
0.4
0.3
0.2
0.1
0
0
50
100
150
200
250
Cycle Number
M60 T=80°C
M60 T=80°C
M60 T=80°C

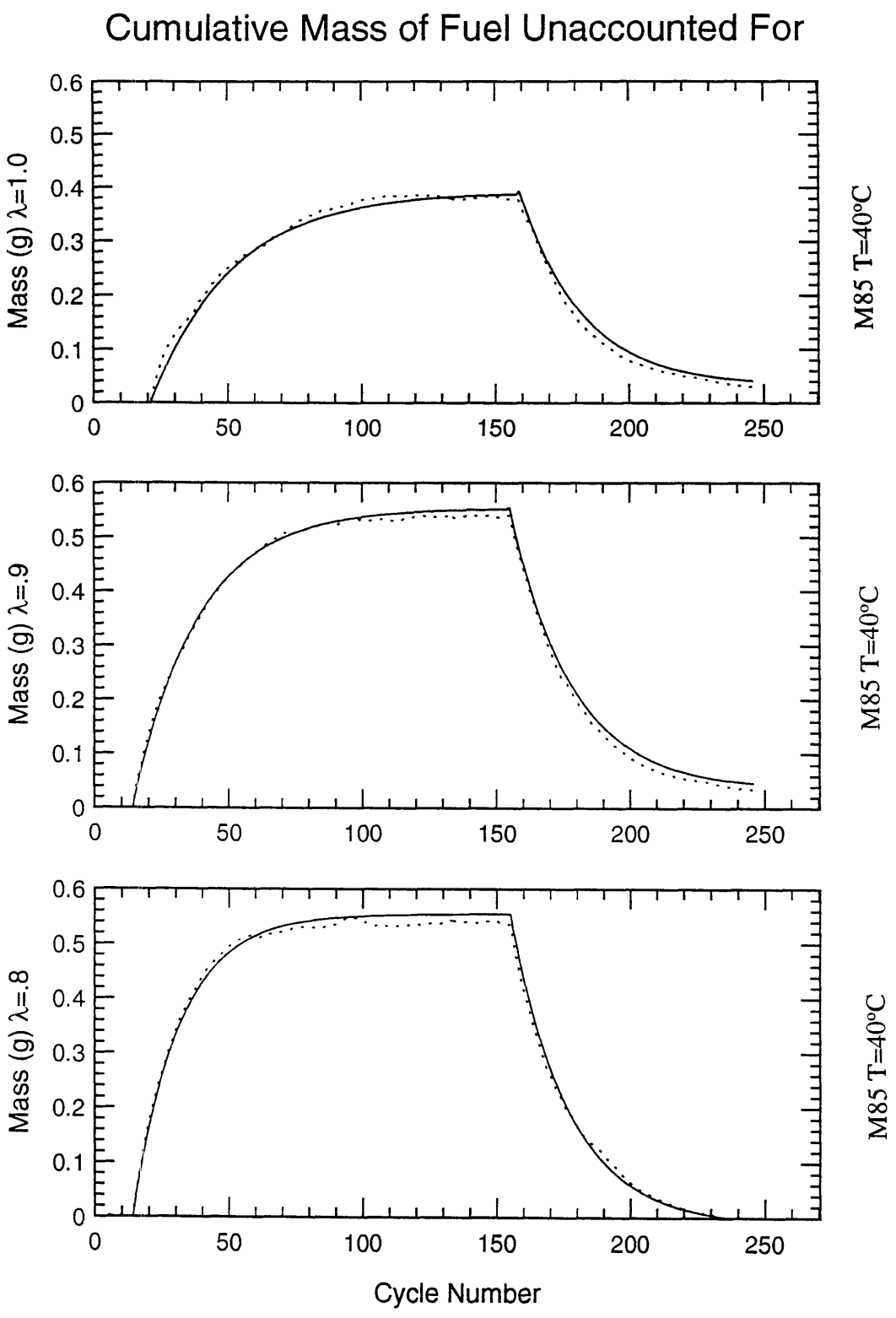
Cumulative Mass of Fuel Unaccounted For
Mass (g) λ=1.0
Mass (g) λ=.9
Mass (g) λ=.8
0.6
0.5
0.4
0.3
0.2
0.1
0
0
50
100
150
200
250
M85 T=40°C
M85 T=40°C
M85 T=40°C
Cycle Number

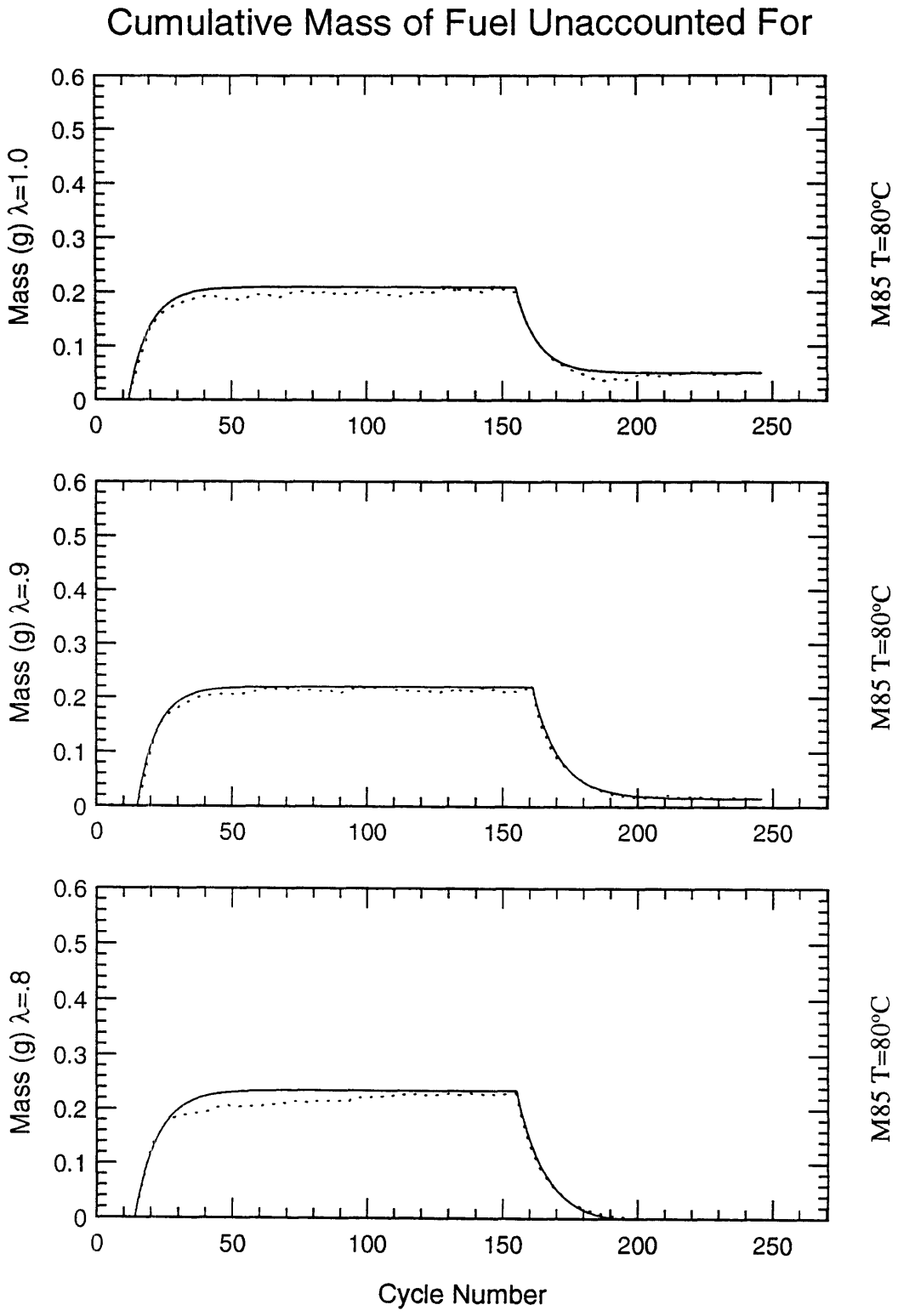
Cumulative Mass of Fuel Unaccounted For
Mass (g) λ=1.0
Mass (g) λ=.9
Mass (g) λ=.8
0.6
0.5
0.4
0.3
0.2
0.1
0
0
50
100
150
200
250
Cycle Number
M85 T=80°C
M85 T=80°C
M85 T=80°C

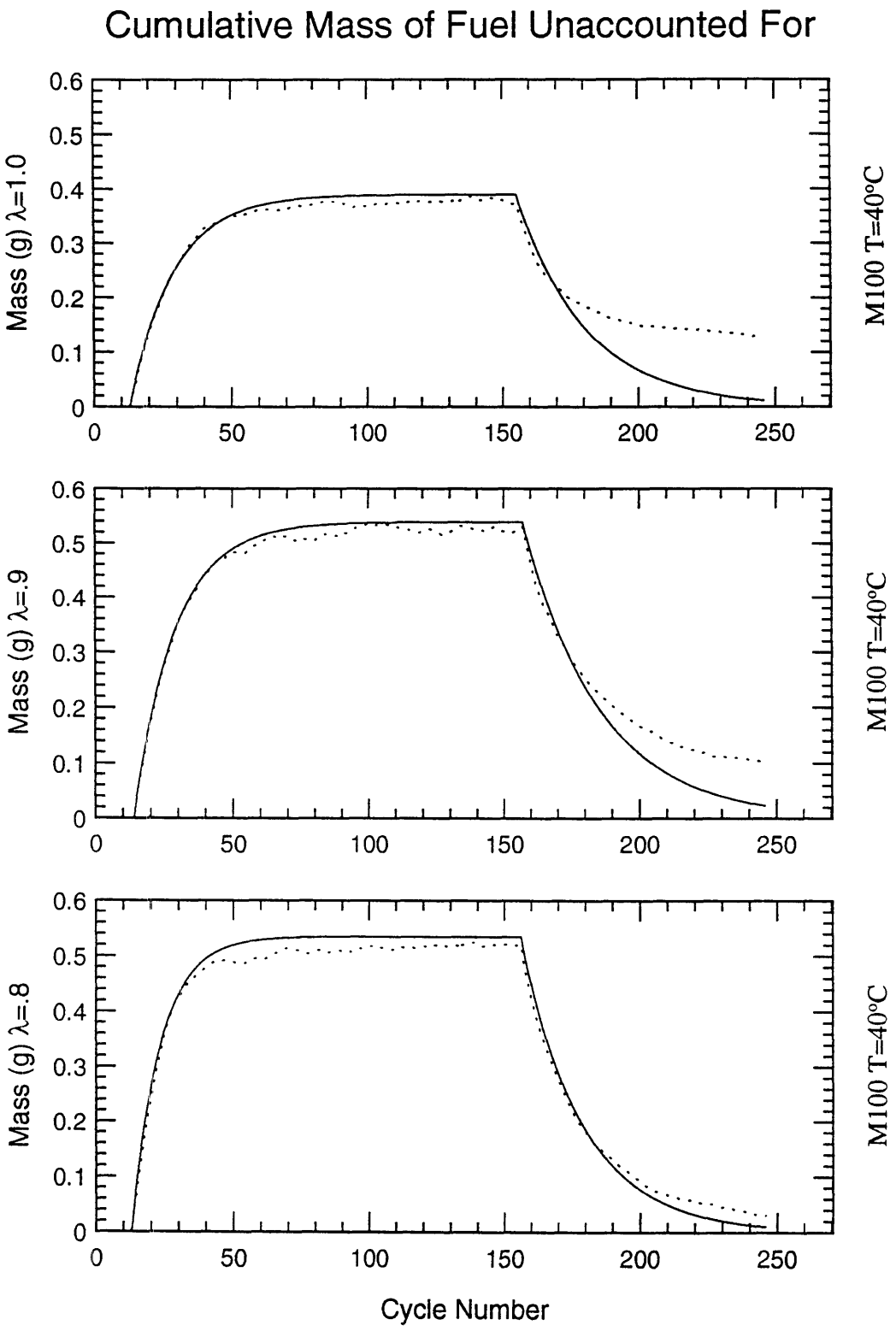
Cumulative Mass of Fuel Unaccounted For
Mass (g) λ=1.0
Mass (g) λ=.9
Mass (g) λ=.8
M100 T=40°C
M100 T=40°C
M100 T=40°C
0.6
0.5
0.4
0.3
0.2
0.1
0
0
50
100
150
200
250
Cycle Number

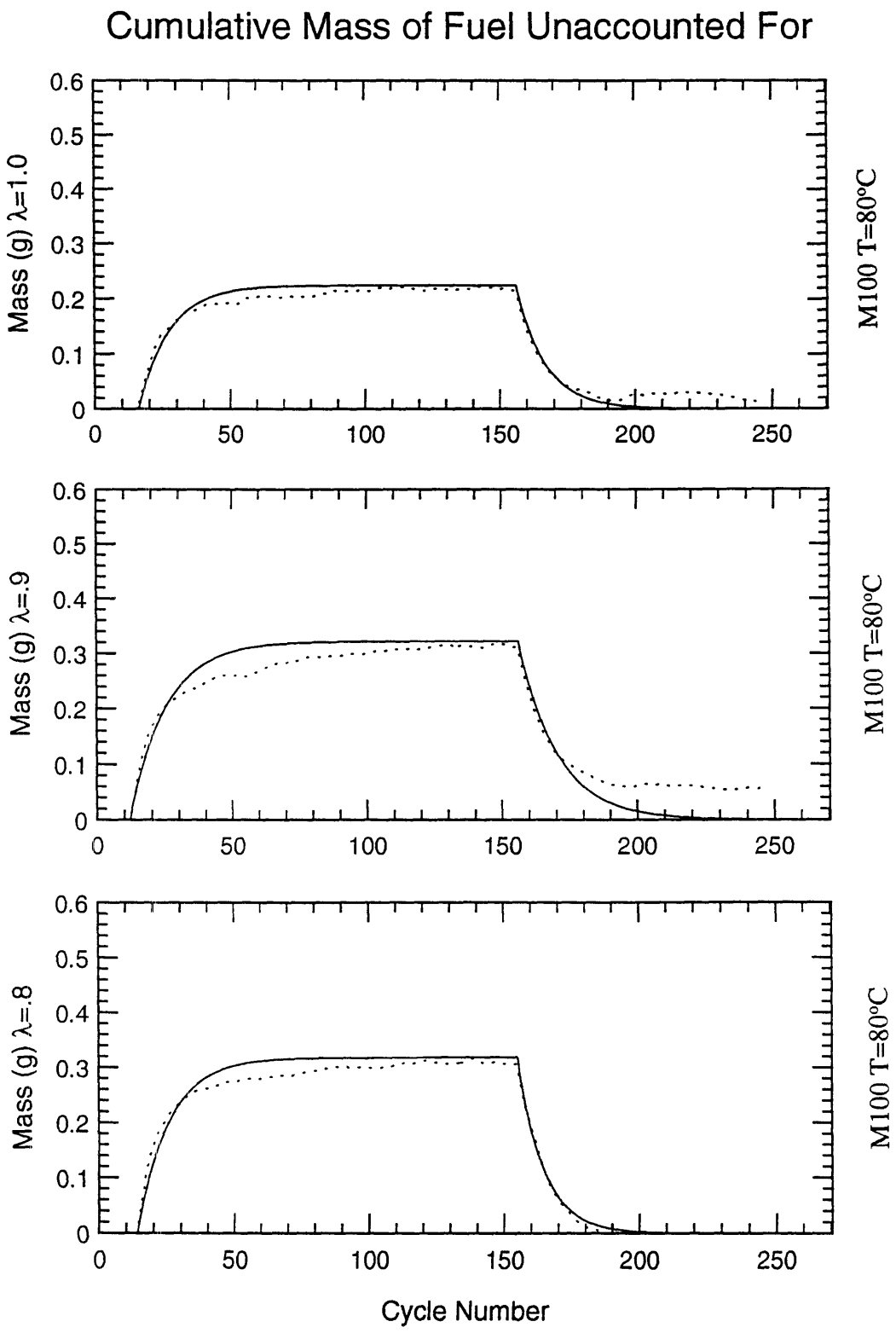
Cumulative Mass of Fuel Unaccounted For
Mass (g) λ=1.0
Mass (g) λ=.9
Mass (g) λ=.8
0.6
0.5
0.4
0.3
0.2
0.1
0
0
50
100
150
200
250
Cycle Number
M100 T=80°C
M100 T=80°C
M100 T=80°C

APPENDIX B

INDOLENE λ=1.0 @ 40°C

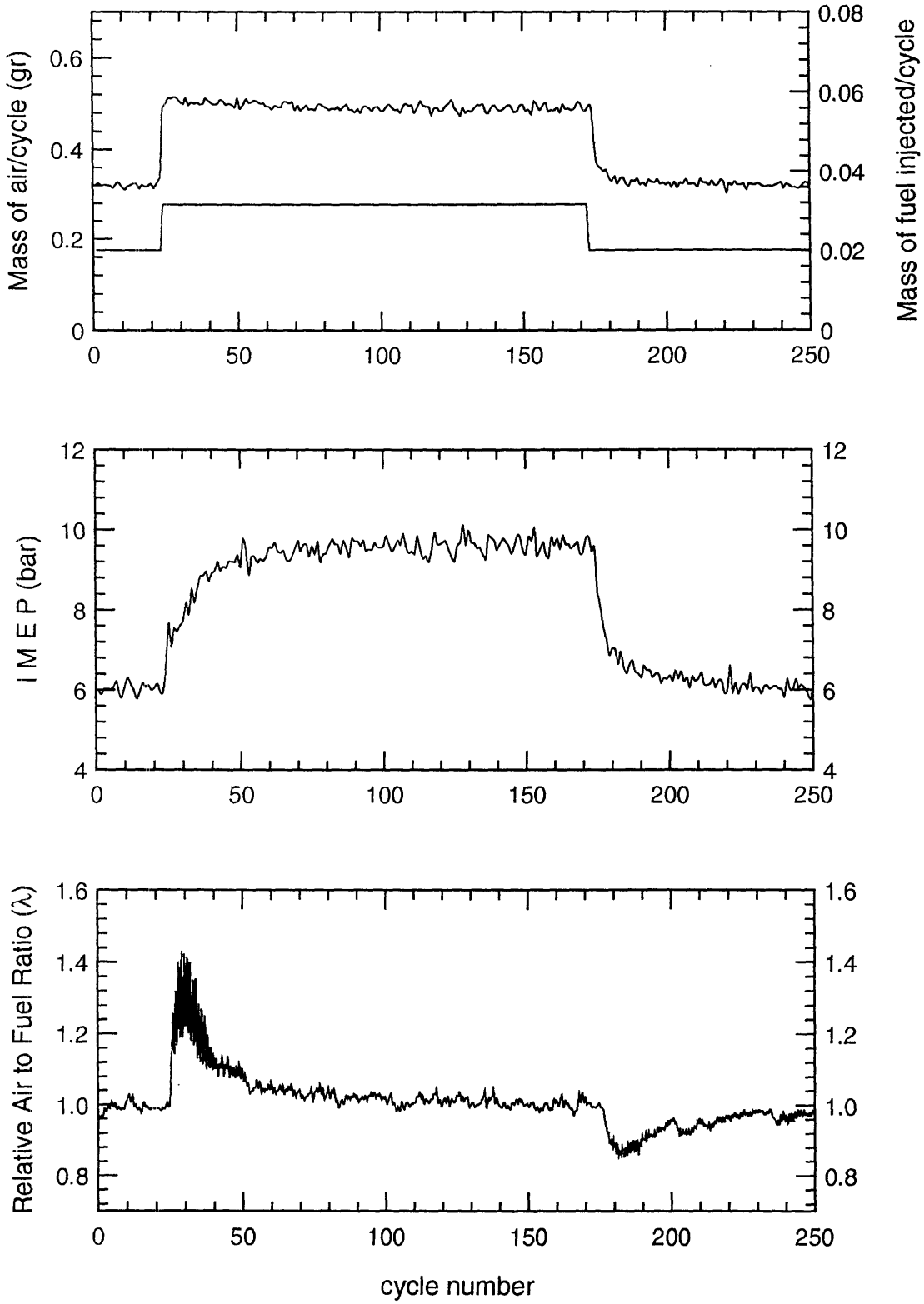

INDOLENE λ=0.9 @ 40°C

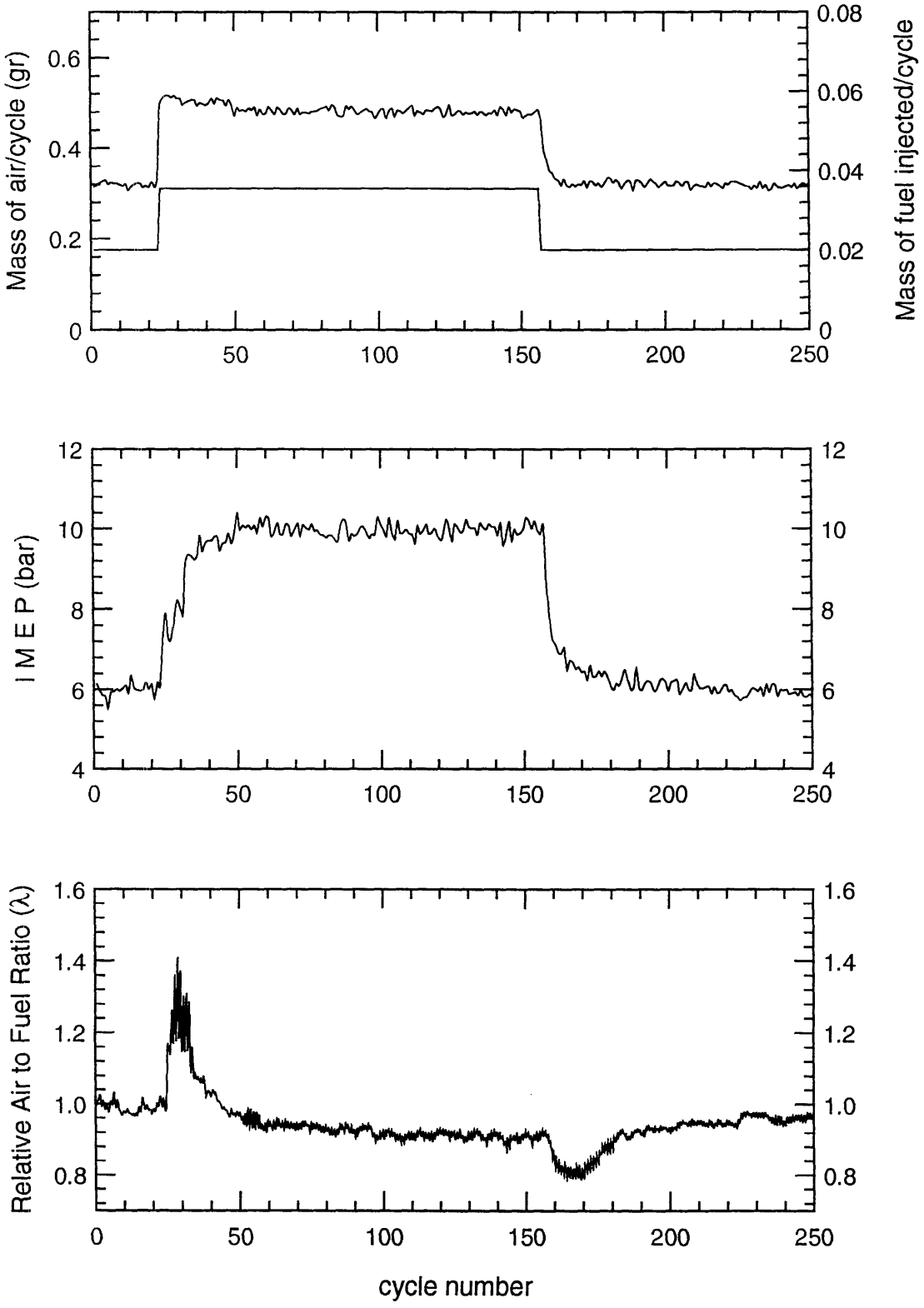

INDOLENE λ=0.8 @ 40°C

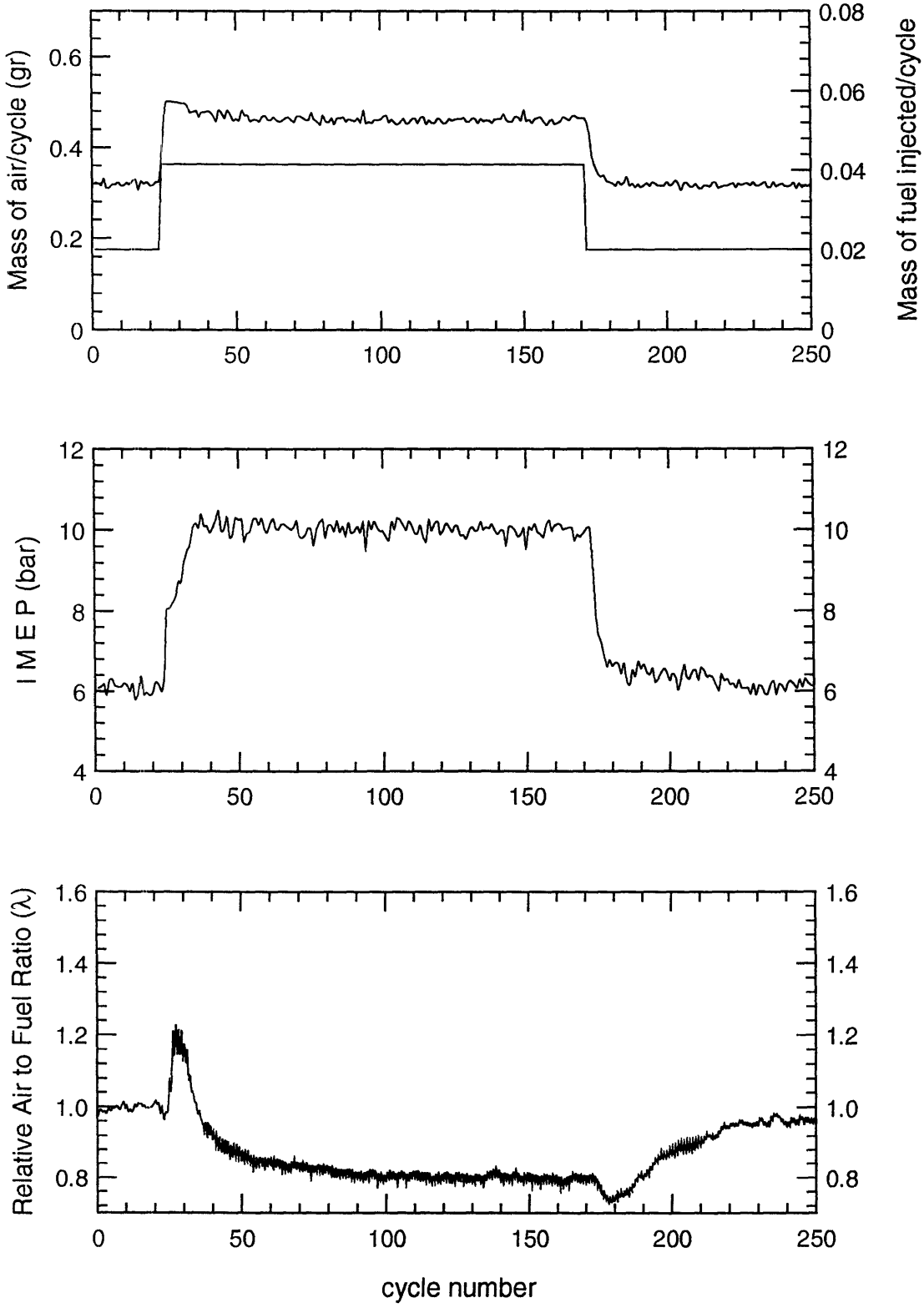

INDOLENE λ=1.0 @ 80°C

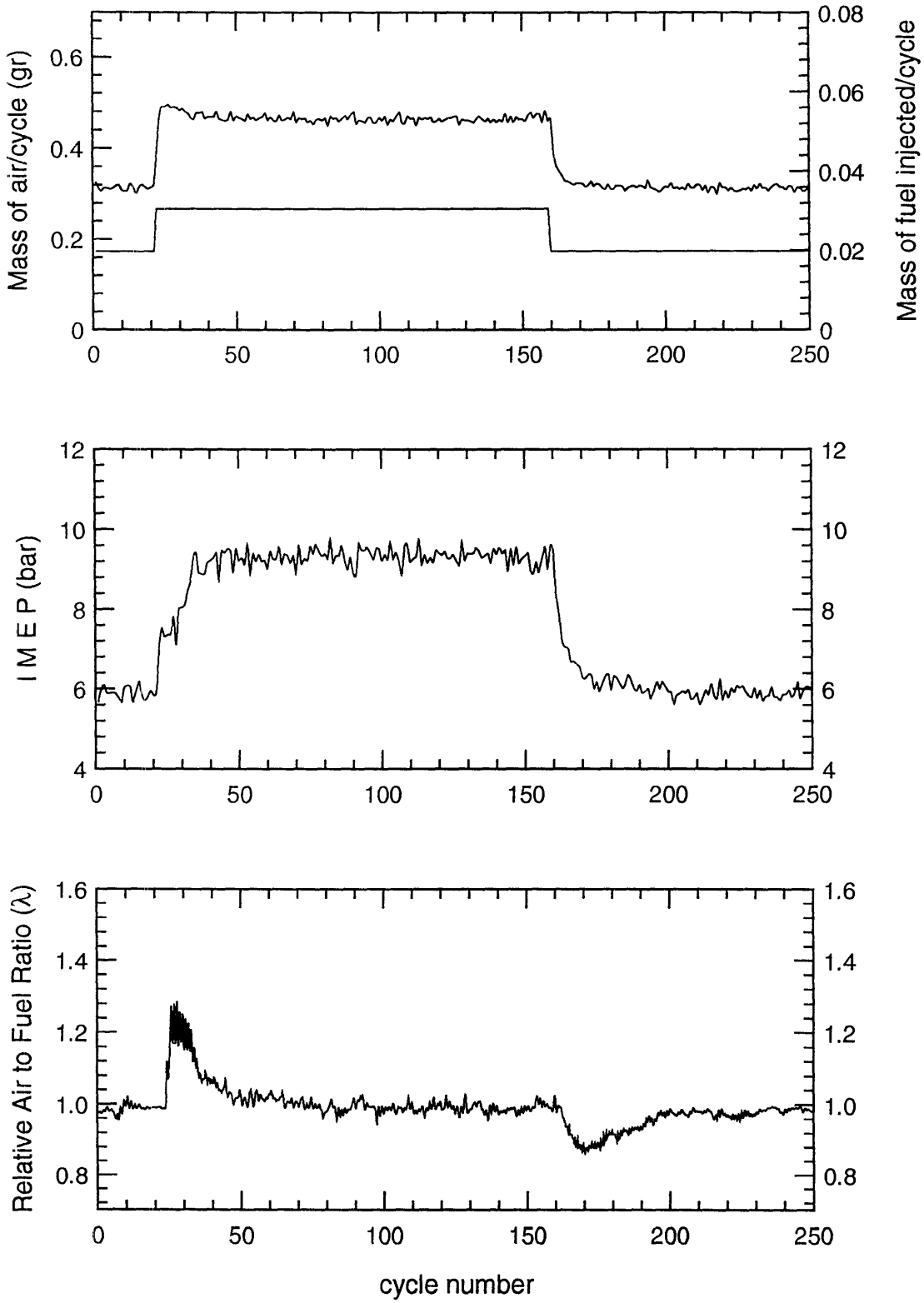

INDOLENE λ=0.9 @ 80°C

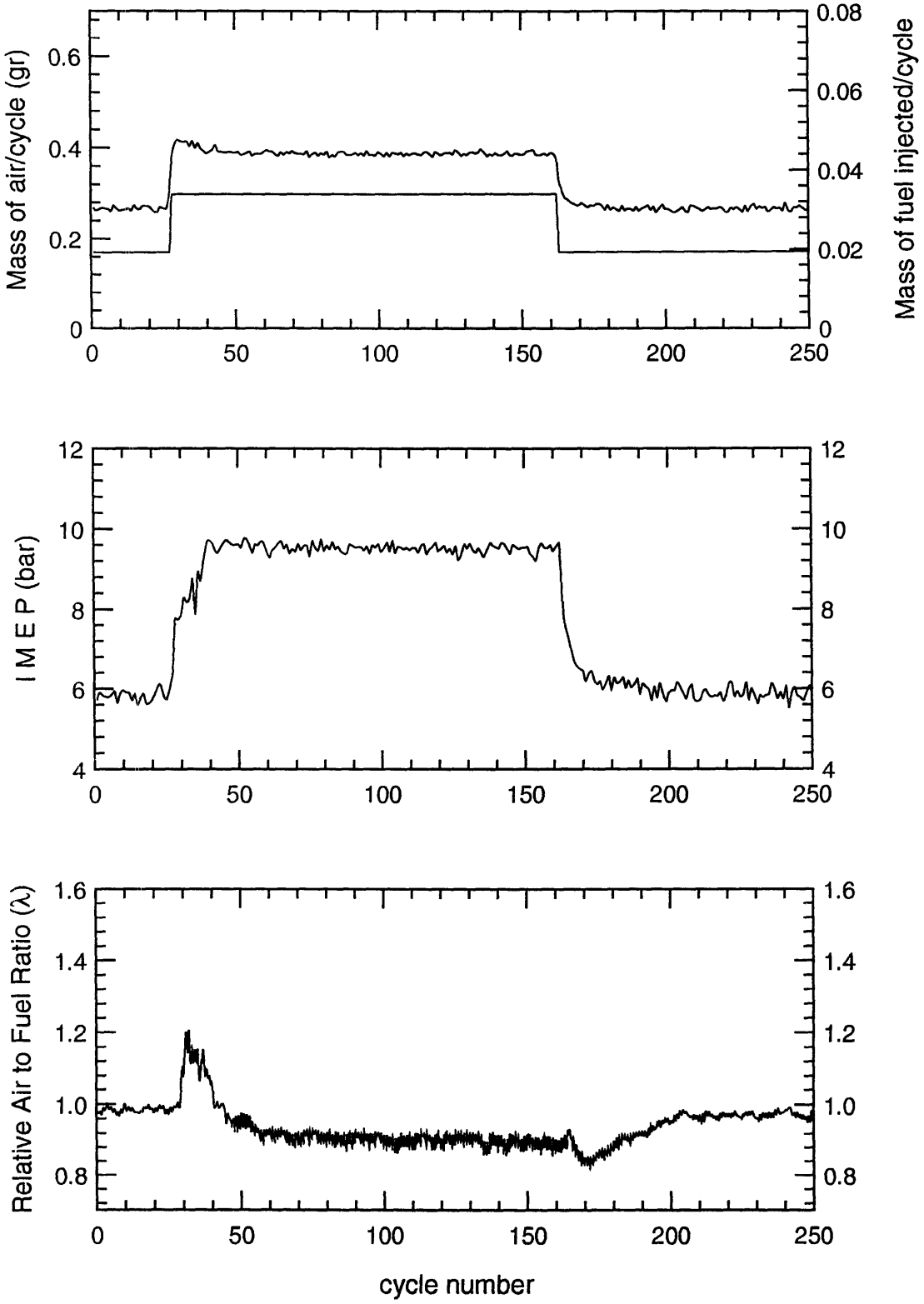

INDOLENE λ=0.8 @ 80°C

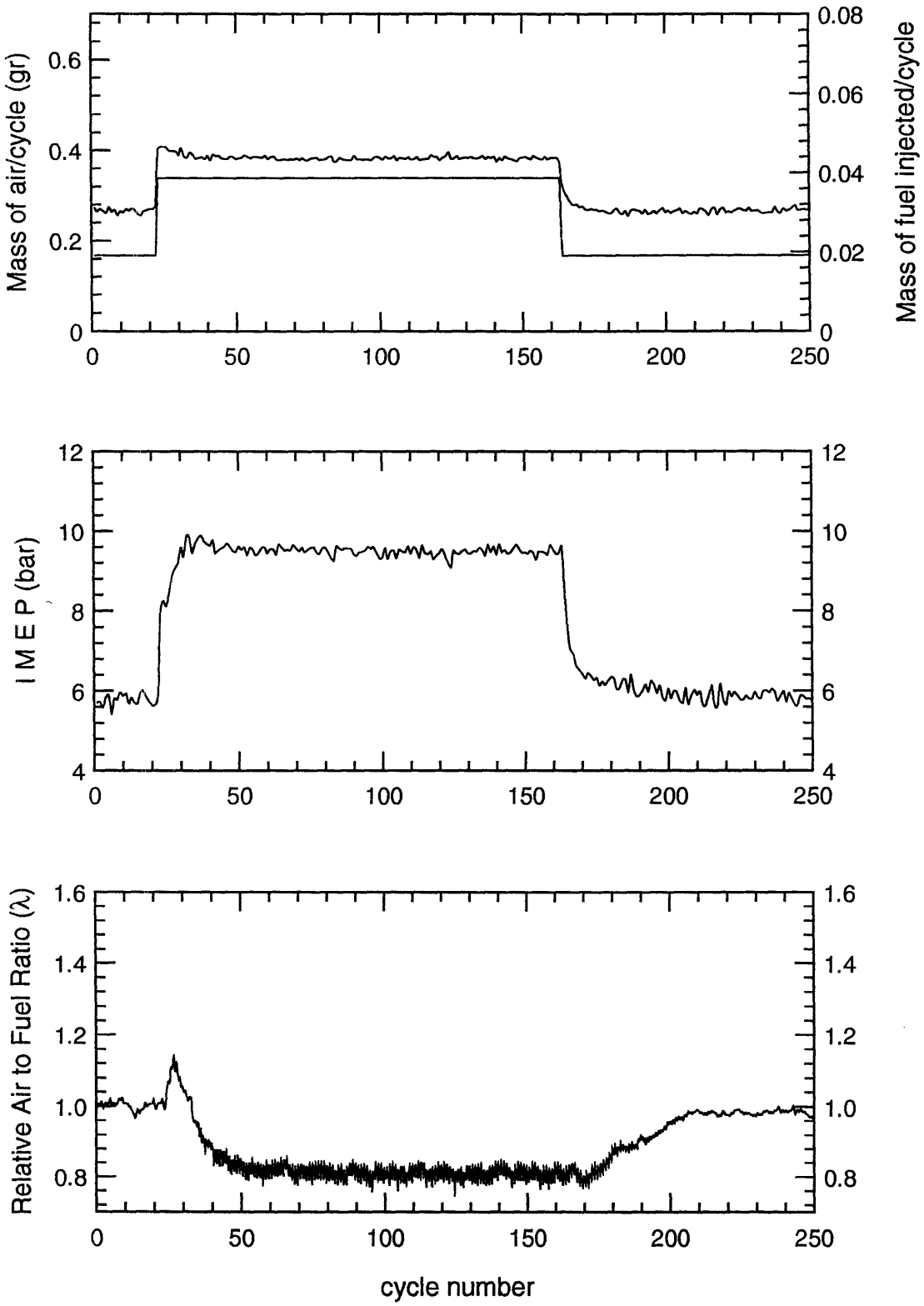

M10 λ=1.0 @ 40°C

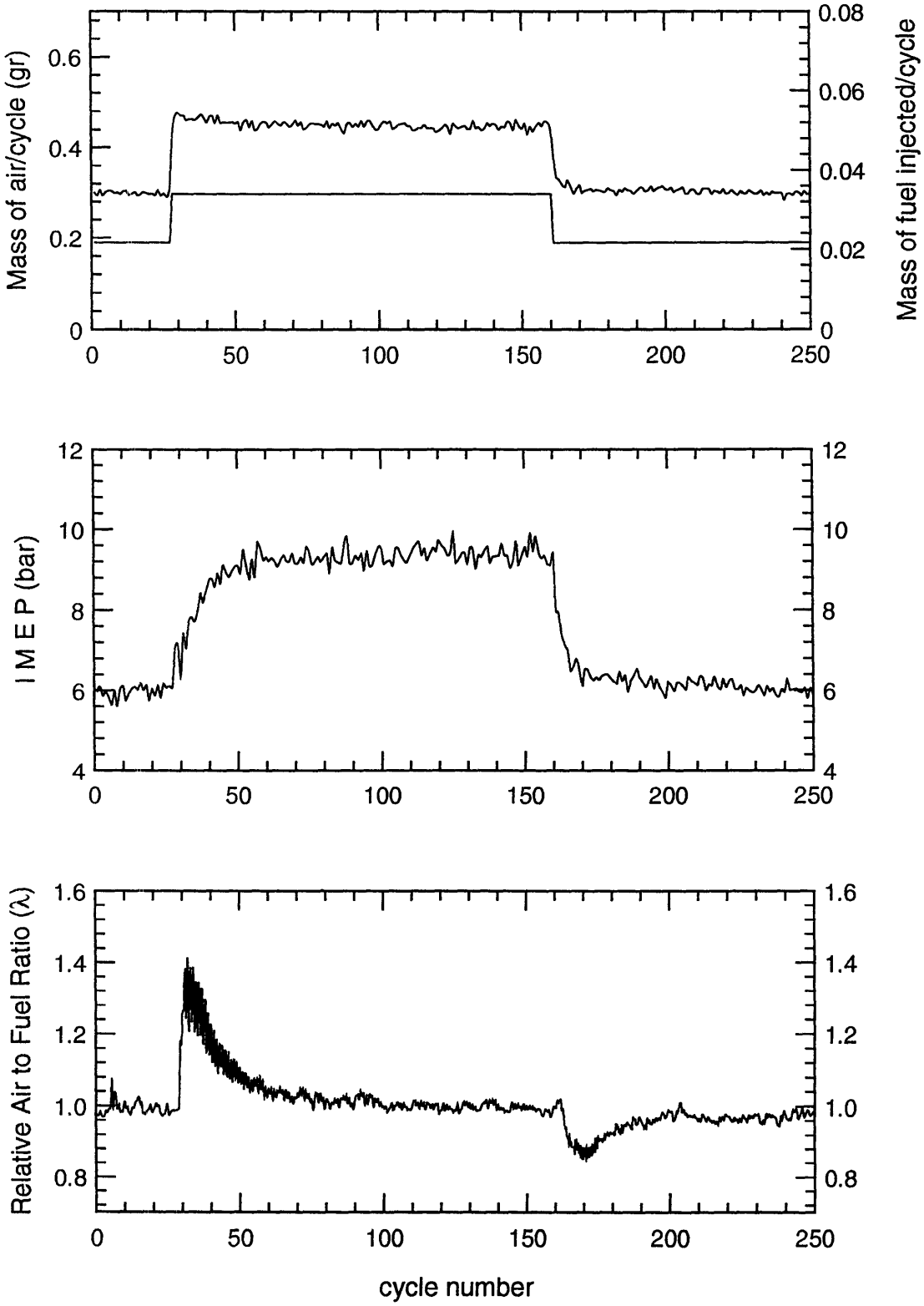
Mass of air/cycle (gr)
Mass of fuel injected/cycle
I M E P (bar)
Relative Air to Fuel Ratio (λ)
cycle number
0
50
100
150
200
250
0.2
0.4
0.6
0.02
0.04
0.06
0.08
4
6
8
10
12
0.8
1.0
1.2
1.4
1.6

M10 λ=0.9 @ 40°C

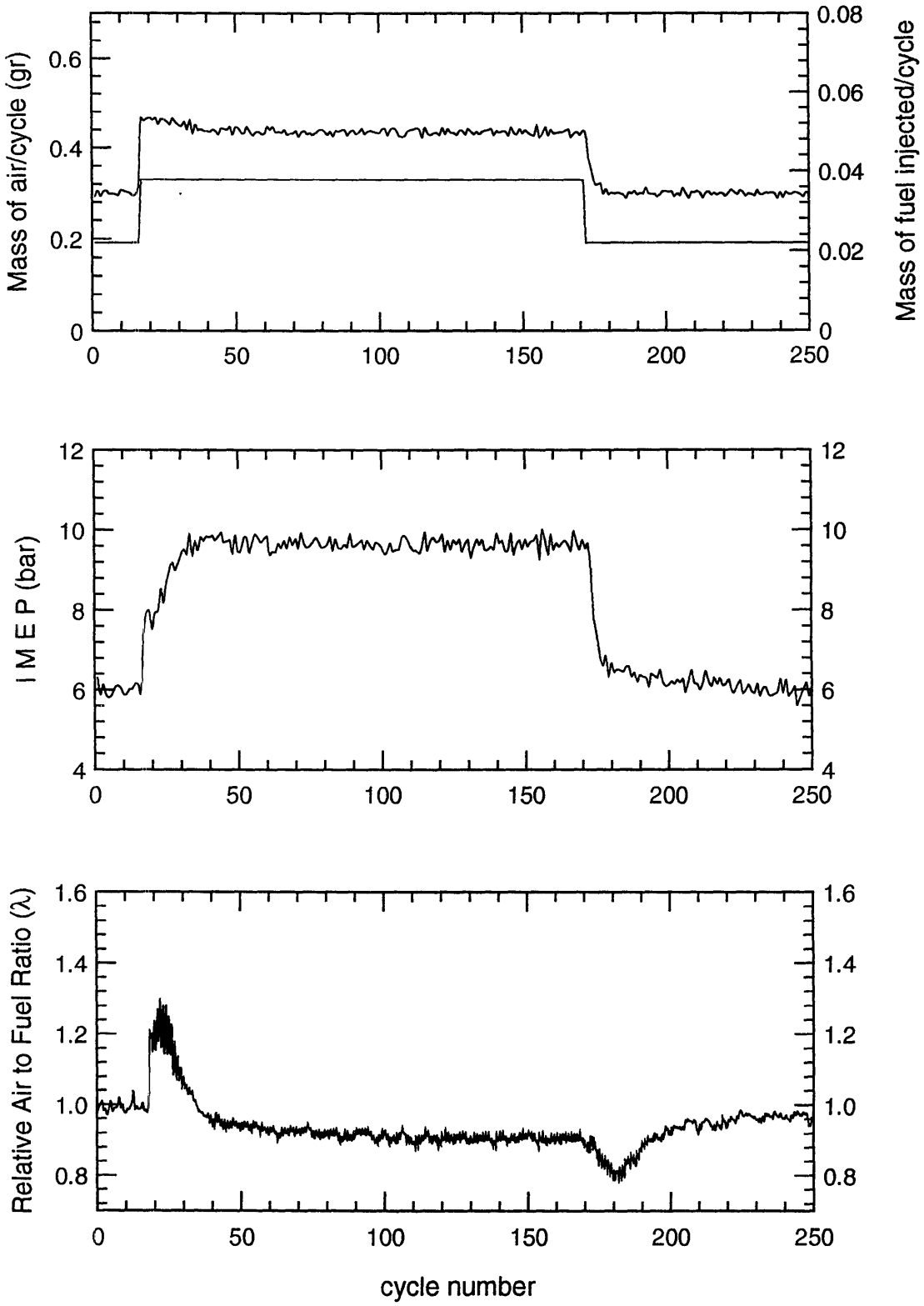
Mass of air/cycle (gr)
0.6
0.4
0.2
0
0.08
0.06
0.04
0.02
0
Mass of fuel injected/cycle
0
50
100
150
200
250
I M E P (bar)
12
10
8
6
4
Relative Air to Fuel Ratio (λ)
1.6
1.4
1.2
1.0
0.8
cycle number

M10 λ=0.8 @ 40°C

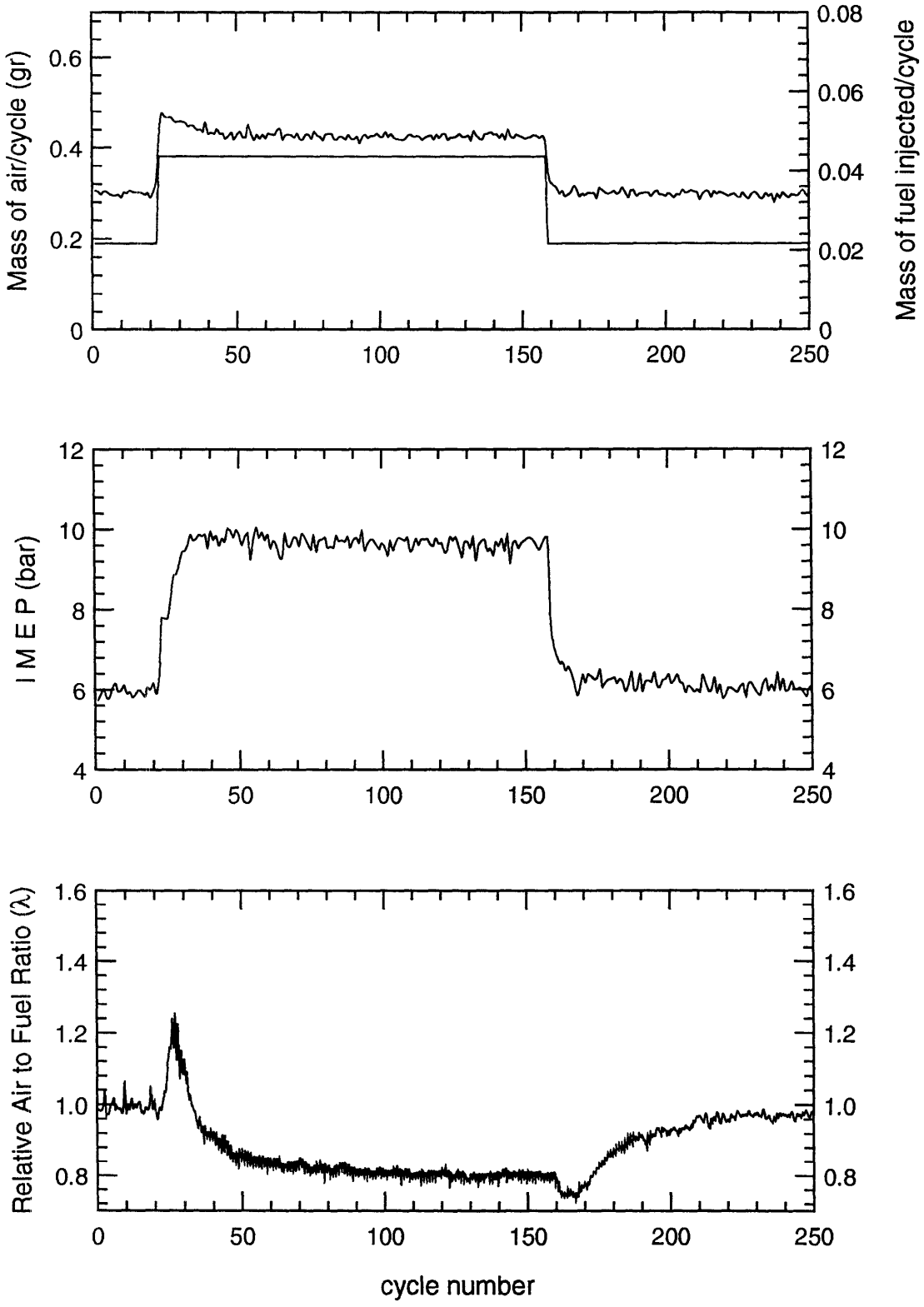
Mass of air/cycle (gr)
Mass of fuel injected/cycle
I M E P (bar)
Relative Air to Fuel Ratio (λ)
cycle number
0
50
100
150
200
250
0.2
0.4
0.6
0.02
0.04
0.06
0.08
4
6
8
10
12
0.8
1.0
1.2
1.4
1.6

M10 λ=1.0 @ 80°C

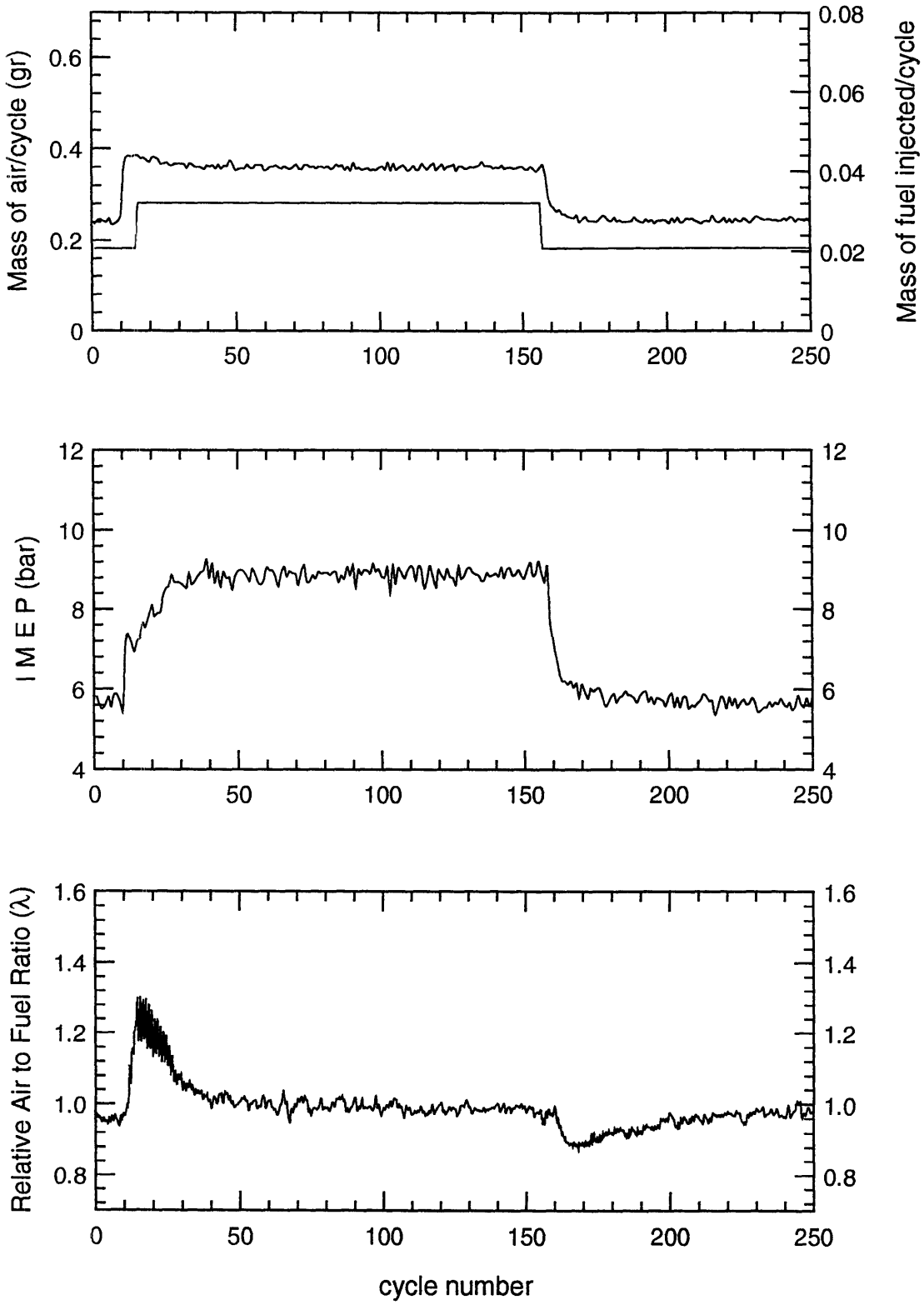
Mass of air/cycle (gr)
Mass of fuel injected/cycle
I M E P (bar)
Relative Air to Fuel Ratio (λ)
cycle number
0
50
100
150
200
250
0.2
0.4
0.6
0.02
0.04
0.06
0.08
4
6
8
10
12
0.8
1.0
1.2
1.4
1.6

M10 λ=0.9 @ 80°C

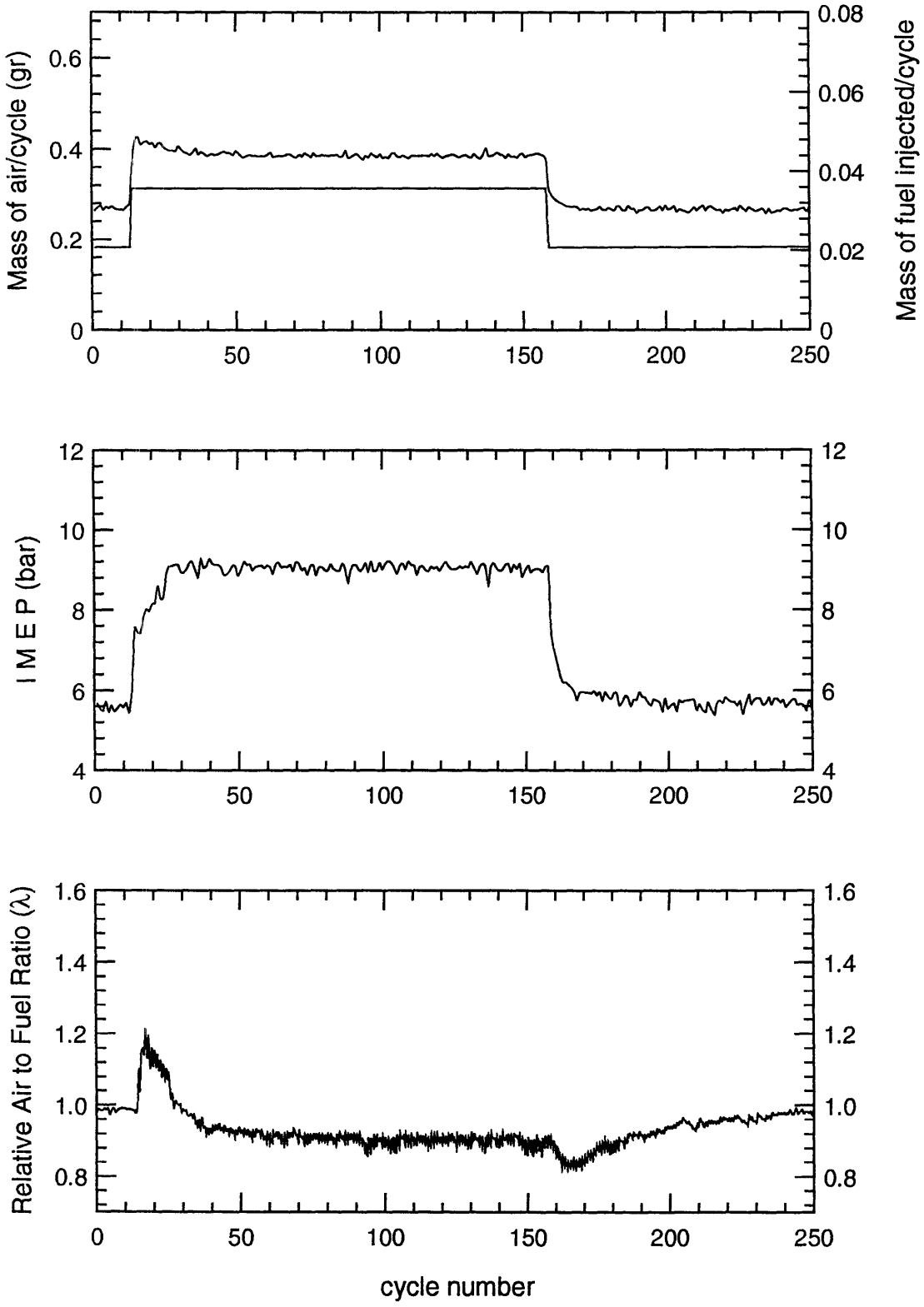
Mass of air/cycle (gr)
Mass of fuel injected/cycle
I M E P (bar)
Relative Air to Fuel Ratio (λ)
cycle number
0
50
100
150
200
250
0.2
0.4
0.6
0.02
0.04
0.06
0.08
4
6
8
10
12
0.8
1.0
1.2
1.4
1.6

M10 λ=0.8 @ 80°C

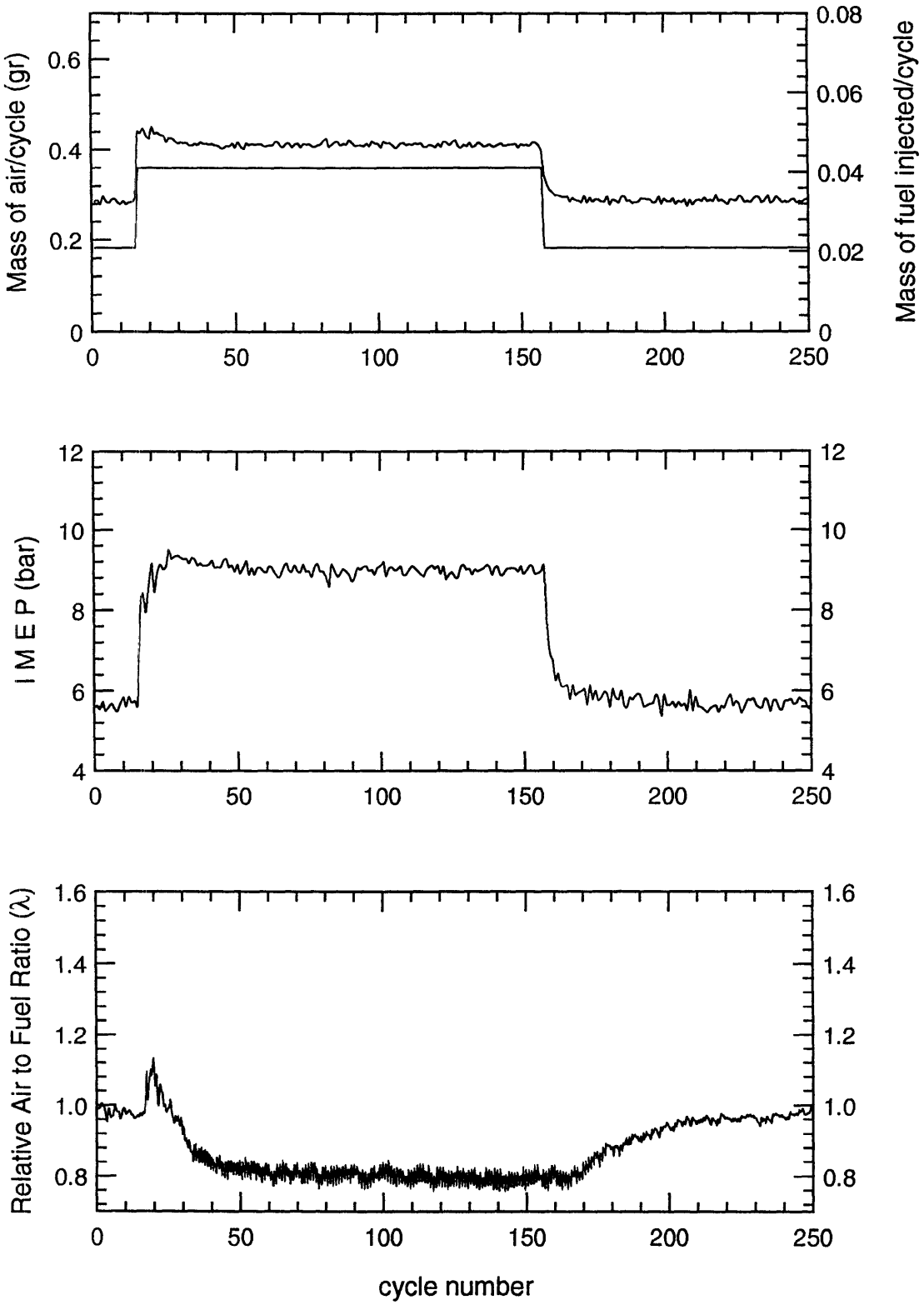
Mass of air/cycle (gr)
0
0.2
0.4
0.6
Mass of fuel injected/cycle
0
0.02
0.04
0.06
0.08
0
50
100
150
200
250
I M E P (bar)
4
6
8
10
12
Relative Air to Fuel Ratio (λ)
0.8
1.0
1.2
1.4
1.6
cycle number

M25 λ=1.0 @ 40°C

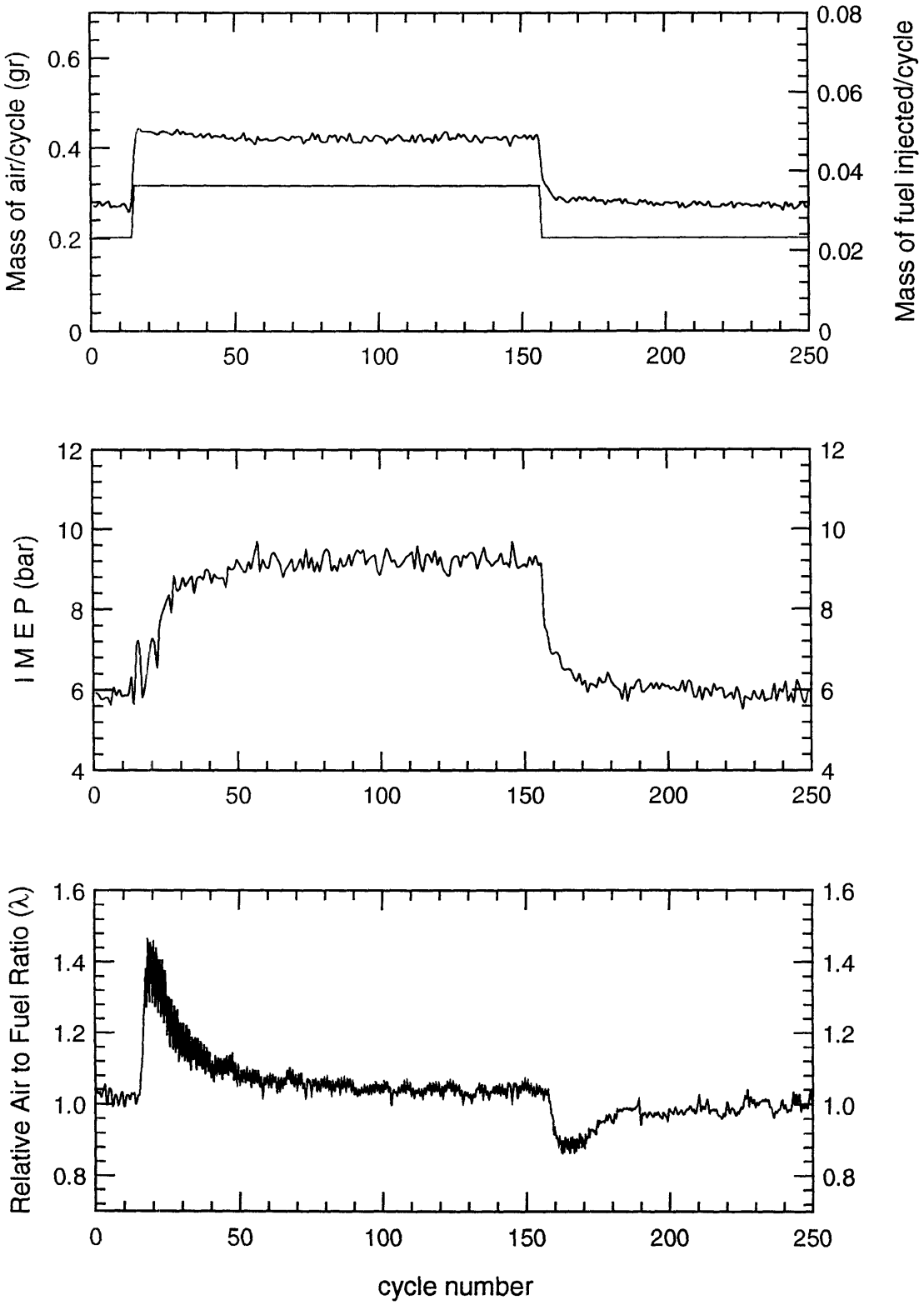
Mass of air/cycle (gr)
Mass of fuel injected/cycle
I M E P (bar)
Relative Air to Fuel Ratio (λ)
cycle number
0
50
100
150
200
250
0.2
0.4
0.6
0.02
0.04
0.06
0.08
4
6
8
10
12
0.8
1.0
1.2
1.4
1.6

M25 λ=0.9 @ 40°C

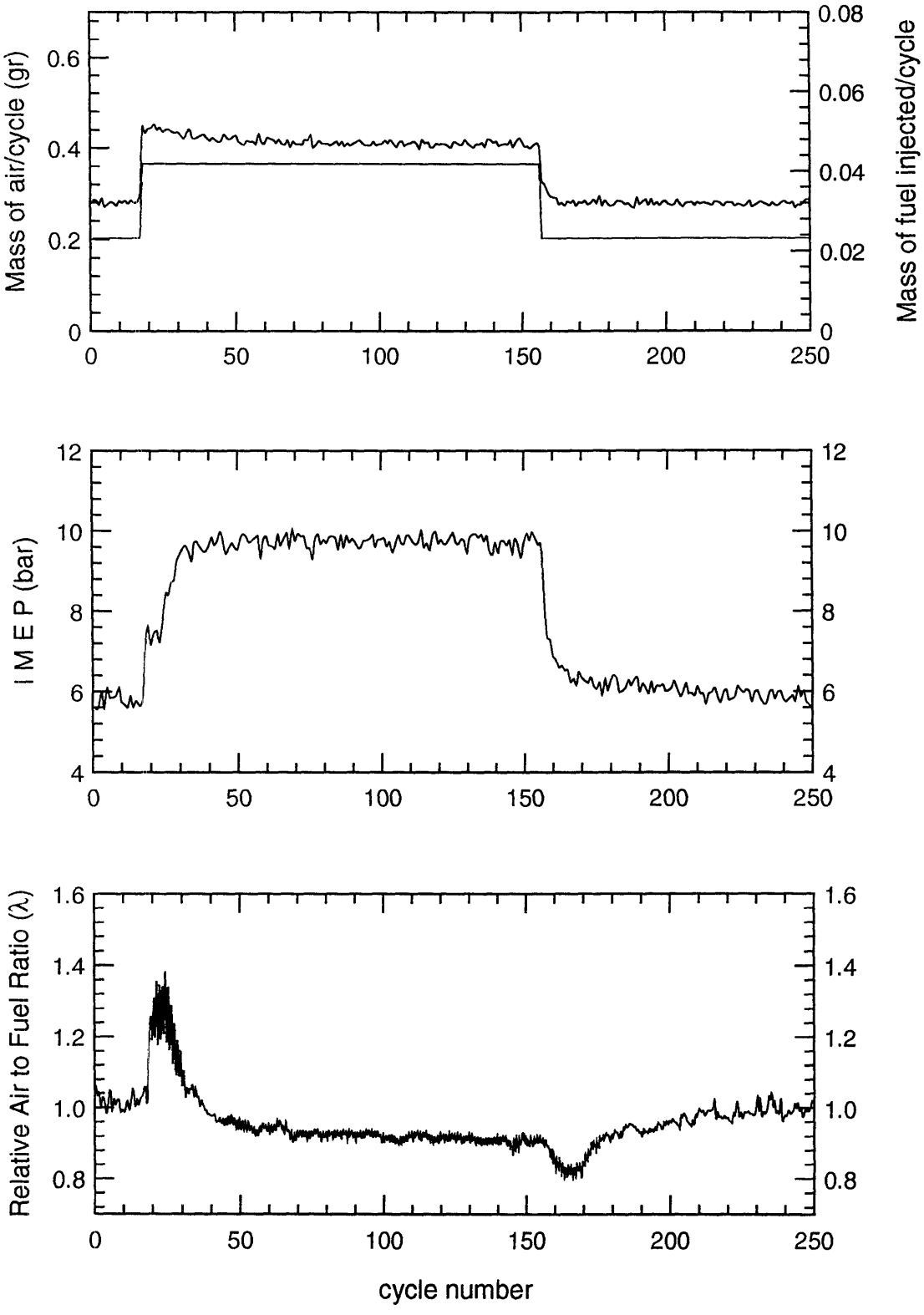
Mass of air/cycle (gr)
Mass of fuel injected/cycle
I M E P (bar)
Relative Air to Fuel Ratio (λ)
cycle number
0
50
100
150
200
250
0.2
0.4
0.6
0.02
0.04
0.06
0.08
4
6
8
10
12
0.8
1.0
1.2
1.4
1.6

M25 λ=0.8 @ 40°C

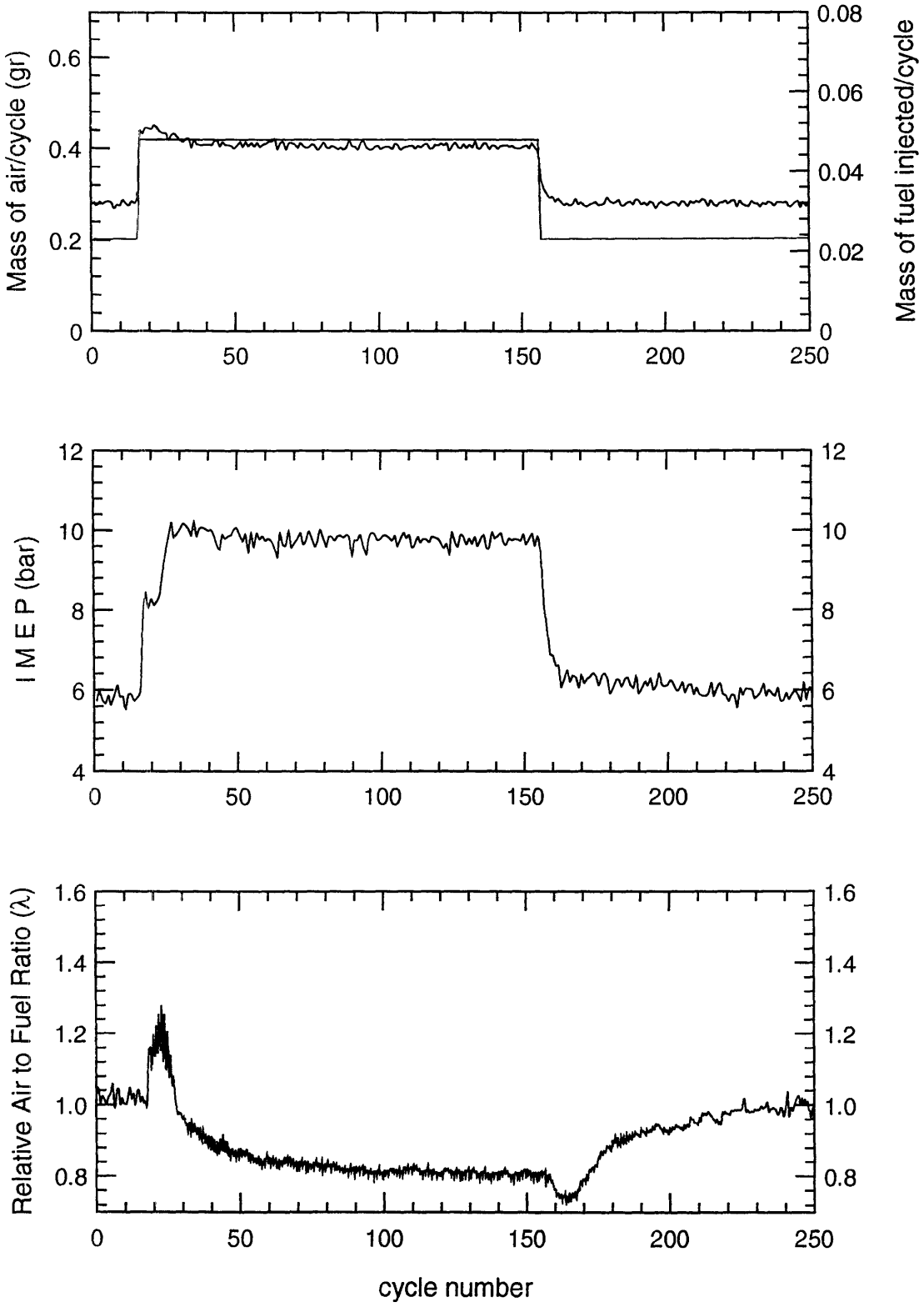
Mass of air/cycle (gr)
Mass of fuel injected/cycle
I M E P (bar)
Relative Air to Fuel Ratio (λ)
cycle number
0
50
100
150
200
250
0.2
0.4
0.6
0.02
0.04
0.06
0.08
4
6
8
10
12
0.8
1.0
1.2
1.4
1.6

M25 λ=1.0 @ 80°C

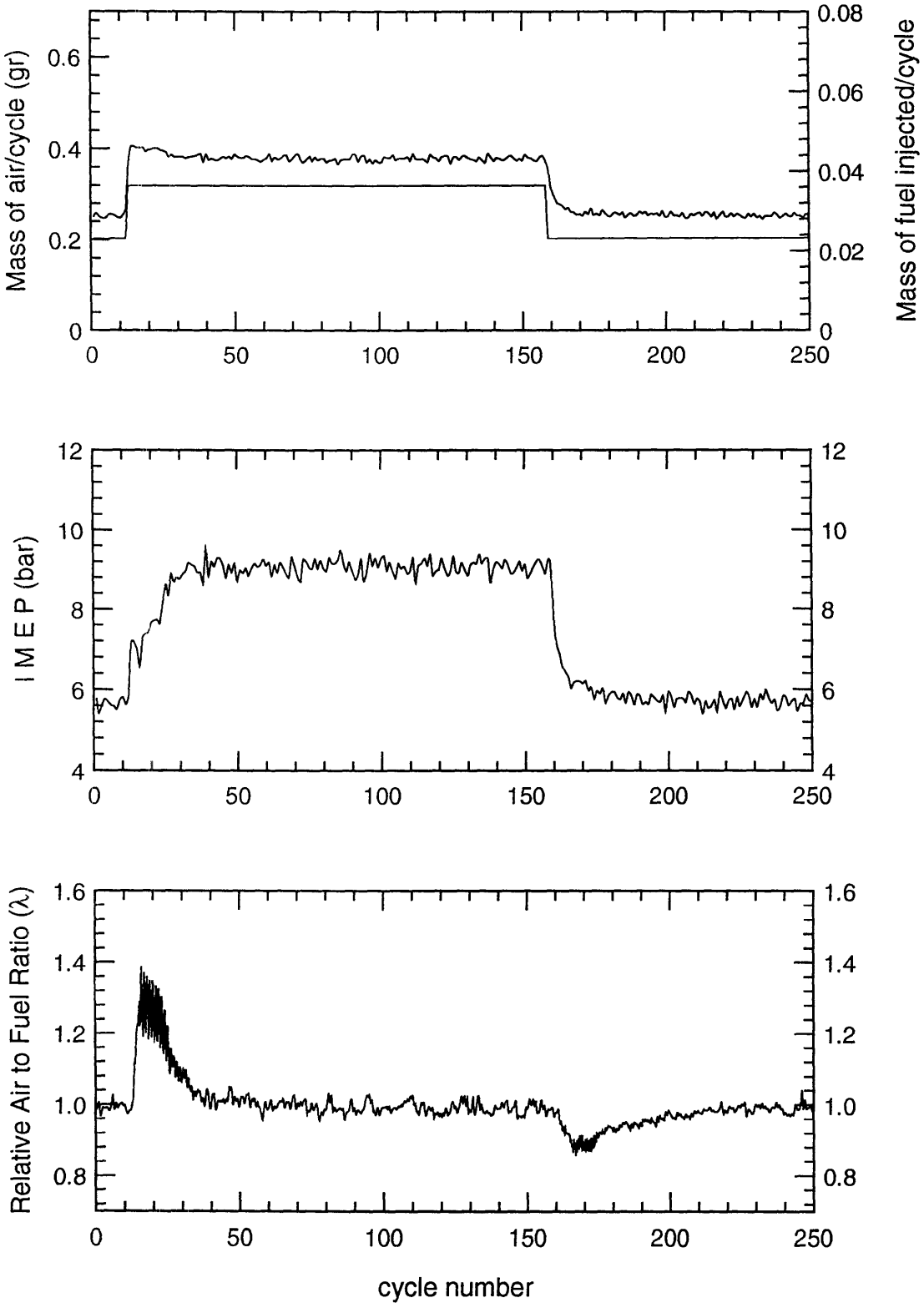
Mass of air/cycle (gr)
Mass of fuel injected/cycle
I M E P (bar)
Relative Air to Fuel Ratio (λ)
cycle number
0
50
100
150
200
250
0.2
0.4
0.6
0.02
0.04
0.06
0.08
4
6
8
10
12
0.8
1.0
1.2
1.4
1.6

M25 λ=0.9 @ 80°C

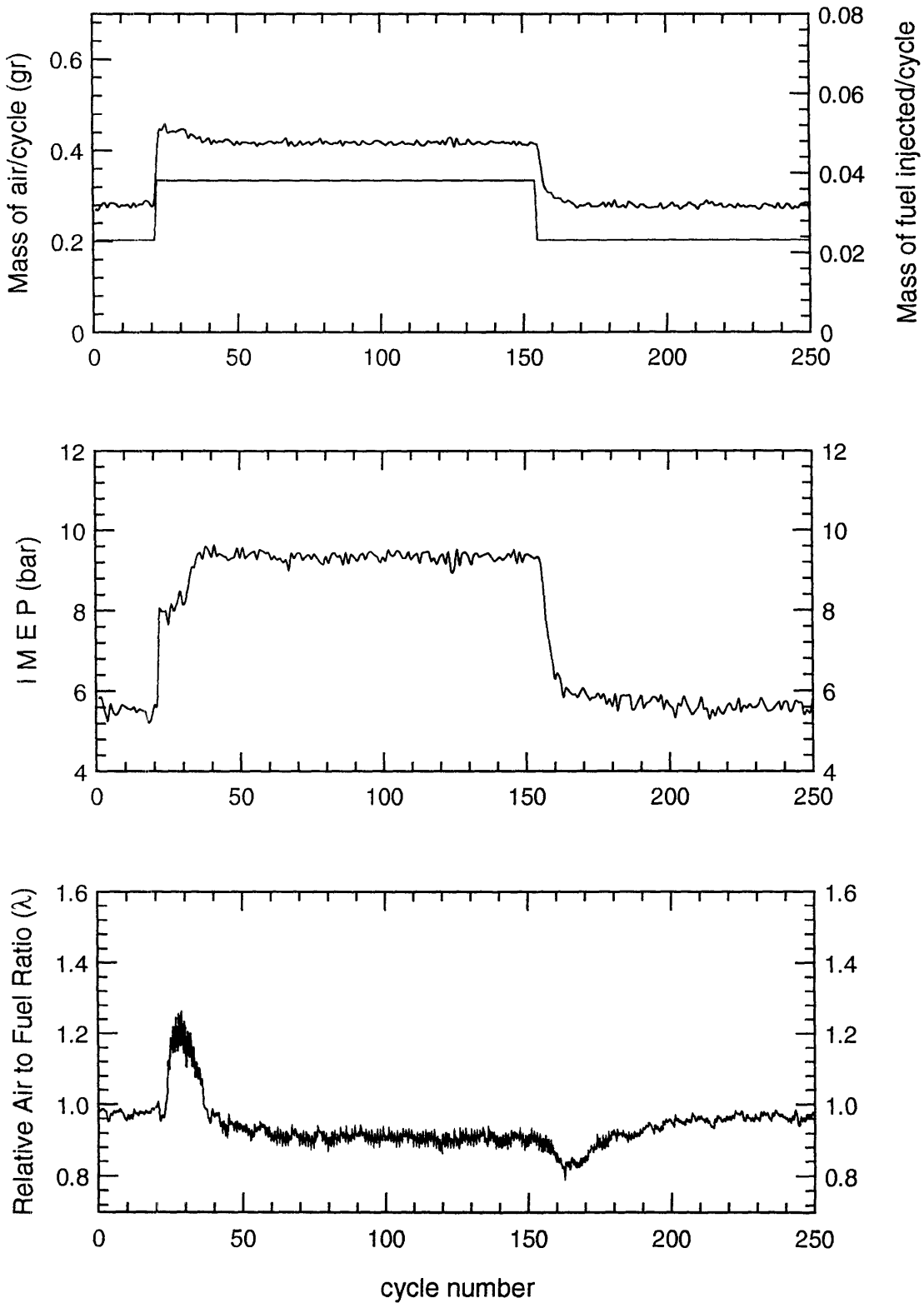
Mass of air/cycle (gr)
Mass of fuel injected/cycle
I M E P (bar)
Relative Air to Fuel Ratio (λ)
cycle number
0
50
100
150
200
250
0.2
0.4
0.6
0.02
0.04
0.06
0.08
4
6
8
10
12
0.8
1.0
1.2
1.4
1.6

M25 λ=0.8 @ 80°C

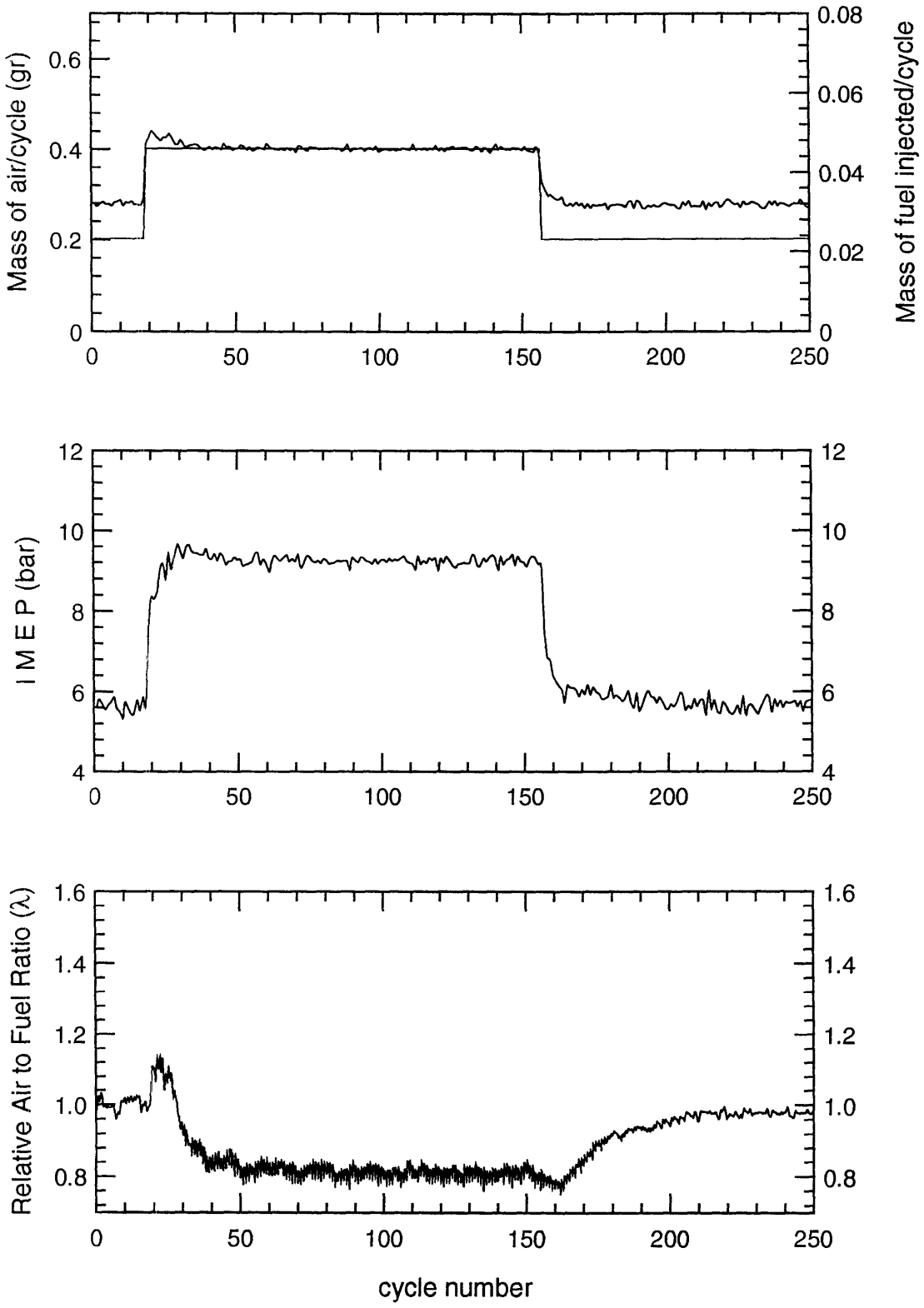
Mass of air/cycle (gr)
Mass of fuel injected/cycle
I M E P (bar)
Relative Air to Fuel Ratio (λ)
cycle number
0
50
100
150
200
250
0.2
0.4
0.6
0.02
0.04
0.06
0.08
4
6
8
10
12
0.8
1.0
1.2
1.4
1.6

M40 λ=1.0 @ 40°C

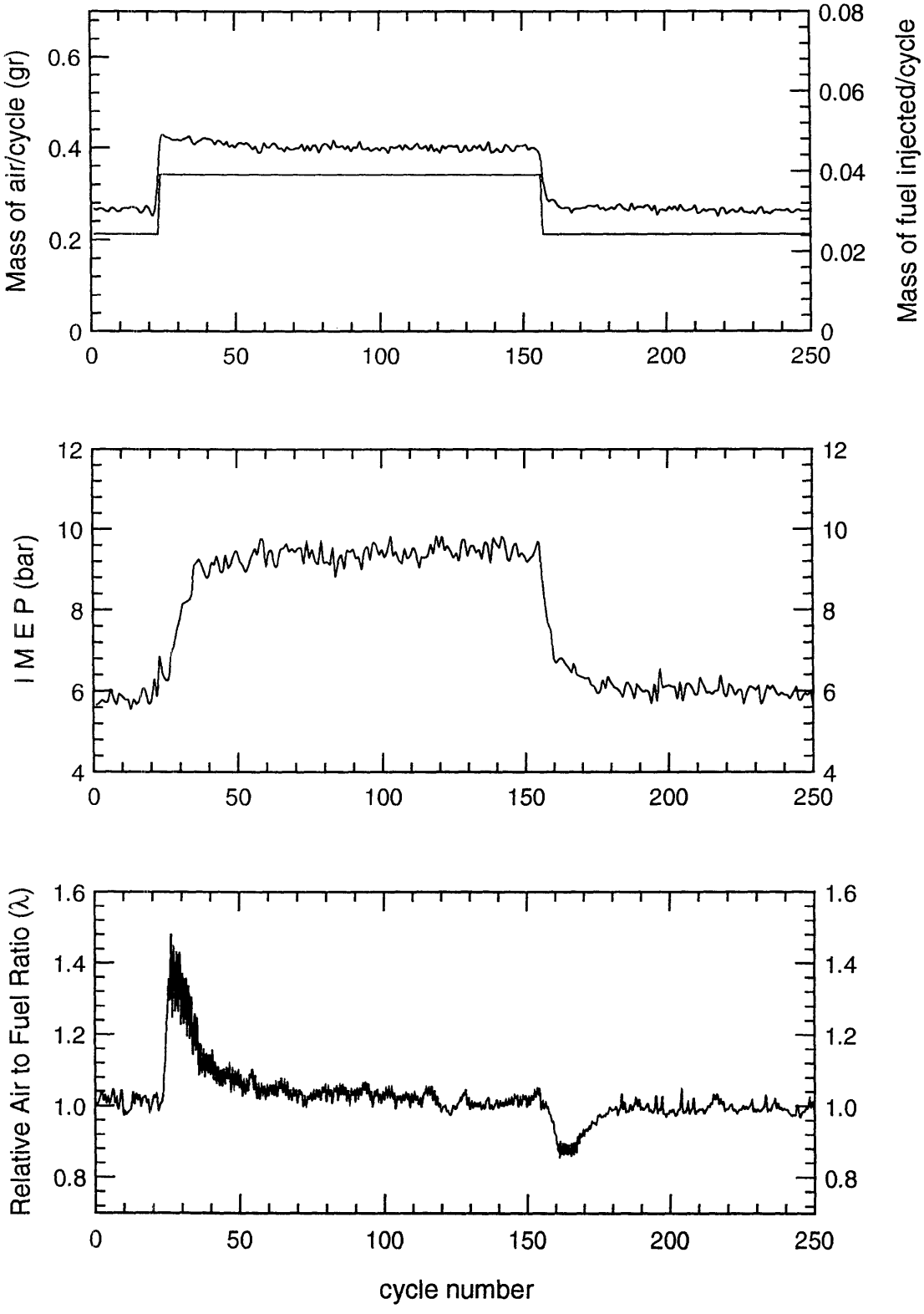
Mass of air/cycle (gr)
0
0.2
0.4
0.6
Mass of fuel injected/cycle
0
0.02
0.04
0.06
0.08
0
50
100
150
200
250
I M E P (bar)
4
6
8
10
12
Relative Air to Fuel Ratio (λ)
0.8
1.0
1.2
1.4
1.6
cycle number

M40 λ=0.9 @ 40°C

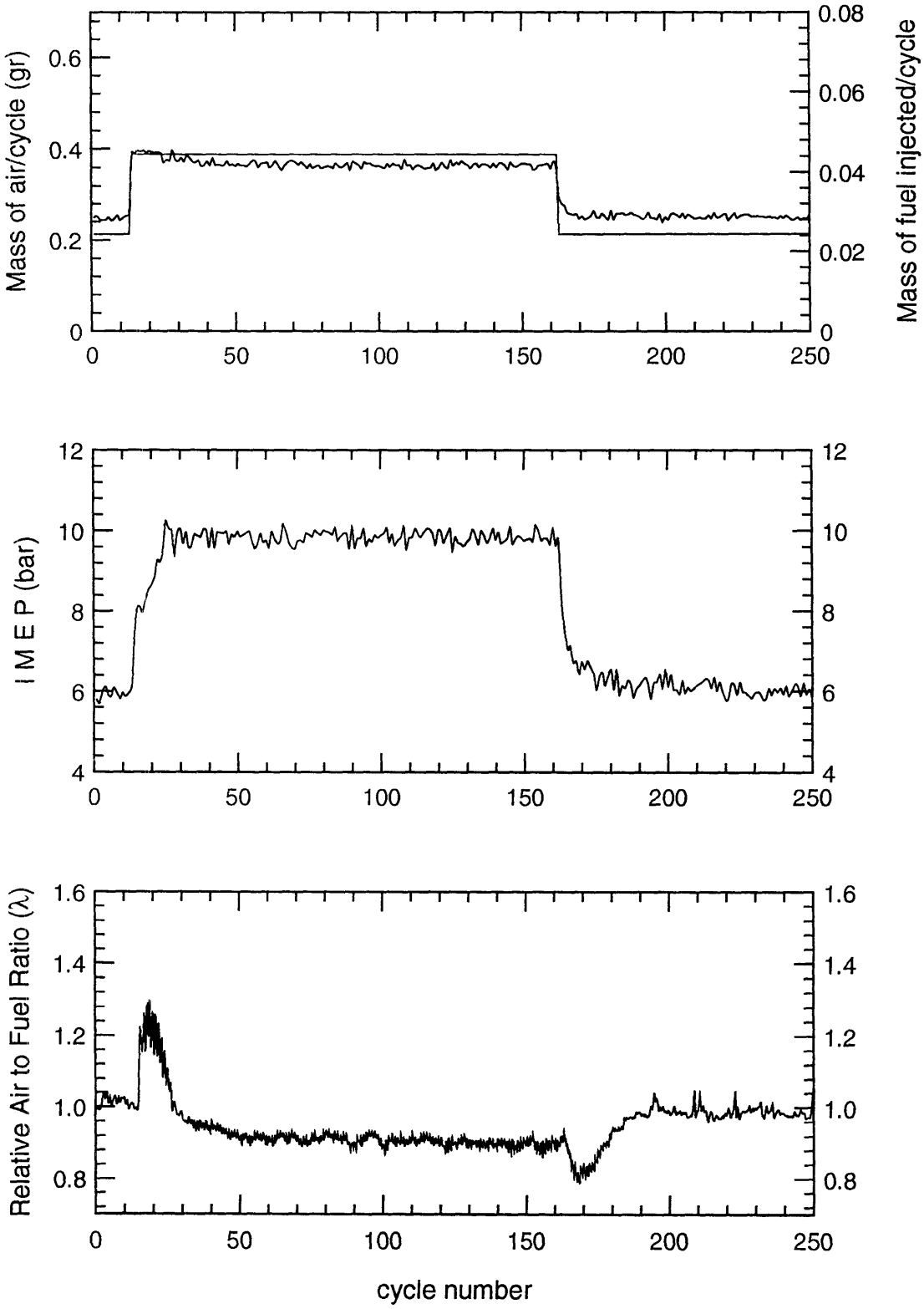
Mass of air/cycle (gr)
Mass of fuel injected/cycle
I M E P (bar)
Relative Air to Fuel Ratio (λ)
cycle number
0
50
100
150
200
250
0.2
0.4
0.6
0.02
0.04
0.06
0.08
4
6
8
10
12
0.8
1.0
1.2
1.4
1.6

M40 λ=0.8 @ 40°C

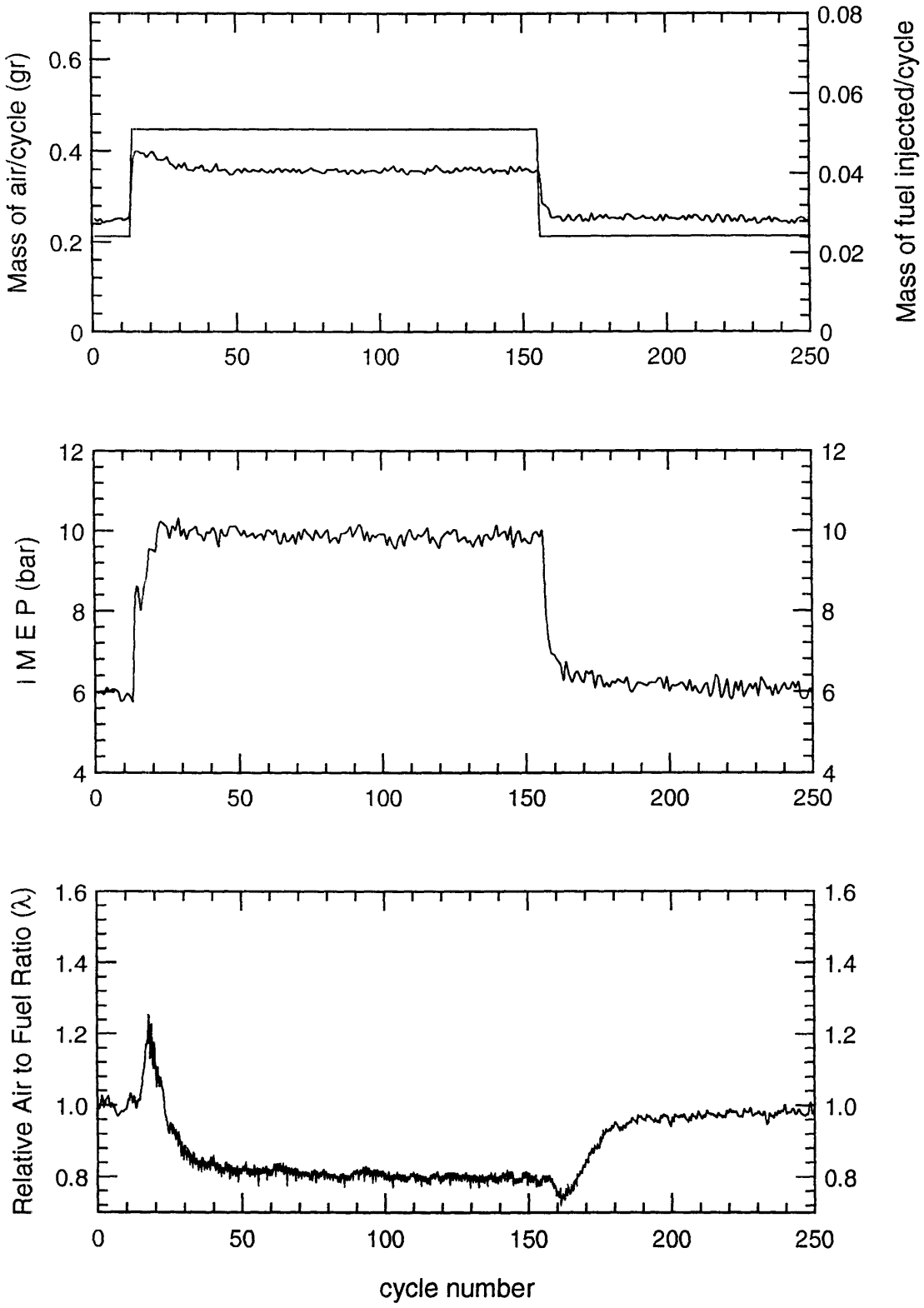
Mass of air/cycle (gr)
Mass of fuel injected/cycle
I M E P (bar)
Relative Air to Fuel Ratio (λ)
cycle number
0
50
100
150
200
250
0.2
0.4
0.6
0.02
0.04
0.06
0.08
4
6
8
10
12
0.8
1.0
1.2
1.4
1.6

M40 λ=1.0 @ 80°C

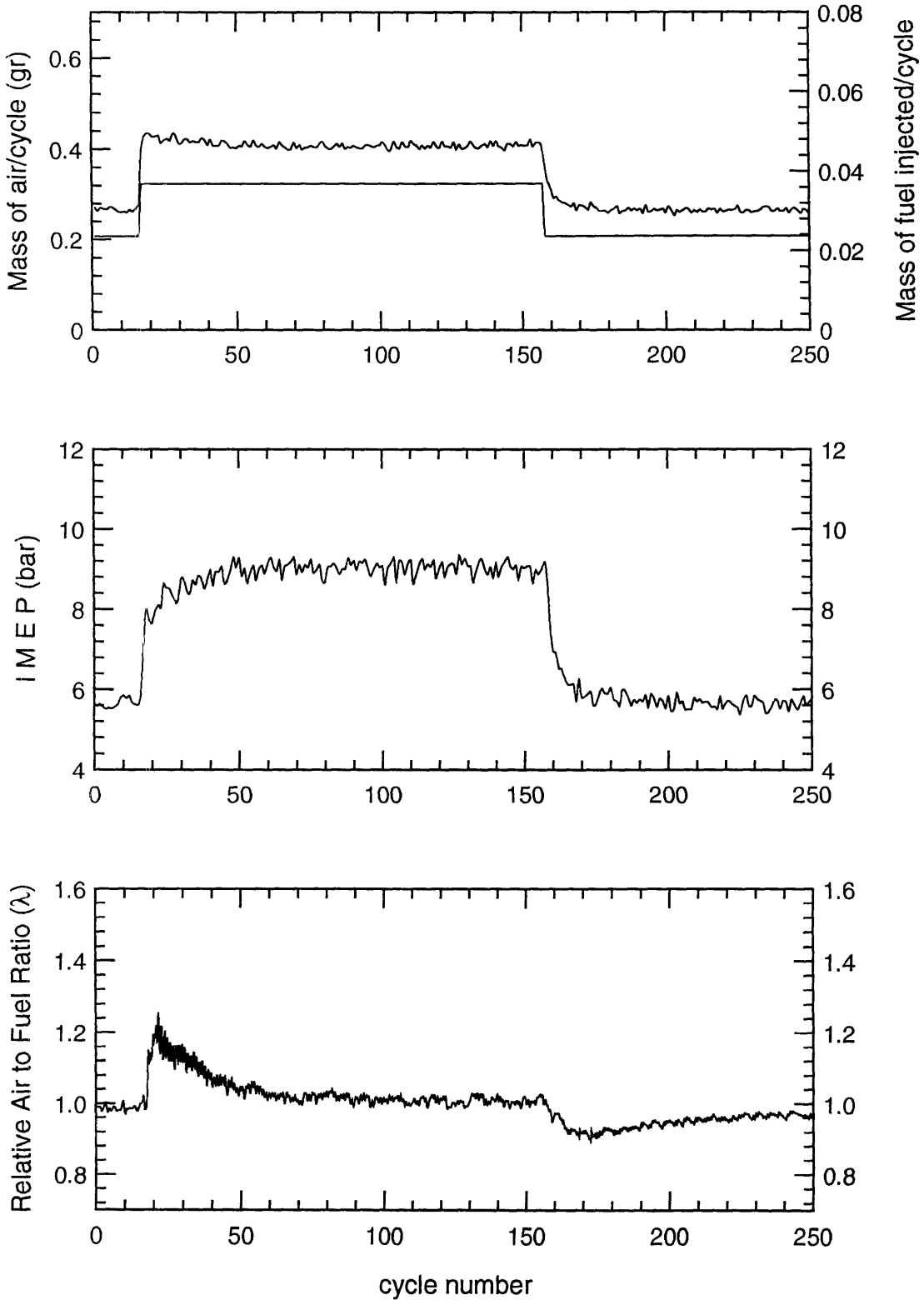
Mass of air/cycle (gr)
Mass of fuel injected/cycle
I M E P (bar)
Relative Air to Fuel Ratio (λ)
cycle number
0
50
100
150
200
250
0.2
0.4
0.6
0.02
0.04
0.06
0.08
4
6
8
10
12
0.8
1.0
1.2
1.4
1.6

M40 λ=0.9 @ 80°C

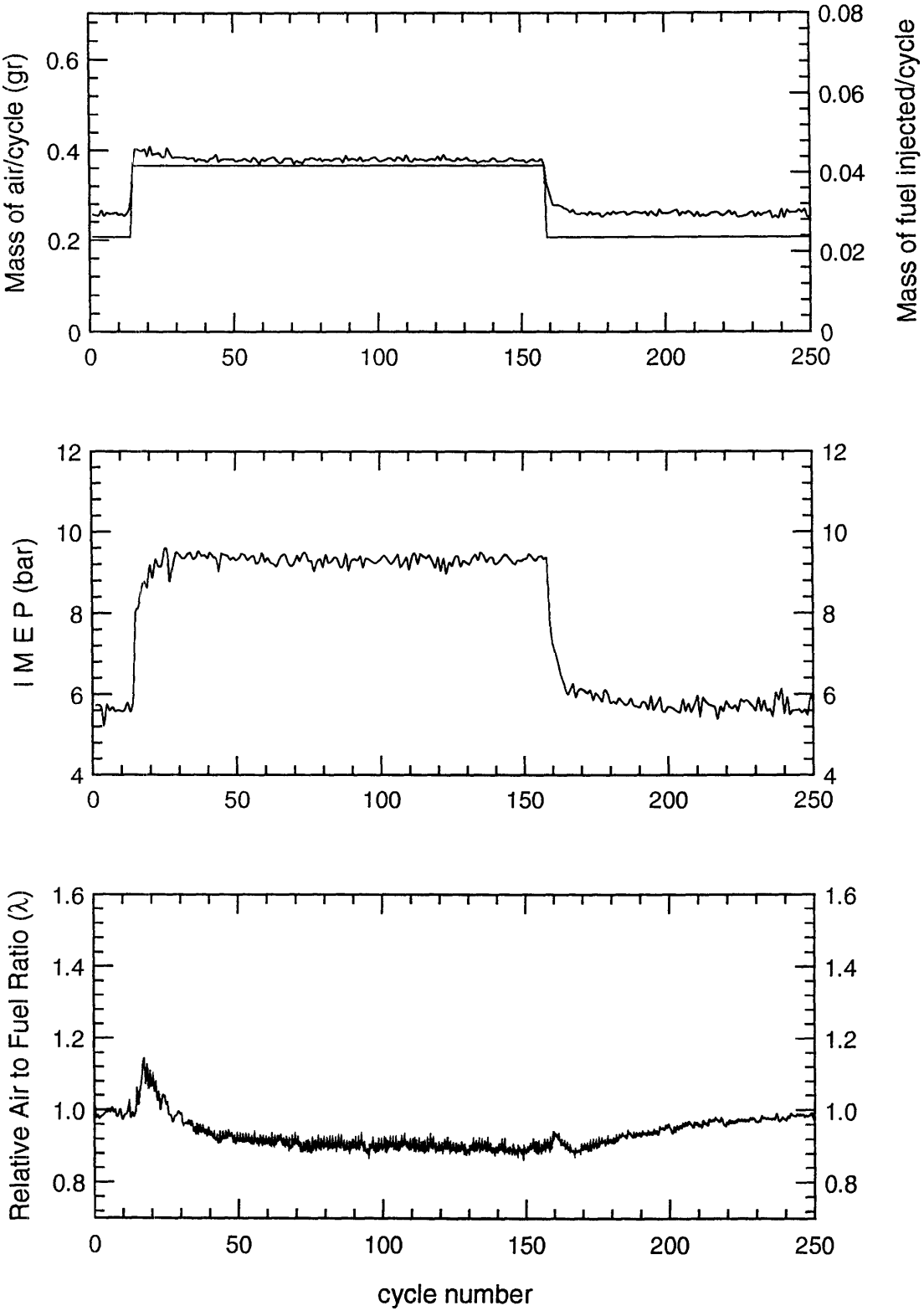
Mass of air/cycle (gr)
Mass of fuel injected/cycle
I M E P (bar)
Relative Air to Fuel Ratio (λ)
cycle number
0
50
100
150
200
250
0.2
0.4
0.6
0.02
0.04
0.06
0.08
4
6
8
10
12
0.8
1.0
1.2
1.4
1.6

M40 λ=0.8 @ 80°C

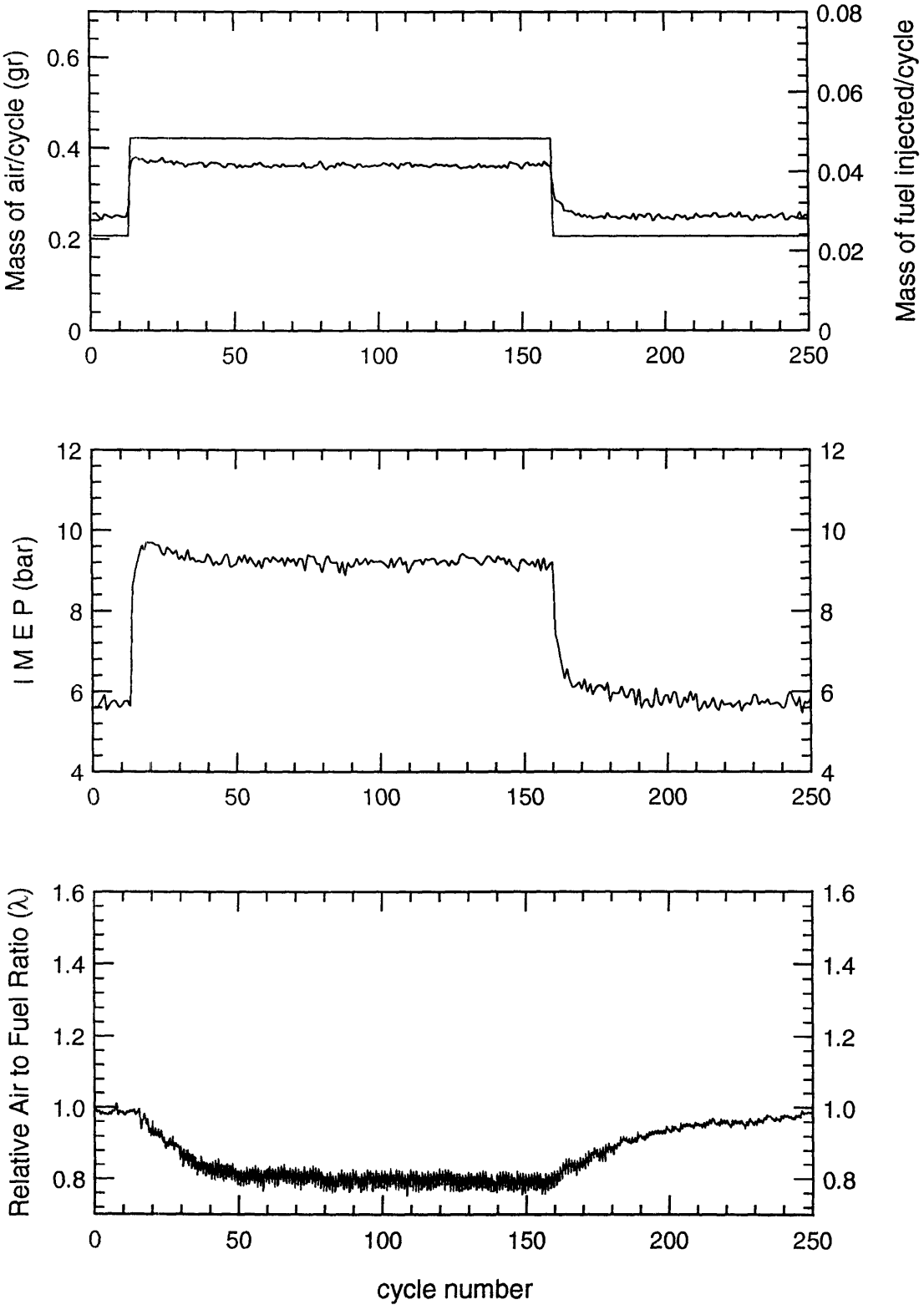
Mass of air/cycle (gr)
Mass of fuel injected/cycle
I M E P (bar)
Relative Air to Fuel Ratio (λ)
cycle number

M60 λ=1.0 @ 40°C

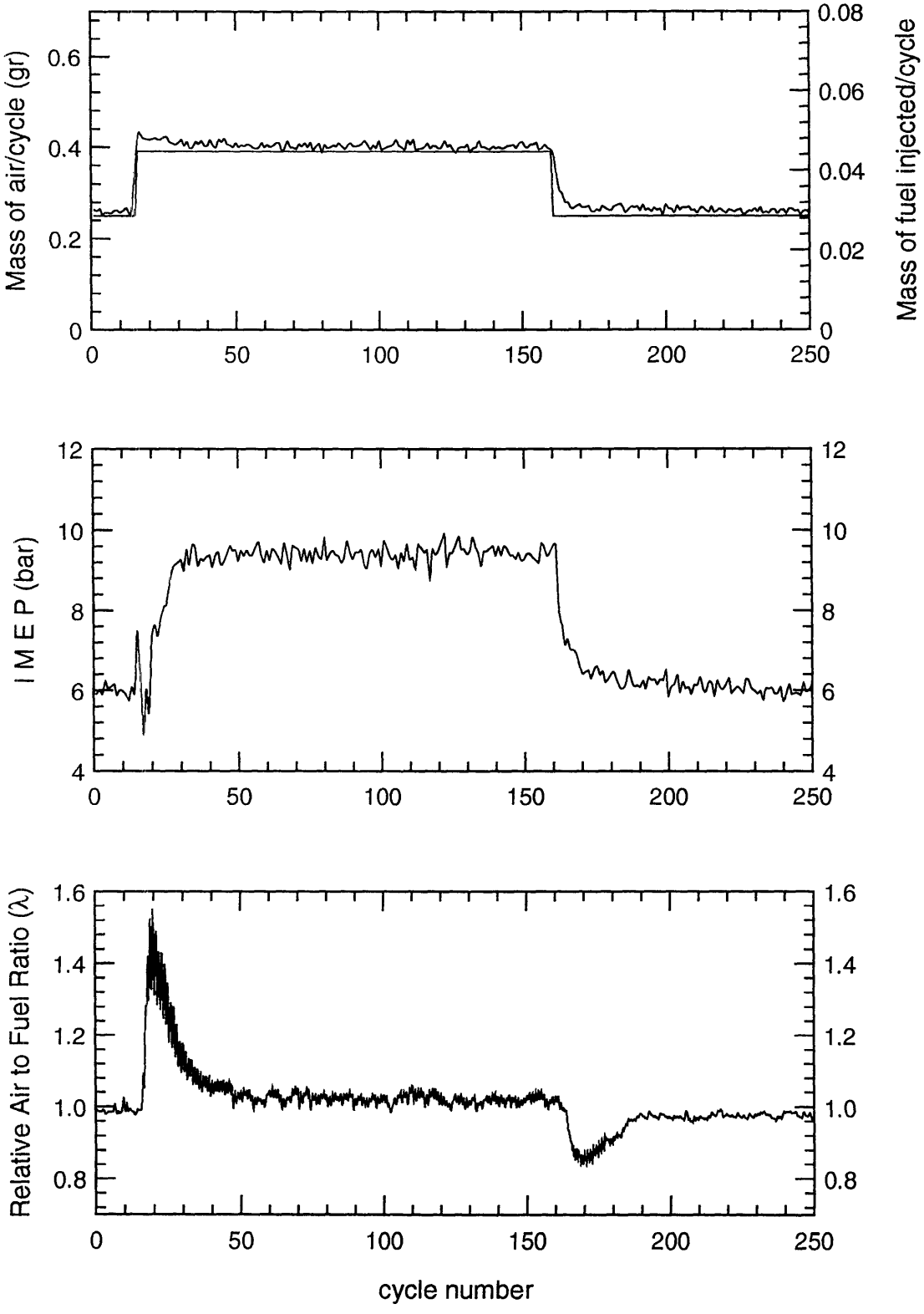
Mass of air/cycle (gr)
Mass of fuel injected/cycle
I M E P (bar)
Relative Air to Fuel Ratio (λ)
cycle number
0
50
100
150
200
250
0.2
0.4
0.6
0.02
0.04
0.06
0.08
4
6
8
10
12
0.8
1.0
1.2
1.4
1.6

M60 λ=0.9 @ 40°C

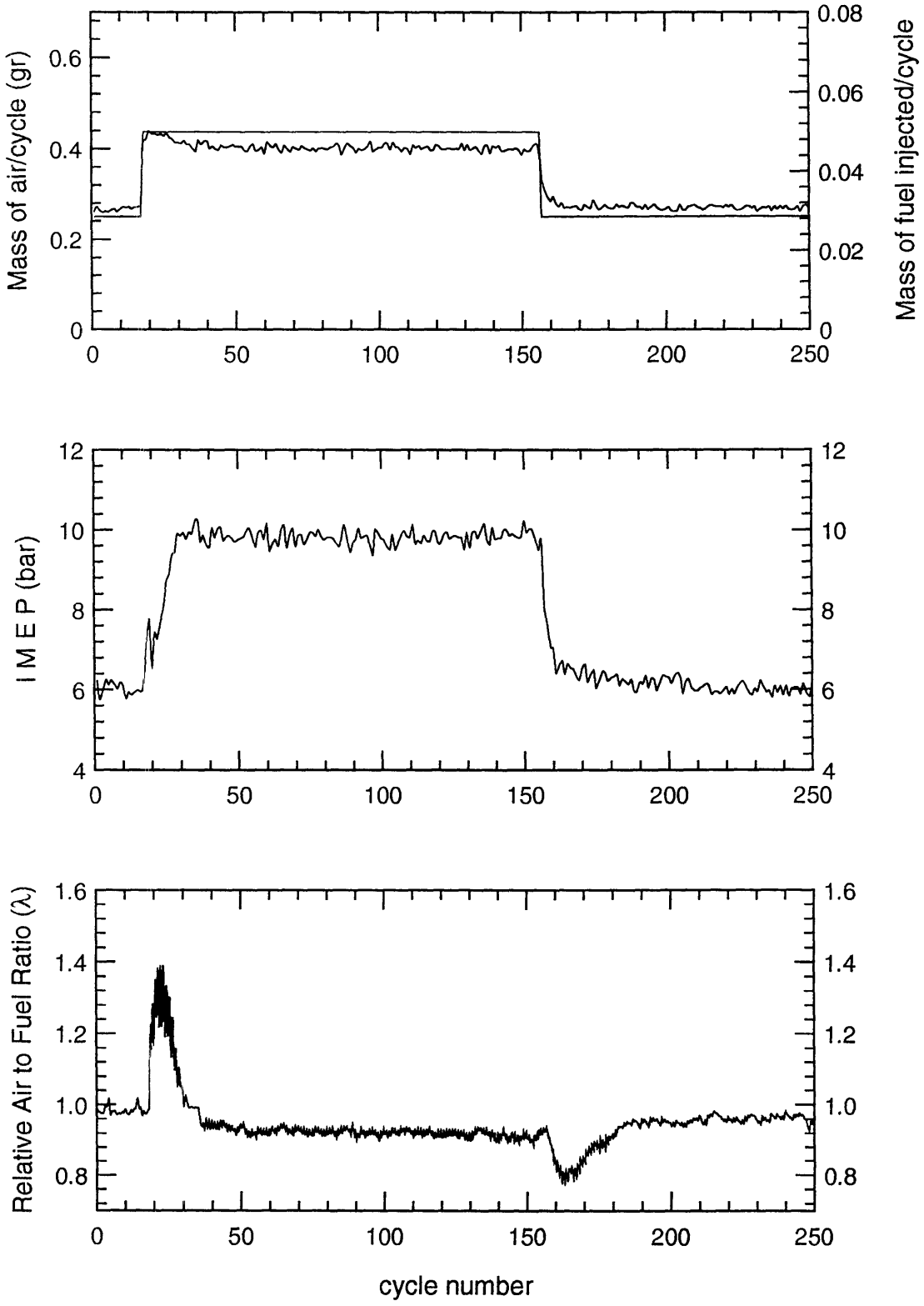
Mass of air/cycle (gr)
Mass of fuel injected/cycle
I M E P (bar)
Relative Air to Fuel Ratio (λ)
cycle number
0
50
100
150
200
250
0.2
0.4
0.6
0.02
0.04
0.06
0.08
4
6
8
10
12
0.8
1.0
1.2
1.4
1.6

M60 λ=0.8 @ 40°C

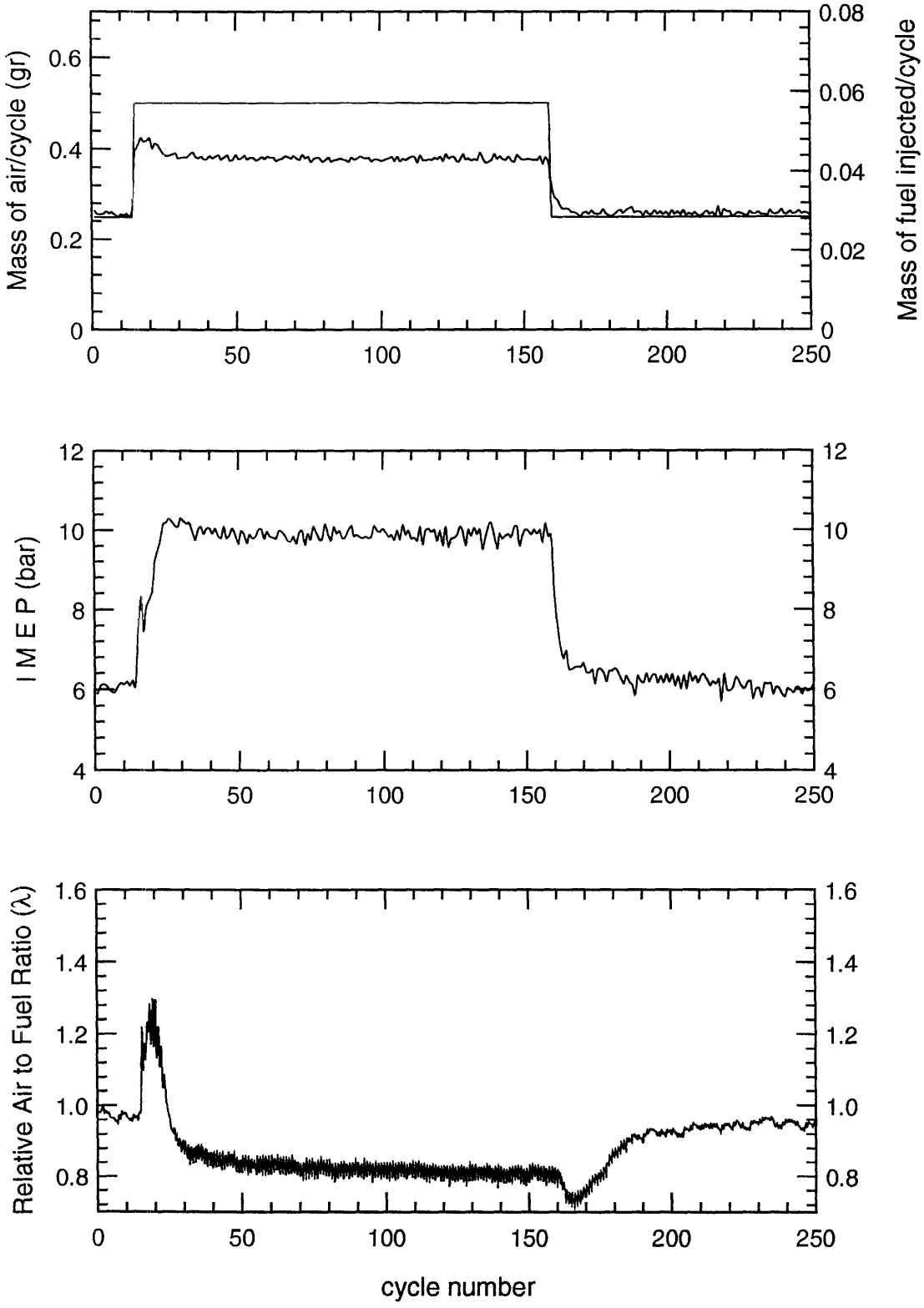
Mass of air/cycle (gr)
Mass of fuel injected/cycle
I M E P (bar)
Relative Air to Fuel Ratio (λ)
cycle number
0
50
100
150
200
250
0.2
0.4
0.6
0.02
0.04
0.06
0.08
4
6
8
10
12
0.8
1.0
1.2
1.4
1.6

M60 λ=1.0 @ 80°C

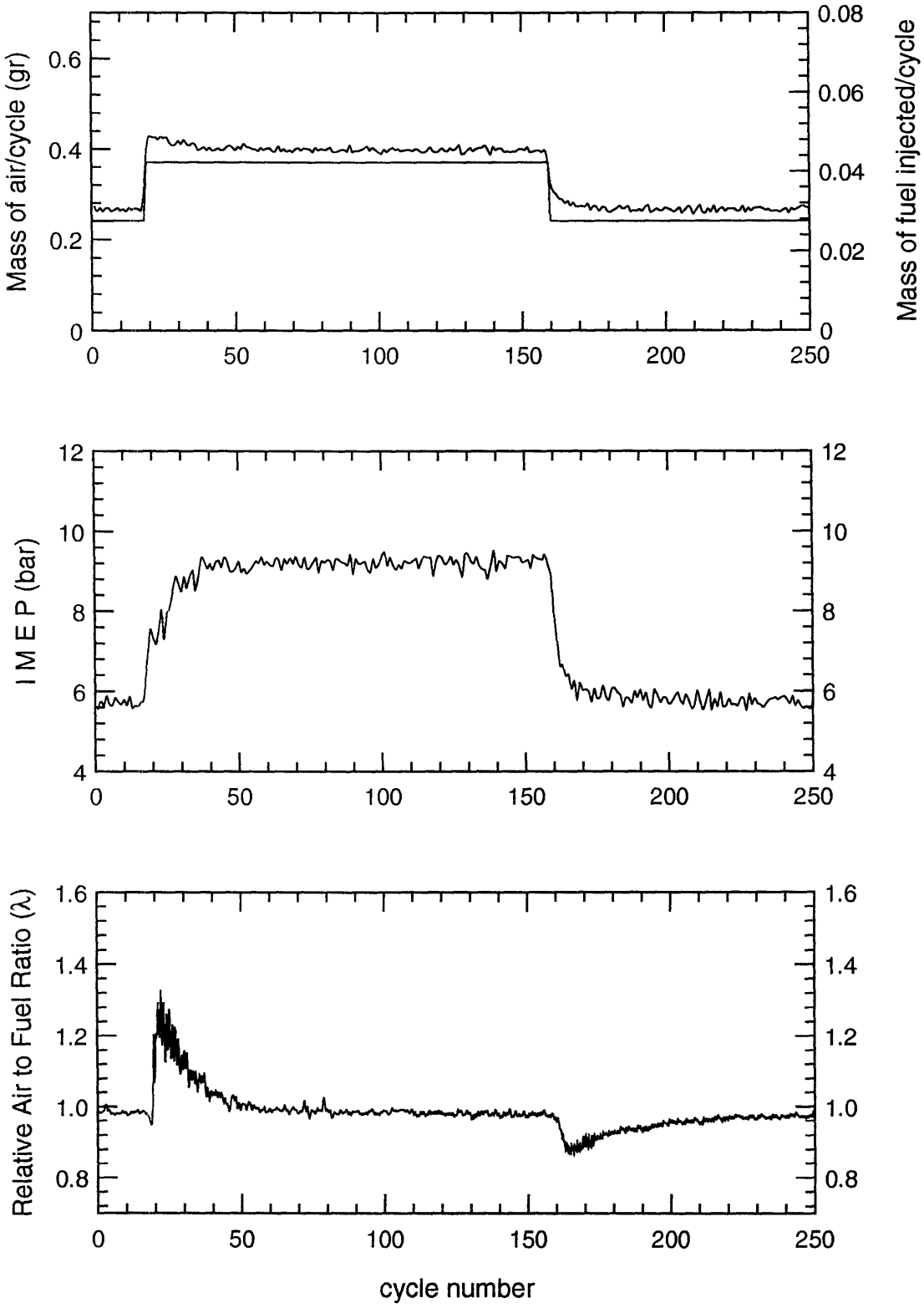
Mass of air/cycle (gr)
Mass of fuel injected/cycle
I M E P (bar)
Relative Air to Fuel Ratio (λ)
cycle number
0
50
100
150
200
250
0.2
0.4
0.6
0.02
0.04
0.06
0.08
4
6
8
10
12
0.8
1.0
1.2
1.4
1.6

M60 λ=0.9 @ 80°C

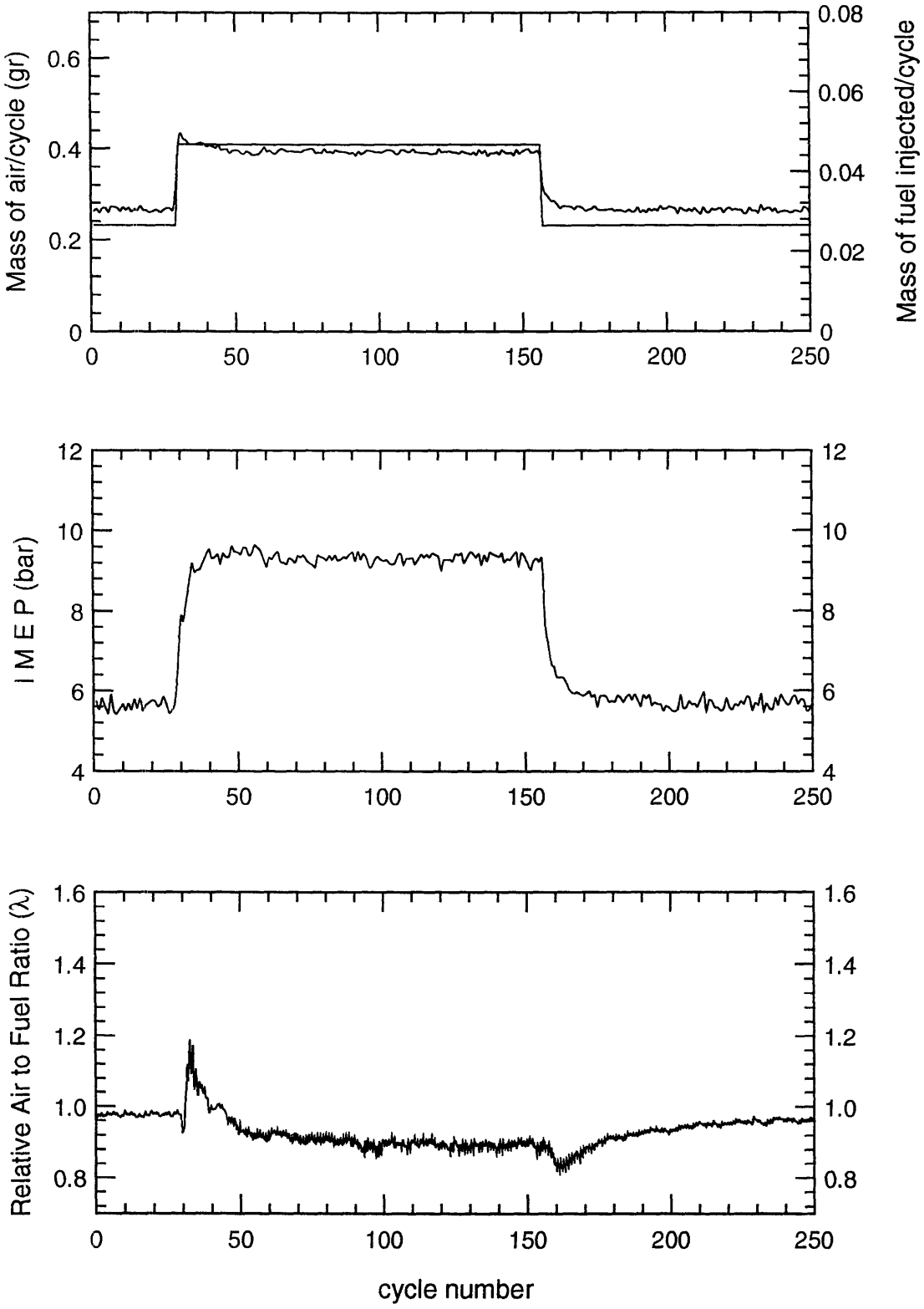
Mass of air/cycle (gr)
Mass of fuel injected/cycle
I M E P (bar)
Relative Air to Fuel Ratio (λ)
cycle number
0
50
100
150
200
250
0.2
0.4
0.6
0.02
0.04
0.06
0.08
4
6
8
10
12
0.8
1.0
1.2
1.4
1.6

M60 λ=0.8 @ 80°C

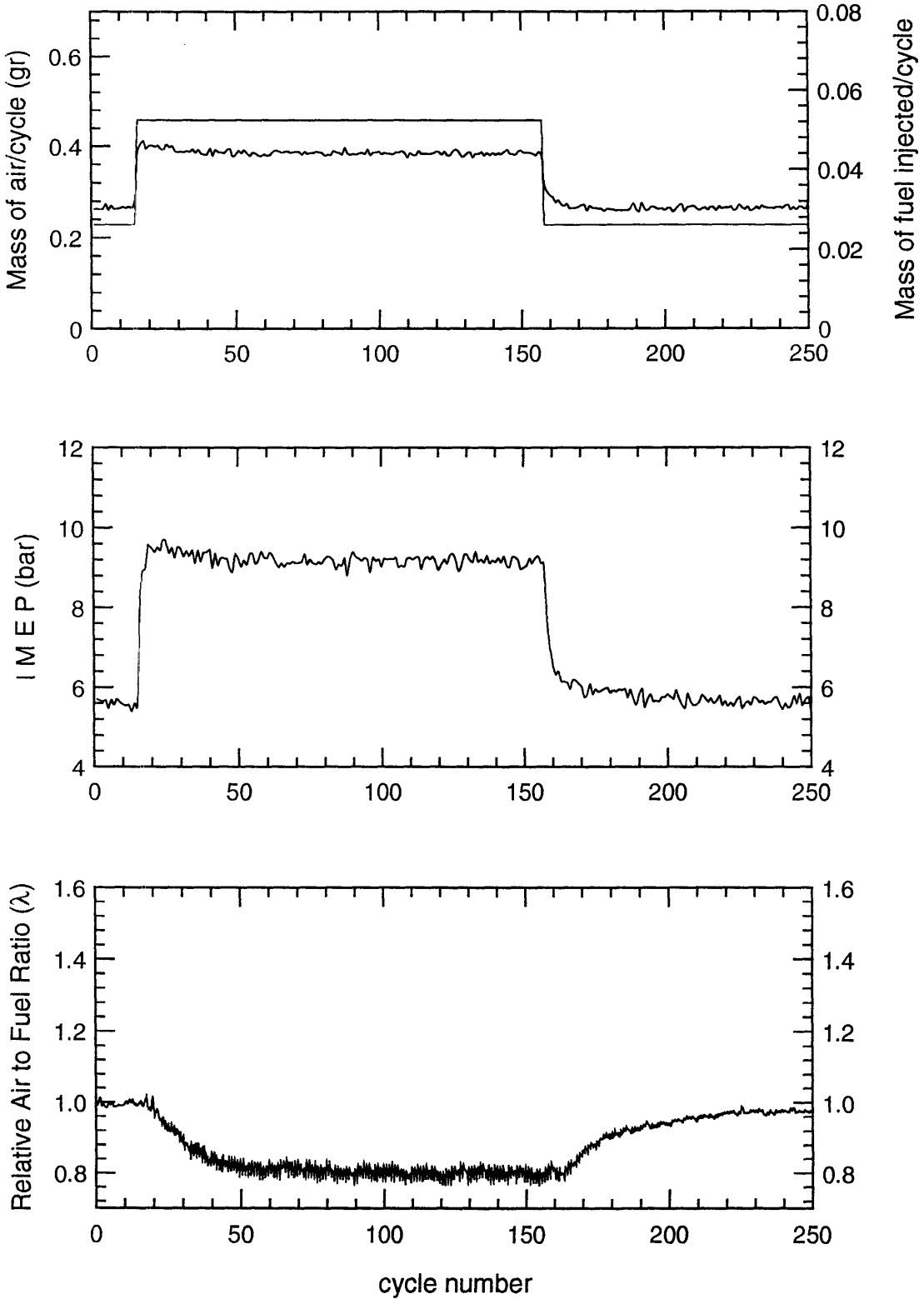
Mass of air/cycle (gr)
Mass of fuel injected/cycle
I M E P (bar)
Relative Air to Fuel Ratio (λ)
cycle number
0
50
100
150
200
250
0.2
0.4
0.6
0.02
0.04
0.06
0.08
4
6
8
10
12
0.8
1.0
1.2
1.4
1.6

M85 λ=1.0 @ 40°C

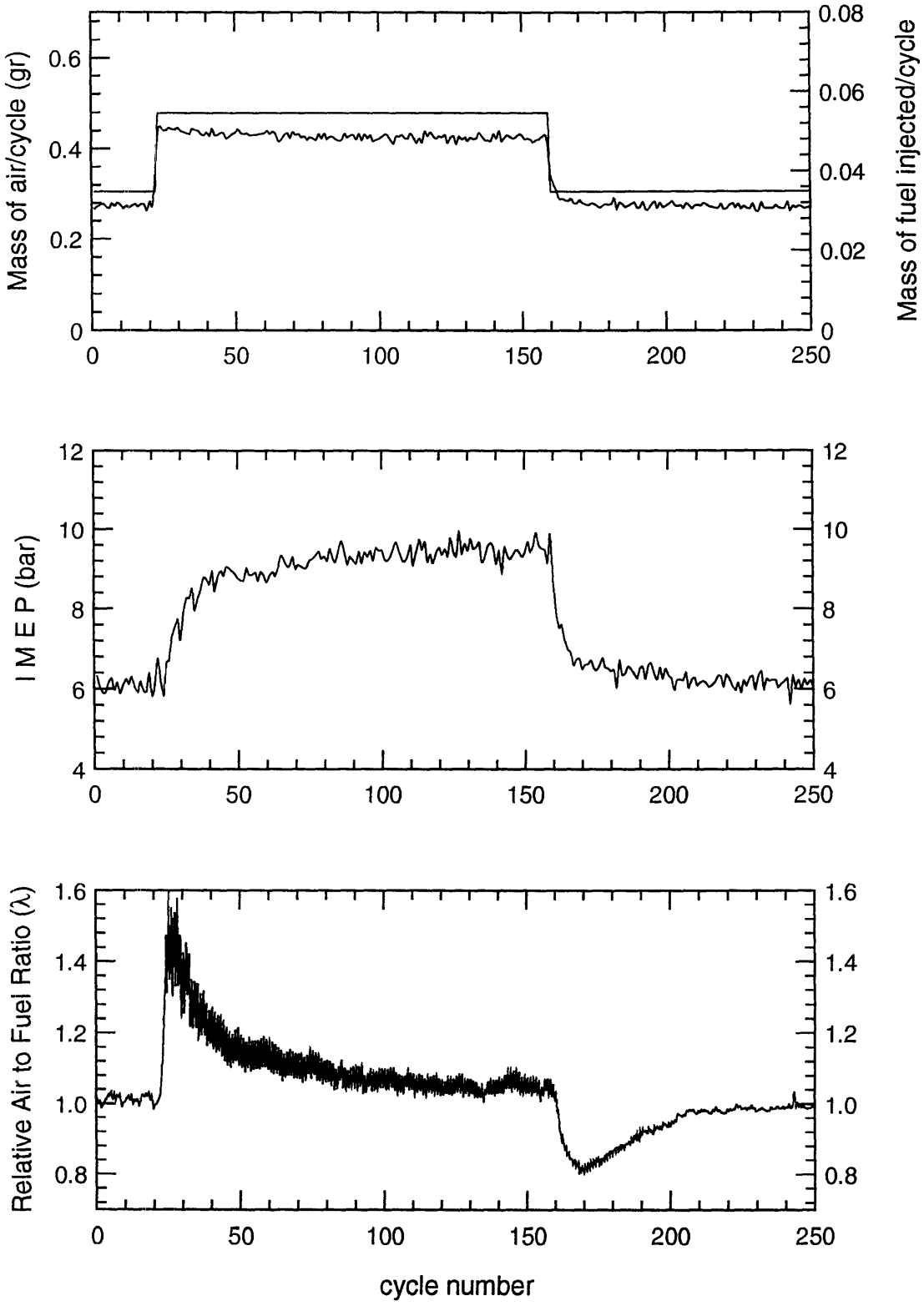
Mass of air/cycle (gr)
Mass of fuel injected/cycle
I M E P (bar)
Relative Air to Fuel Ratio (λ)
cycle number
0
50
100
150
200
250
0.2
0.4
0.6
0.02
0.04
0.06
0.08
4
6
8
10
12
0.8
1.0
1.2
1.4
1.6

M85 λ=0.9 @ 40°C

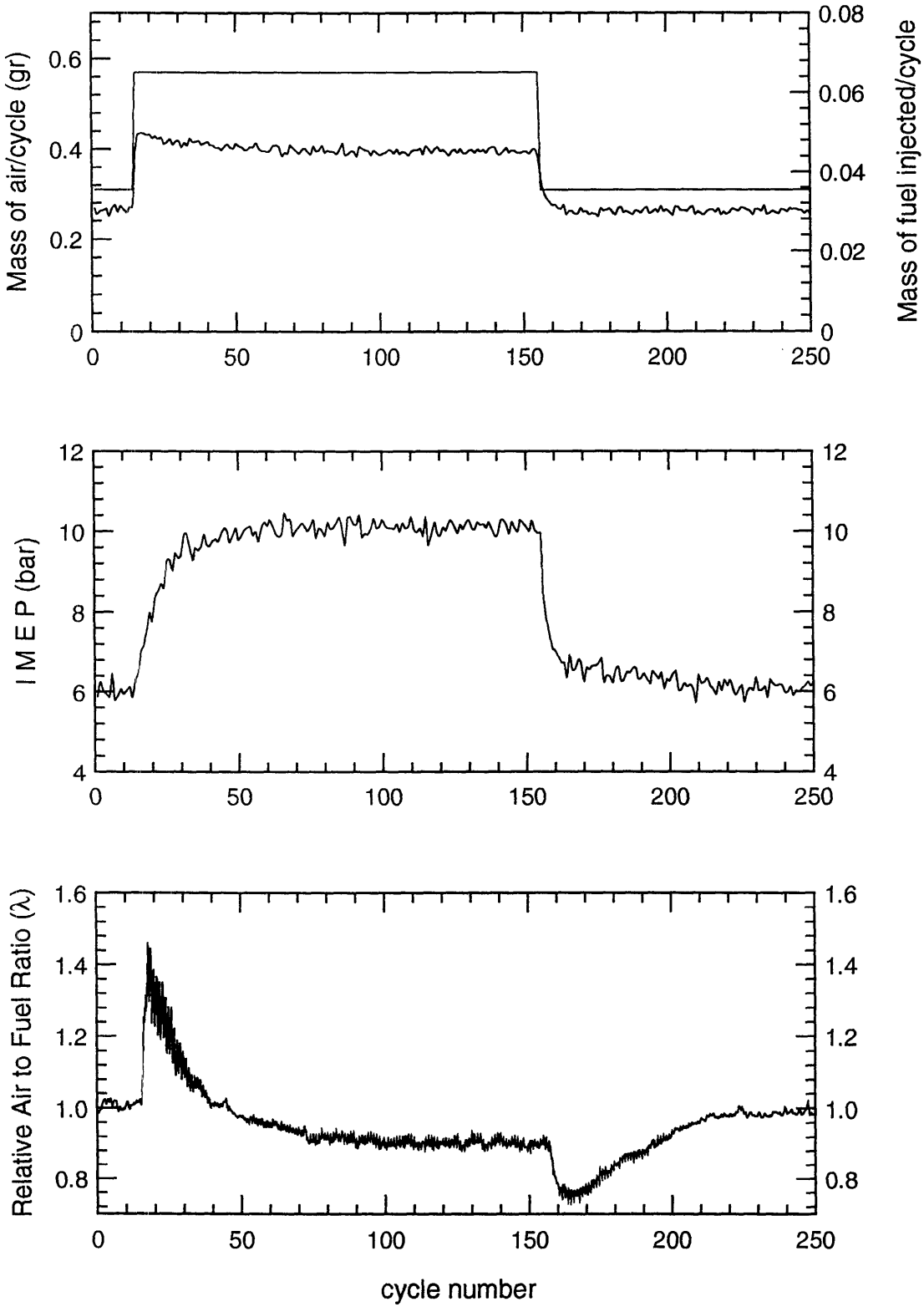
Mass of air/cycle (gr)
Mass of fuel injected/cycle
I M E P (bar)
Relative Air to Fuel Ratio (λ)
cycle number
0
50
100
150
200
250
0.2
0.4
0.6
0.02
0.04
0.06
0.08
4
6
8
10
12
0.8
1.0
1.2
1.4
1.6

M85 λ=0.8 @ 40°C

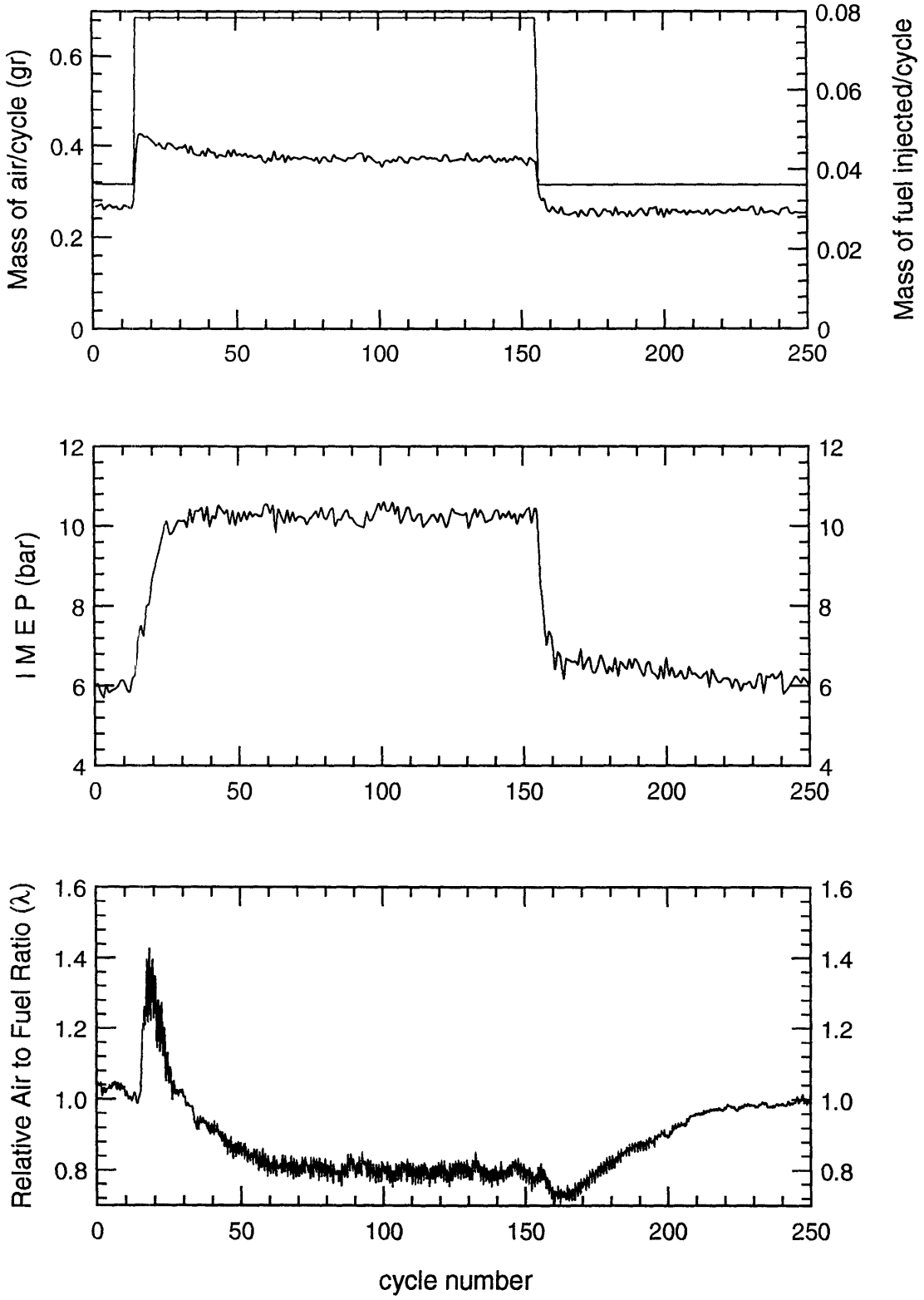
Mass of air/cycle (gr)
Mass of fuel injected/cycle
I M E P (bar)
Relative Air to Fuel Ratio (λ)
cycle number
0
50
100
150
200
250
0.2
0.4
0.6
0.02
0.04
0.06
0.08
4
6
8
10
12
0.8
1.0
1.2
1.4
1.6

M85 λ=1.0 @ 80°C

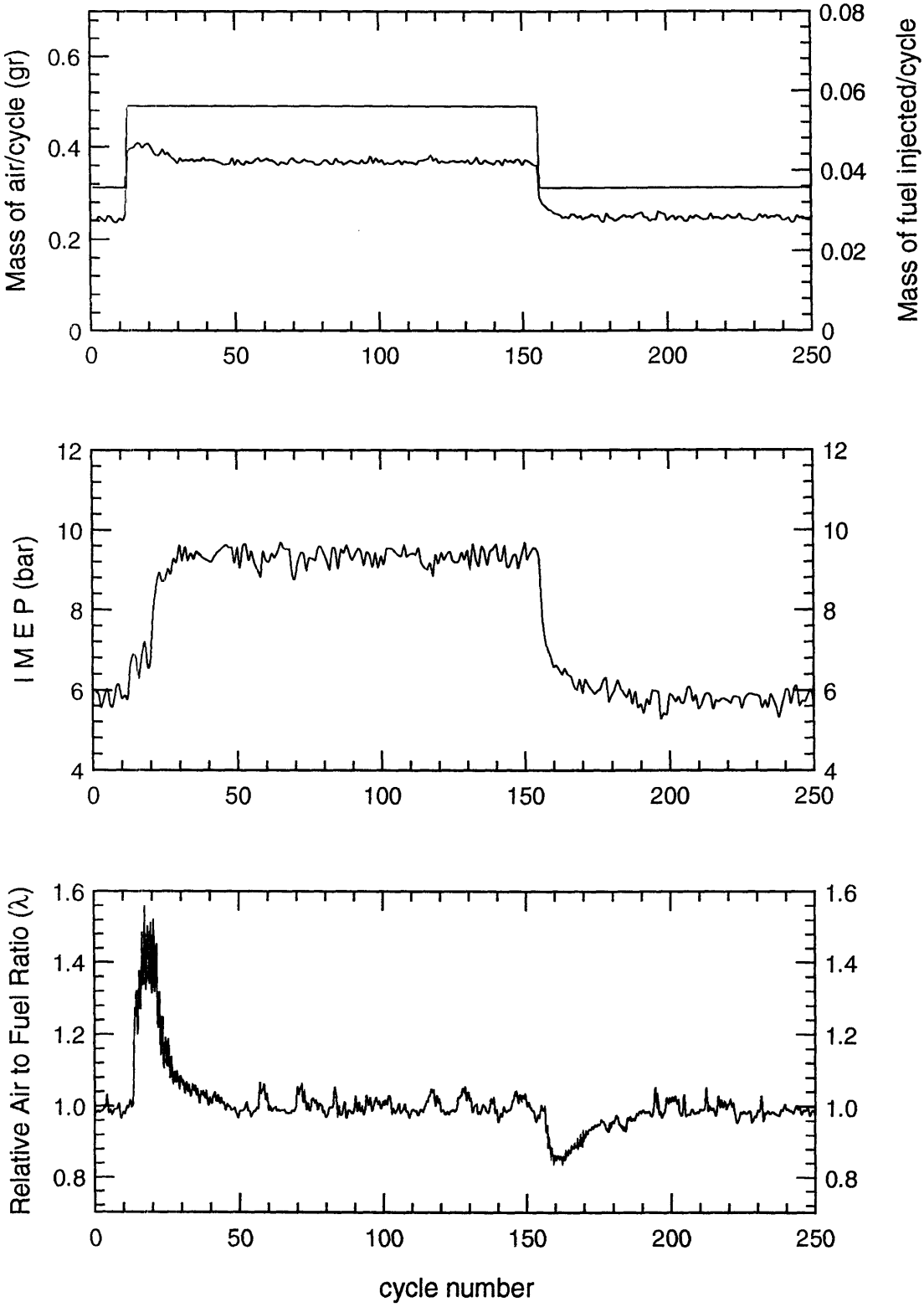
Mass of air/cycle (gr)
Mass of fuel injected/cycle
I M E P (bar)
Relative Air to Fuel Ratio (λ)
cycle number
0
50
100
150
200
250
0.2
0.4
0.6
0.02
0.04
0.06
0.08
4
6
8
10
12
0.8
1.0
1.2
1.4
1.6

M85 λ=0.9 @ 80°C

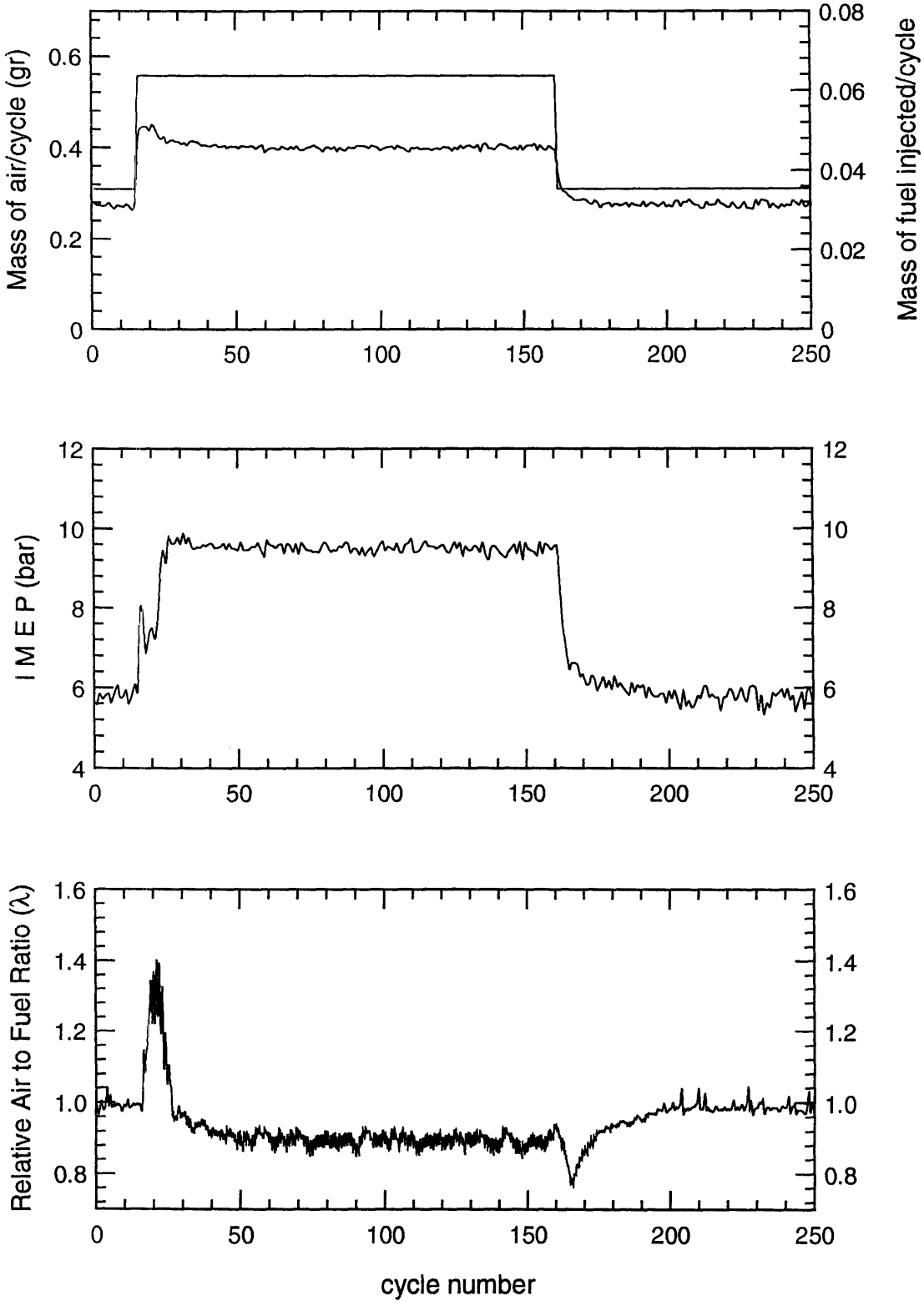
Mass of air/cycle (gr)
Mass of fuel injected/cycle
I M E P (bar)
Relative Air to Fuel Ratio (λ)
cycle number
0
50
100
150
200
250
0.2
0.4
0.6
0.02
0.04
0.06
0.08
4
6
8
10
12
0.8
1.0
1.2
1.4
1.6

M85 λ=0.8 @ 80°C

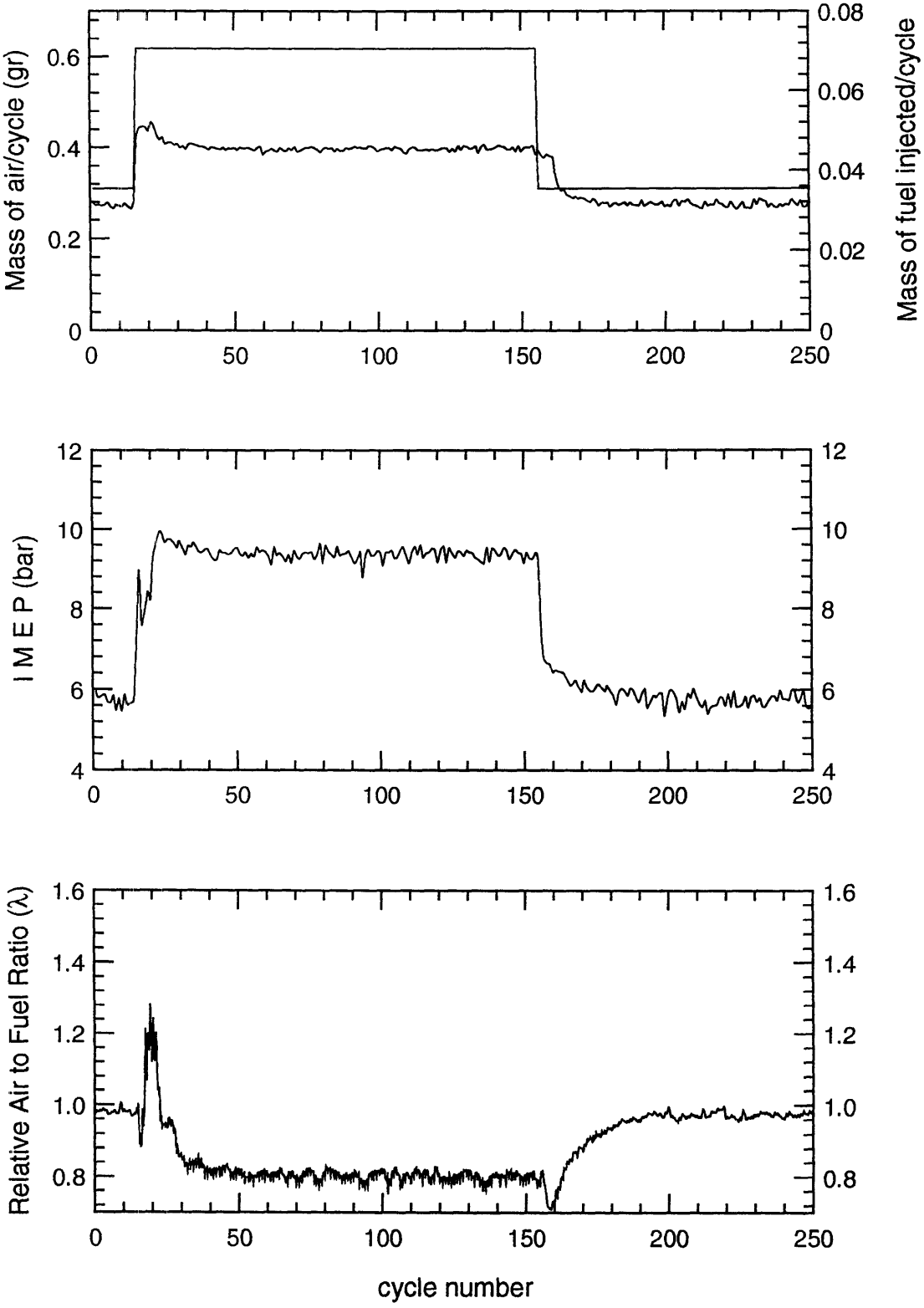
Mass of air/cycle (gr)
Mass of fuel injected/cycle
I M E P (bar)
Relative Air to Fuel Ratio (λ)
cycle number
0
50
100
150
200
250
0.2
0.4
0.6
0.02
0.04
0.06
0.08
4
6
8
10
12
0.8
1.0
1.2
1.4
1.6

M100 λ=1.0 @ 40°C

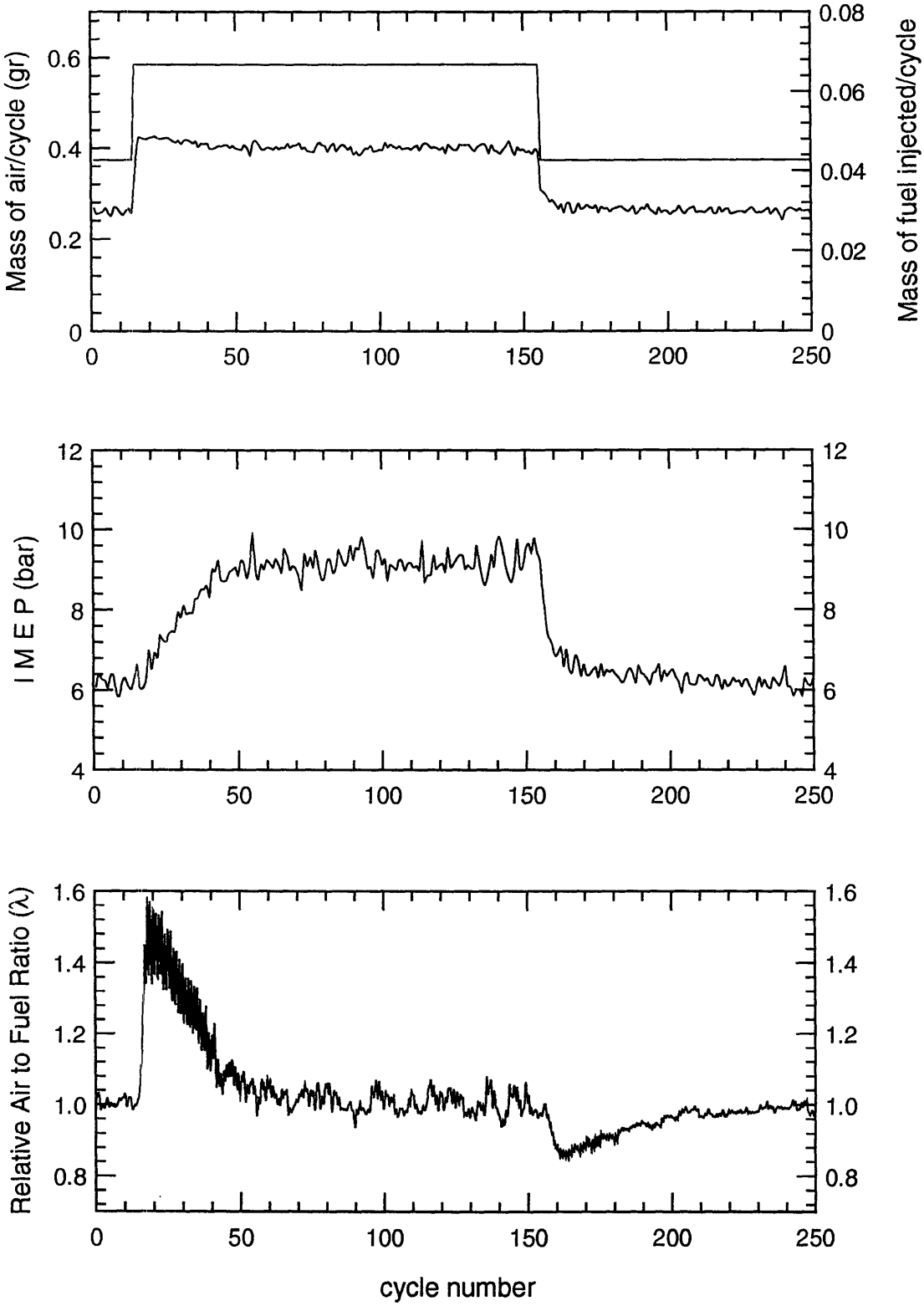
Mass of air/cycle (gr)
Mass of fuel injected/cycle
0
0.2
0.4
0.6
0.02
0.04
0.06
0.08
0
50
100
150
200
250
I M E P (bar)
4
6
8
10
12
Relative Air to Fuel Ratio (λ)
0.8
1.0
1.2
1.4
1.6
cycle number

M100 λ=0.9 @ 40°C

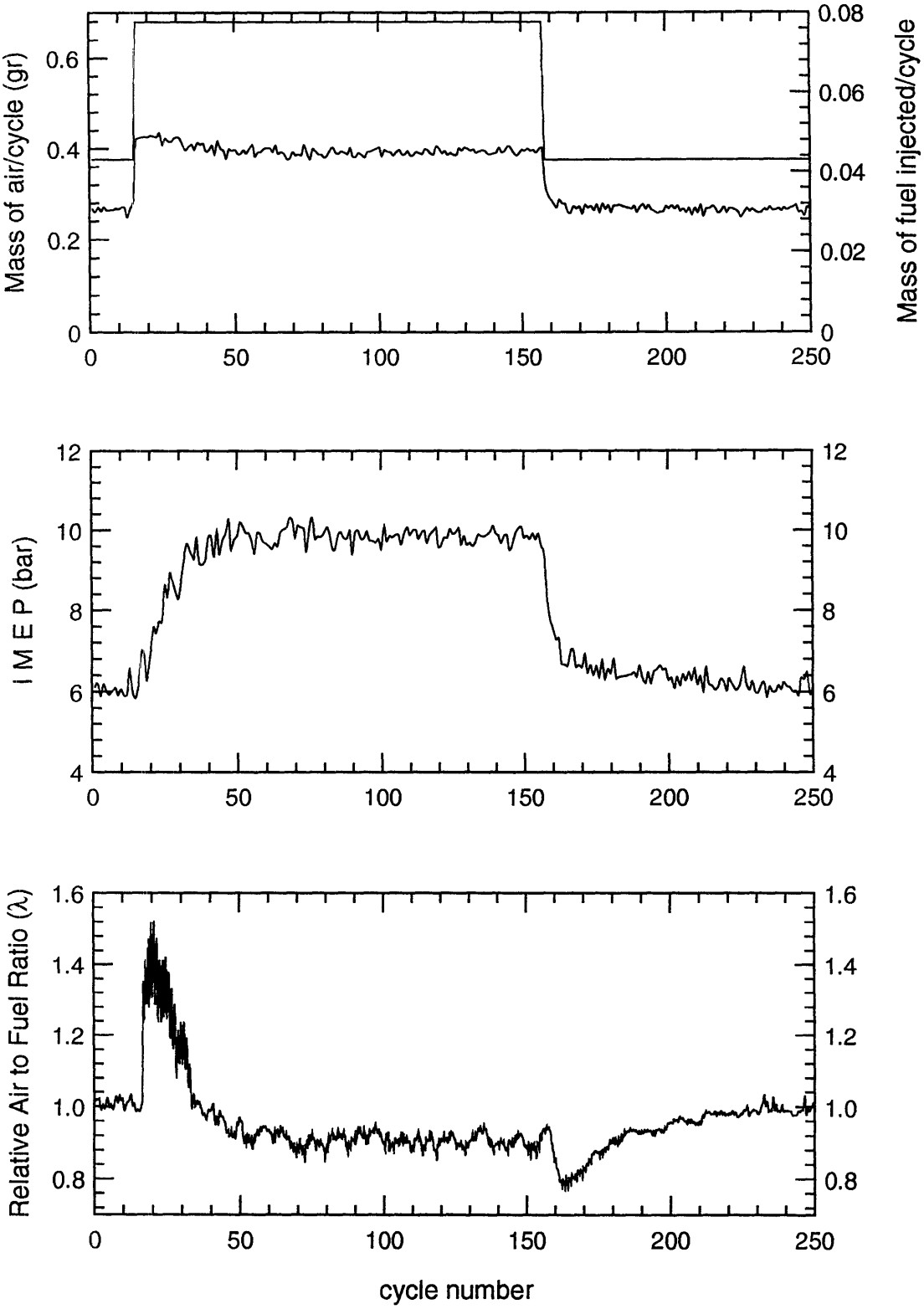
Mass of air/cycle (gr)
Mass of fuel injected/cycle
I M E P (bar)
Relative Air to Fuel Ratio (λ)
cycle number
0
50
100
150
200
250
0.2
0.4
0.6
0.02
0.04
0.06
0.08
4
6
8
10
12
0.8
1.0
1.2
1.4
1.6

M100 λ=0.8 @ 40°C

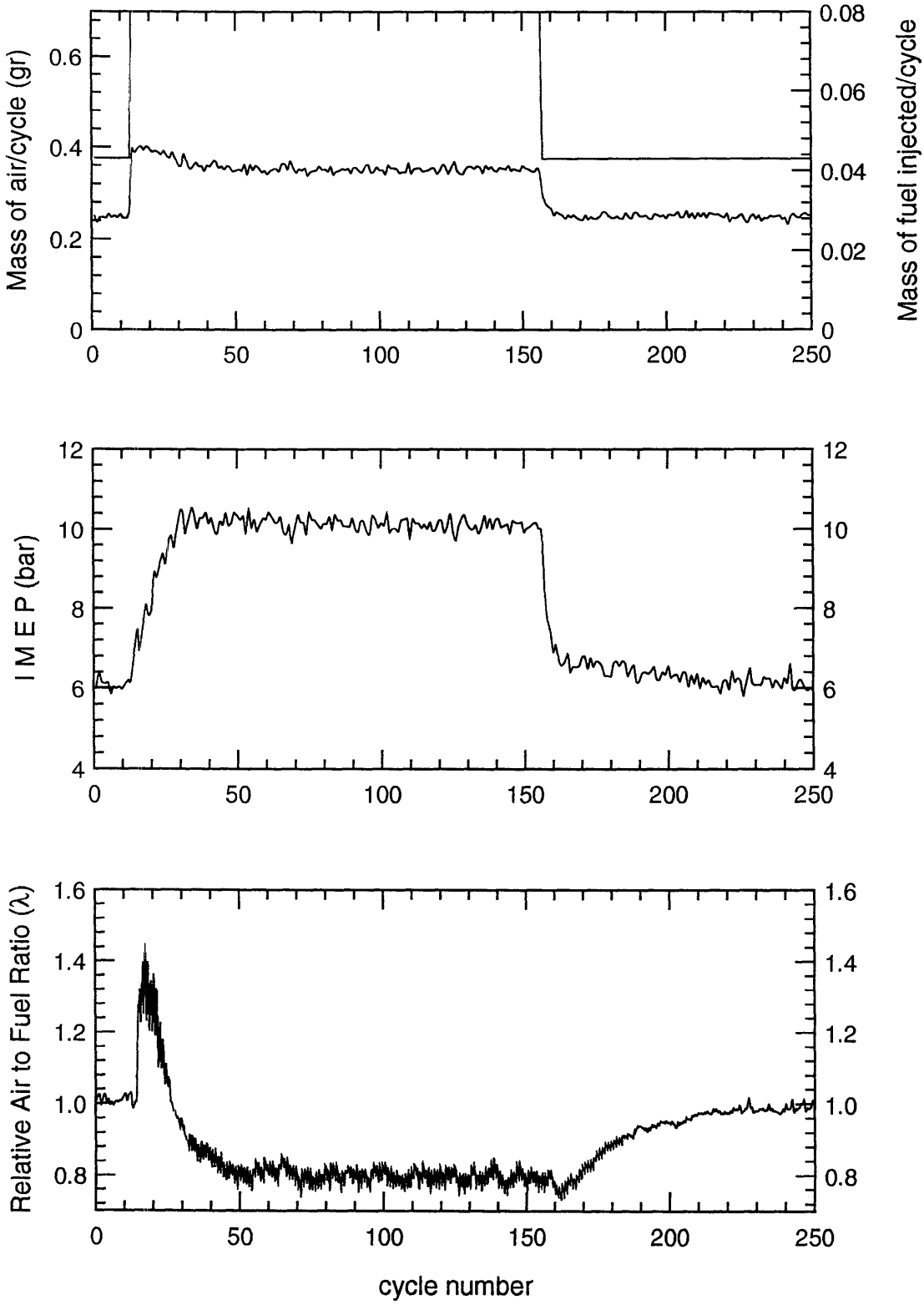
Mass of air/cycle (gr)
Mass of fuel injected/cycle
I M E P (bar)
Relative Air to Fuel Ratio (λ)
cycle number
0
50
100
150
200
250
0.2
0.4
0.6
0.02
0.04
0.06
0.08
4
6
8
10
12
0.8
1.0
1.2
1.4
1.6

M100 λ=1.0 @ 80°C

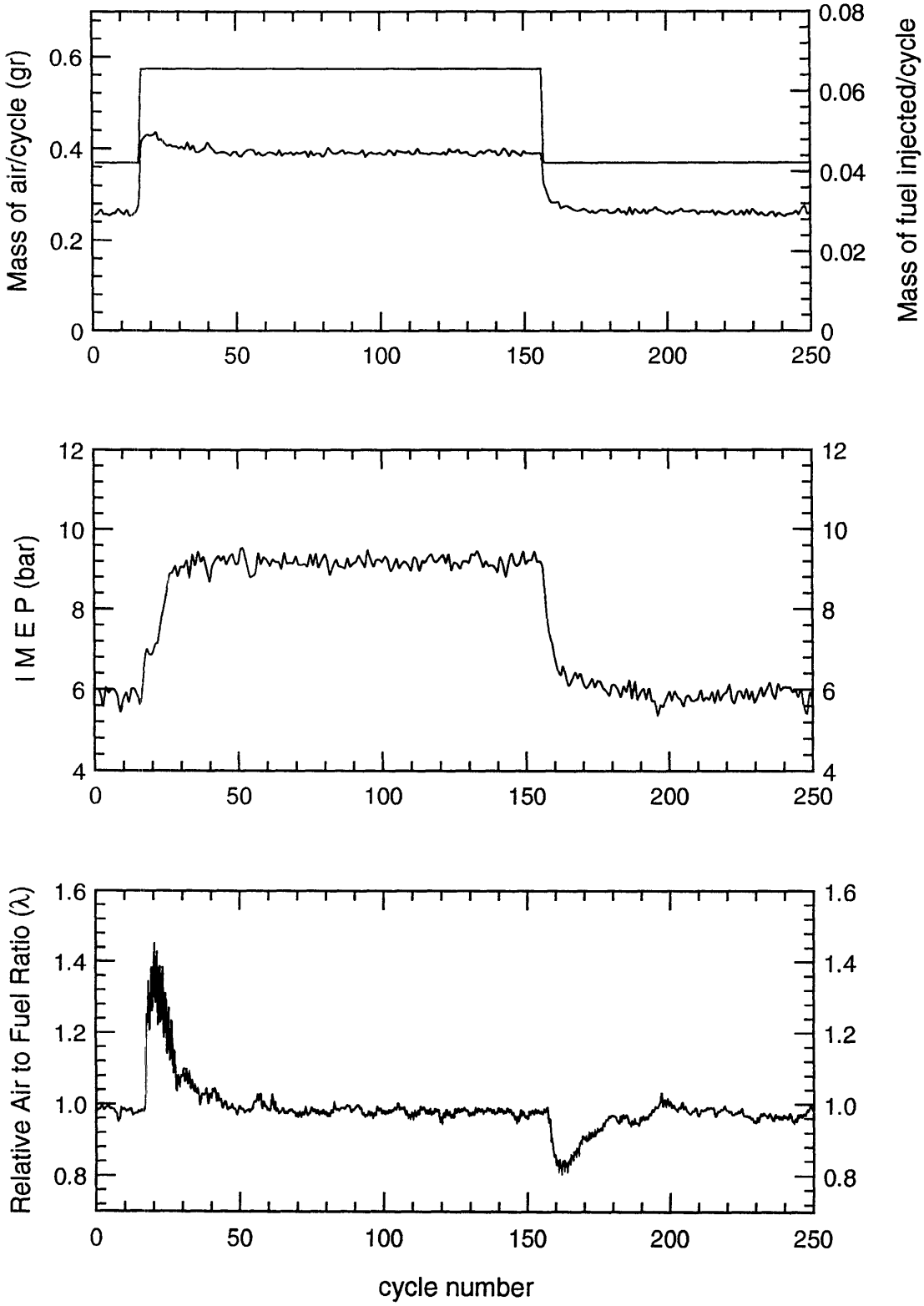
Mass of air/cycle (gr)
Mass of fuel injected/cycle
I M E P (bar)
Relative Air to Fuel Ratio (λ)
cycle number
0
50
100
150
200
250
0.2
0.4
0.6
0.02
0.04
0.06
0.08
4
6
8
10
12
0.8
1.0
1.2
1.4
1.6

M100 λ=0.9 @ 80°C

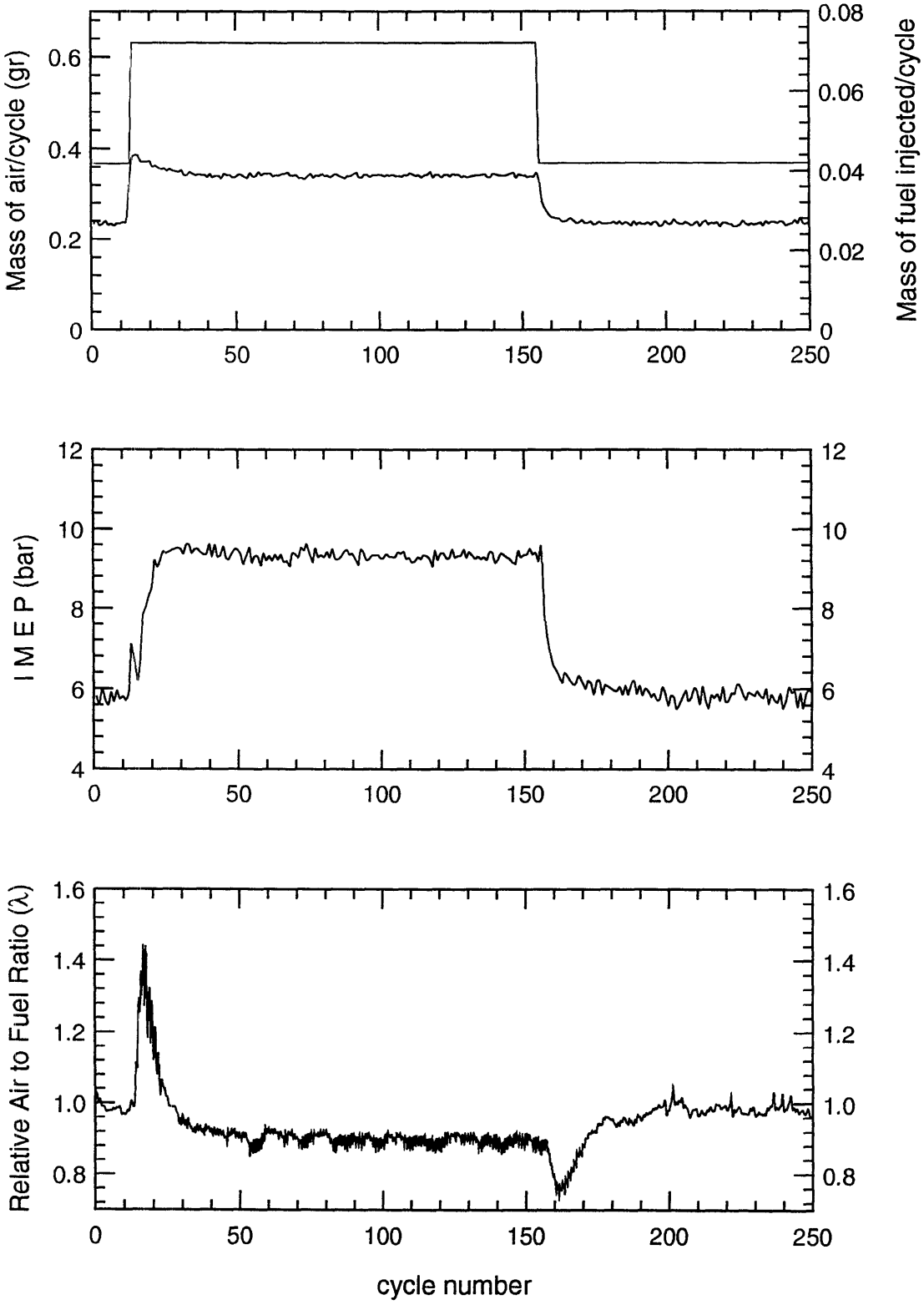
Mass of air/cycle (gr)
Mass of fuel injected/cycle
I M E P (bar)
Relative Air to Fuel Ratio (λ)
cycle number
0
50
100
150
200
250
0.2
0.4
0.6
0.02
0.04
0.06
0.08
4
6
8
10
12
0.8
1.0
1.2
1.4
1.6

M100 λ=0.8 @ 80°C

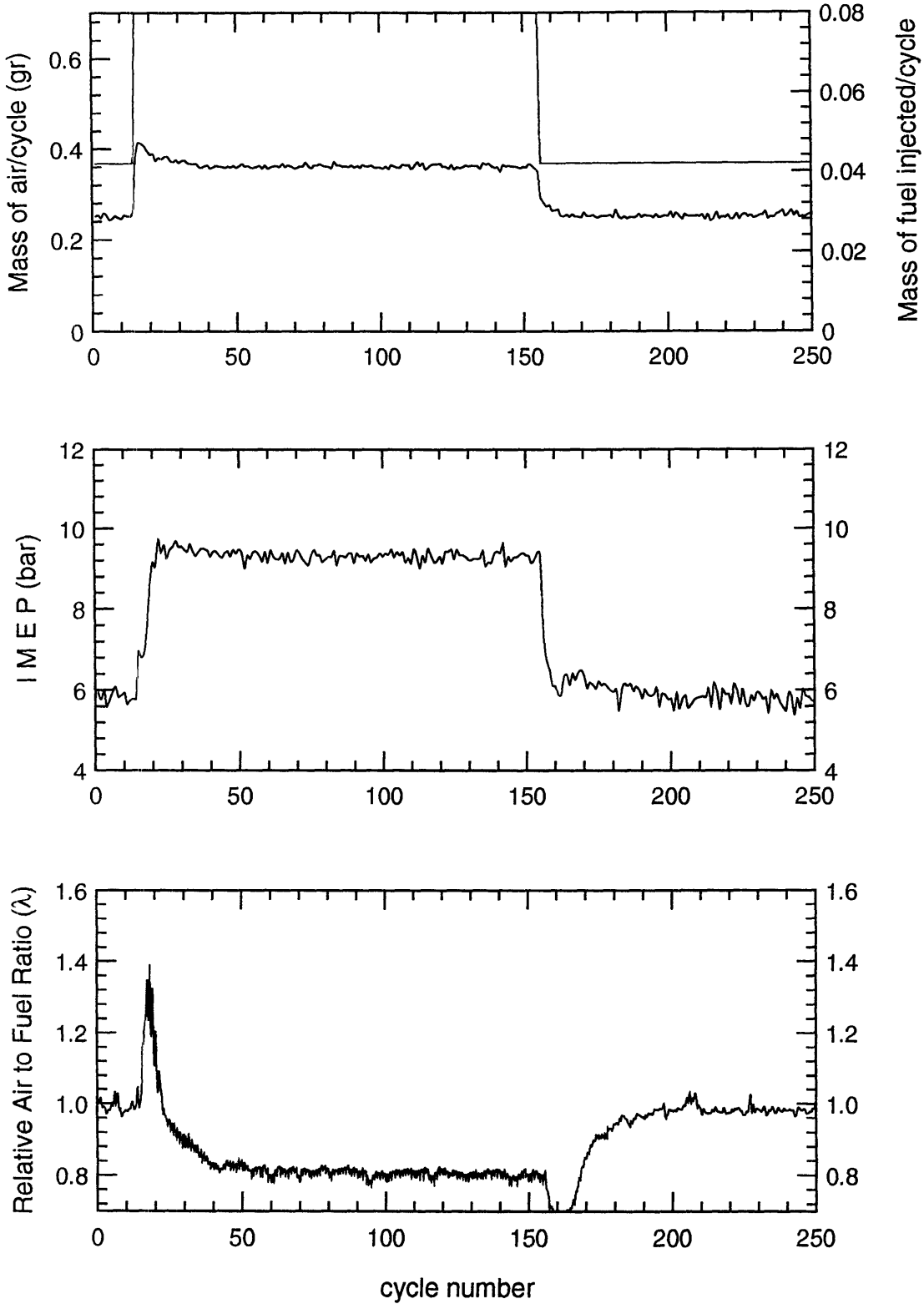
Mass of air/cycle (gr)
Mass of fuel injected/cycle
I M E P (bar)
Relative Air to Fuel Ratio (λ)
cycle number
0
50
100
150
200
250
0.2
0.4
0.6
0.02
0.04
0.06
0.08
4
6
8
10
12
0.8
1.0
1.2
1.4
1.6